AD-783 531

OCEAN MICROSTRUCTURES AND THEIR EFFECTS ON SOUND PROPAGATION IN THE CARIBBEAN SEA

Takashi Ichiye

Texas A and M University

Prepared for:

Office of Naval Research
National Science Foundation
Gulf Universities Research Consortium

May 1974

Texas A&M University
Department of Oceanography
College Station, Texas

Ocean Microstructures and Their Effects on Sound Propagation in the Caribbean Sea

by

Takashi Ichiye

for

Gulf Universities Research Consortium

A & M Project 934

Reference 74-3-T

TABLE OF CONTENTS

Page

ABSTRACT

In spring of 1972, 32 STD stations with 14 Nansen casts were occupied in the Cayman Sea and Yucatan Channel. Vertical sections of temperature, salinity and sigma-t along the central axis of the sea indicate four layered major water types. A computer program is developed for correcting digitized STD data for time lag of the temperature sensor against the conductivity sensor and for removing sharp spikes. From temperature, salinity and sigma-t values thus determined every meter at five stations, mean values and the perturbations are obtained to a depth of 1500 m. The perturbation amplitudes are proportional to the vertical gradient of the mean values of each quantity. Power spectra of the perturbations are computed by dividing the series into two depth ranges of 0 to 600 m and 600 m to 1200 m. The powers of temperature and salinity spectra are larger in the upper layer by one order of magnitude than in the lower layer. Slopes of the spectra against vertical wave numbers are steeper in the upper layer with minus three power of the buoyancy-subrange than in the lower layer with approximately minus five thirds power of the inertial subrange. Slopes of the sigma-t spectra are less steep than those of temperature and salinity spectra. A theoretical equation for the effective cross section of sound scattering by temperature irregularities indicate dependence on both horizontal and vertical wave number spectra of perturbations. There is a possibility with this equation to determine both spectra by measuring scattering cross section of initial plane sound waves propagating on a horizontal plane.

Ocean Microstructures and Their Effects on Sound Propagation in the Caribbean Sea

Takashi Ichiye

Dept. of Oceanography, Texas A&M University, College Station, Texas

1. Introduction

Sound propagation in the sea is influenced not only by a large scale density structure but also by microstructures of temperature and salinity and, to a lesser degree, of currents. Scattering of sound waves by a randomly inhomogeneous field of isotropic turbulence was mathematically treated by Tatarski (1961). More generalized problems of wave propagation in continuous random media was reviewed in a monograph by Frisch (1969). These theoretical works have been somewhat deprived of their practical purposes, because information of randomness of the oceanic environment was scarce until recently.

Although there were a number of attempts to monitor oceanic turbulence and microstructures of temperature and salinity in the past two decades, it is only after invention of STD (salinity-temperature-depth recorder) that the continuous vertical profiles of temperature and salinity can be obtained routinely. Even with an STD temperature and salinity profiling is not free from various problems. Particularly, difference in response time between temperature and conductivity sensors causes errors in determining salinity.

During the present work, computer programs are developed to correct

salinity readouts of an STD by compensating the difference in response time between temperature and conductivity sensors and to smooth out noises inherent in electronics of the STD instrumentation. Then sigma-t values are determined from the corrected values of temperature and salinity at each meter.

Smoothed vertical profiles at each station are obtained for temperature, salinity and sigma-t by using a binomial low pass filter. Deviations of corrected individual values from smoothed profiles are determined for each station. The power spectra of the perturbations (deviations) against vertical wave numbers are then calculated at upper and lower depth ranges for each station by use of the Tukey method. The power spectra indicate different power relationships about the vertical wave numbers. Theoretical models on scattering of sound waves by microstructures are presented based on the spectra thus determined.

2. Description of a Hydrographic Section Along the Cayman Sea

Cruise 72-A-8 was carried out on board the R/V ALAMINOS in the Cayman Sea, Yucatan Channel and the Florida Straits from April 22 to May 1, 1972. During the cruise, thirty-two CTD stations were occupied to a maximum depth of 1500 m. At fourteen of these STD stations Nansen casts were carried out to a depth of 4000 m. Between STD stations XBT's were operated almost every ten nautical miles to record water temperature down to 500 m. Locations of such stations are plotted in Fig. 1.

Temperature, salinity and sigma-t cross sections across the western Windward Passage and along the Cayman Sea are plotted in Figs. 2, 3 and 4, respectively. Temperature and sigma-t sections indicate that the water flows into and out of the Cayman Sea, respectively, in the northern and southern half of the western Windward Passage (Worthington, 1966; Ichiye and Sudo, 1971). In the central Cayman Sea the current seems to be northward judging from the trend of isotherms and isopicnals. The thermocline can be located between 100 m and 600 m with the maximum vertical gradient in temperatures between 120 m and 240 m. The depth of the thermocline decreases in general towards the west. The pycnocline is shallower than the thermocline and is located between 60 m and 250 m with the maximum vertical gradient around 150 m. The depth of the pycnocline decreases slightly toward the west.

Water types or water masses in the Cayman Sea can be recognized more clearly by the salinity section than by the temperature or sigma-t section. Particularly the high salinity core above 36.75 $^{o}/_{oo}$ is located at the depth

between 125 m and 200 m and signifies the westward spreading of the North Atlantic Subtropical Water which enters the Windward Passage (Wüst, 1963). Below this water, the low salinity core of salinity less than 34.90 °/oo is found between 600 m and 950 m. This core indicates the presence of the Subantarctic Intermediate Water which is ubiquitous in the North Atlantic Ocean. The trend of the isopycnals in the western part of the section suggests that this water comes up northward from the Colombia Basin. The isohalines suggest that the Intermediate Water may move eastwards in the Cayman Sea after crossing the Jamaica Ridge from the Colombia Basin, in an opposite direction to the movement of the Subtropical Water in the upper layer. Below the Intermediate Water, presence of the North Atlantic Deep Water is indicated by salinity slightly higher than 35.00 °/oo below 1200 m. High salinity above 35.05 °/oo near the Windward Passage suggests that this water enters the Cayman Sea through the passage.

3. Recording and Processing of Data

In order to determine oceanic microstructure with conventional STD's (Plessy 9006 and 9040) special care was taken in two points. One was lower the sensor at slower speed (about 0.3 m/sec) than the standard speed (1 to 2 m/sec) and the other was to record the data with Hewlet-Packard data logger using magnetic tapes as well as in strip charts with the manufacturer's recorder. Also temperature and salinity data from Nansen casts at the same stations were always used to calibrate the STD.

Seven-track tapes recorded the data with density of 200 bytes per inch and 120 characters per logical record. Nine data sets of salinity, temperature, depth and time (S, T, D, t) are recorded in 0.99 seconds. Thus nine readings can be obtained if the STD is lowered at 1 m/sec. Each of the three variables (S, T, D) is recorded by frequencies and is assigned a time interval.

Salinity, temperature, and depth frequencies are converted to conventional oceanographic units and a relative time in seconds is assigned to each data set. Conductivity is then calculated by using observed salinity and temperature from Weyl's (1964) formula. (It is obvious from this procedure that conductivity and temperature should be recorded instead of salinity and temperature, since recorded salinity includes errors due to time lag of the temperature probe against the conductivity sensor.)

It is assumed that response of the conductivity sensor is instantaneous while the temperature probe has time lag of 0.35 seconds as stated by the manufacturer. Therefore the salinity recorded by the instrument corresponds

to the conductivity at the instant but to temperature at the time 0.35 seconds before. Thus the salinity is calculated from the conductivity and the temperature at the time 0.33 seconds later by use of Weyl's formula, disregarding the difference of 0.02 seconds in time interval.

There are still some errors caused by electronic noises. In order to eliminate such noises as much as possible, values which show sudden change are deleted. Criterions for sudden change are considered as $|S_i - S_{i-1}| > 0.1$ °/oo and $|S_{i+1} + S_{i-1} - 2S_i| > 0.1$ °/oo for salinity and $|T_i - T_{i-1}| > 0.2°C$ and $|T_{i+1} + T_{i-1} - 2T_i| > 0.2°C$, where subscripts i-1, i, i+1 designate successive data points taken at an interval of about 0.11 sec.

Each set of data is averaged to represent the value at the depth interval of about 1 meter. Since in the upper 200 m the lowering rate is slower than 1 m/sec, more than nine values are averaged for giving each value even when values with sudden change are deleted. The mean depth of such averaged values is truncated to the unit of one meter.

In order to obtain the mean vertical profiles of temperature, salinity and sigma-t at each station from the data corrected for each meter of the depth, the low-pass filter of binomial weighting coefficients is used. The mean values at each meter $q^*(z)$ can be obtained from the original corrected values $q(z)$ by use of a formula

$$q^*(z) = \sum_{i=-n}^{n} w(i)\, q(z+i) \qquad (1)$$

where w(i) is a weighting coefficient given by

$$w(i) = \frac{(2n)!}{(2n-i)!\,i!} \Big/ \sum_{i} \frac{(2n)!}{(2n-i)!\,i!} \qquad (2)$$

Although the larger n the greater is the degree of smoothing, too large an n means including values of different types of waters (or statistically different sets of values) as well as shortens numbers of the original series of data. Therefore n is taken as 20. This is equivalent to taking weighting means of the values 20 m above and below the original value at each meter of depth.

4. Average Profiles and Perturbations at Microstructure Study Stations

The profiles of temperature, salinity and sigma-t determined by the binomial low pass filter at each meter are shown in Figs. 5, 6 and 7 at Stations 9, 10, 11, 15 and 16 (micro-structure study stations). The upper mixed layer was not discernable as in the mid-latitude ocean, though Station 16 may show presence in the upper tens of meters. There are four layers with different vertical gradients at all stations. The uppermost layer (including St. 16) has small gradient of 0.1 to 0.2°C per 10 m and reaches 125 to 175 meters. The second layer reaches 250 to 300 meters with gradient of 0.5 to 0.7°C per 10 m, the third layer reaches 800 to 1000 meters with gradient of 0.2 to 0.3°C per 10 m and the fourth layer is located below the third layer with gradient less than 0.05°C per 10 m.

Vertical profiles of salinity show also four water types (Wüst, 1963). In the upper 100 to 150 m, salinity increases from the surface values of less than 36.00 °/oo. At about 200 m there is a salinity maximum of about 36.8 °/oo which marks the core of the Atlantic Subtropical Water. The core seems to decrease its maximum value westwards from 36.85 to 36.75 °/oo as also indicated by the vertical salinity section of Fig. 3. Salinity decreases downwards from the core to about 800 to 900 m, where the minimum salinity of 34.9 °/oo is encountered. This represents the core of the Antarctic Intermediate Water. In contrast to the salinity maximum, the minimum value of the core seems to decrease slightly westwards and also its thickness seems to decrease westwards. Zonal change of these two cores suggests westward and eastward advection of the Atlantic Subtropical and the Antarctic

Intermediate Water, respectively. Below the Antarctic Intermediate Water core, salinity increases to above 35.0 °/oo. This indicates ubiquitous North Atlantic Deep Water.

The behavior of the vertical profiles of sigma-t reflects temperature and salinity profiles but influence of the former is stronger. Again four layers are distinguished according to the vertical gradient of sigma-t which represents vertical stability. The average stabilities (in 10^{-8} cm^{-1}) in the four layers are 6 from the surface to about 100 m, 25 from 100 m to 200 m, 1.8 from 200 m to 1000 m and 0.3 from 1000 m to 1500 m.

In Figs. 8, 9 and 10 the perturbations of temperature, salinity and sigma-t from the average profiles are plotted against the depth. Temperature perturbations indicate larger amplitudes above 600 m at most stations except at Station 15 where large perturbations occur between 800 m and 1000 m. At three eastern stations (Stations 9, 10 and 11) particularly large perturbations occur above 300 m. These large perturbations in the upper layers with ranges of more than 0.5°C seem to be coherent among the three stations with slight change in depths of maxima and minima. The perturbations gradually diminish below 1000 m with ranges less than 0.1°C. Such large perturbations in the upper layer seem to be generated by internal wave action rather than turbulence because of three reasons. One reason is that the perturbations have rather regular depth intervals (vertical wave lengths). The second reason is that they concur with larger vertical temperature gradient. The third is that they occur in the layer with larger vertical stability,

although the Richardson number is unknown because of lack of velocity data. Rather high horizontal coherence of larger deviations at three eastern stations with station-to-station distances of about 70 km further strengthens this assumption, although this coherence is not certain at two western stations. Previous works of microstructures (Cooper and Stommel, 1968; Tait and Howe, 1968; Ichiye, 1973) showed that significant coherence exists only within a distance of an order of 10 km.

Salinity perturbations of Fig. 9 also reflect the vertical salinity gradient. In this case large perturbations occur in the upper 200 m which is above the salinity maximum. The perturbations are small near the salinity maximum and they remain almost of the same magnitudes down to about 700 m except at St. 9 where they become maximum in the layer between 300 m and 500 m.

Sigma-t perturbations of Fig. 10 show the higher correlations between their amplitudes and vertical gradients than temperature and salinity perturbations. Amplitudes of the perturbations distinguish three layers: the upper layer above 250 m, the middle layer between 250 m and 900 m, and the lower layer below 1000 m. These layers correspond to three layers of different vertical gradients (Fig. 7), though the uppermost layer of Fig. 7 cannot be recognized in Fig. 10 because the intervals of the perturbation extrema are almost of the same order as the layer thickness. Also horizontal coherence for the large perturbations in the upper layer is clearly recognized between Stations 9 and 10 and seems to be higher than the temperature perturbations.

5. Spectral Analysis

The averaged profiles and perturbations of temperature, salinity and sigma-t at five stations suggest presence of four layers of distinct features. Therefore it seems to be reasonable to determine spectra of perturbations in each of the four layers. However, if the data points are grouped by these layers, numbers in each group become too small to compute spectra with sufficient reliability. Therefore the data are divided only into two depth ranges: from 0 to 600 m and from 600 m to 1200 m. The former includes the upper layer and the thermocline. The latter consists of the Antarctic Intermediate Water and the Atlantic Deep Water but excludes the deeper part having no significant perturbations. Each group thus contains about 600 data points.

It is suitable to determine spectra in a high frequency range with low-pass filtering which was used in obtaining smooth profiles. However, such low-pass filtering modifies the spectra in a low frequency range. Therefore it is necessary to correct the effect of the low-pass filter on the high frequency part of the spectra.

In general, a time series function $x(t)$ is subjected to a filtering function $w(t)$ to obtain the smoothed function $\overline{x}(t)$. These three functions are related by an equation

$$\overline{x}(t) = \int_{-\infty}^{\infty} w(\lambda)\, x(t-\lambda)\, d\lambda \qquad (3)$$

The spectra of $x(t)$ and $\bar{x}(t)$ can be expressed with Fourier integrals as

$$X(\sigma) = \int_{-\infty}^{\infty} x(t)\ e^{i\sigma t}\, dt \tag{4}$$

$$\bar{X}(\sigma) = \int_{-\infty}^{\infty} \bar{x}(t)\ e^{i\sigma t}\, dt \tag{5}$$

Because of (3), integral (5) can be written as

$$\begin{aligned} \bar{X}(\sigma) &= \int_{-\infty}^{\infty} \int_{-\infty}^{\infty} w(\lambda)\ x(t-\lambda)\, d\lambda\ e^{i\sigma t}\, dt \\ &= \int_{-\infty}^{\infty} w(\lambda)\, e^{i\lambda\sigma}\, d\lambda \int_{-\infty}^{\infty} x(t)\, e^{i\sigma t} dt \\ &= R(\sigma)\ X(\sigma) \end{aligned} \tag{6}$$

Therefore the spectrum $X(\sigma)$ of the original time series can be obtained by dividing the spectrum $\bar{X}(\sigma)$ of the filtered time series with the spectrum $R(\sigma)$ of the filtering function. The function $R(\sigma)$ is called frequency response of the filtering function. The perturbations are obtained by subtracting the smoothed values from the original data in a form of series in depths of every meter. Therefore they are results of subjecting the original series (m depth) to the high-pass filter. The frequency response of the latter is given by

$$R_h(\sigma) = 1 - R_\ell(\sigma) \tag{7}$$

where $R_\ell(\sigma)$ is the response (in wave number in the present case) of the low-pass filter given by (2) (Holloway, 1959). The discrete form of the wave number response is given by

$$R_h(k) = 1 - w(o) - 2 \sum_{i=1}^{n} w(i) \cos(2\pi k i \Delta \ell) \tag{8}$$

where $\Delta \ell$ is the depth interval (1 m) and $w(i)$ is given by (2).

Figures 11-1 to 11-10 and 12-1 to 12-10 indicate wave number spectra uncorrected and corrected for the filtering function, respectively, of temperature perturbations at five stations for shallow (0-600 m) and deep layers (600-1200 m). In these figures the lines representing k^{-2} and k^{-3} are superposed. It is seen clearly that in the high wave number range (above 60 cycles per km) the spectra for the upper layer are almost proportional to k^{-3}, whereas those for the lower layer behave more likely as k^{-2}. Also the powers of the spectra are higher for the upper layer by one order of magnitude than for the lower layer. Small maxima and minima of power are present in the higher wave number range for all the spectra and might be of local nature. However, the maximum is present at log wave number of about 1.9 for spectra of each station in both layers. This corresponds to 79 cycles per KM or wave length of 12 m. Visual inspection of temperature perturbations plotted in Fig. 8 indicate that the peak-to-peak lengths of such perturbations are about 30 m in the upper layer and 24 m in the lower layer, corresponding to wave numbers 33 and 42

cycles per KM. Therefore the observed peak of power can be interpreted as the biharmonics of the observed predominant perturbations, whose principal harmonics are masked in the spectra due to effects of low-pass filtering.

The power in a low frequency range (below 1.8 in log C. P. KM) of spectra corrected for the high-pass filter are larger by more than one order of magnitude than those uncorrected. The lower wave number part of corrected spectra do not have reliability as high as those of the high wave number range because of smaller number of data values. However, it can be concluded that the spectra in the upper layer are larger by one order of magnitude than those in the lower layer also in the lower wave number range. Similarity in spectra among stations is stronger in the lower wave number range than in the higher wave number range.

Salinity spectra without and with correction for the high-pass filter are shown in Figs. 13-1 to 13-10 and Figs. 14-1 to 14-10, respectively. These spectra have the same features as temperature spectra: (1) the power in the higher wave number range behaves as k^{-3} in the upper layer but they are close to k^{-2} in the lower layer, (2) the power in the high wave number range is larger by one order of magnitude in the upper range than in the lower layer, and (3) a peak is found in all the spectra at the log wave number of about 1.9. The difference of salinity spectra from temperature spectra is mainly in the lower frequency range, where the power difference between the upper layer and the lower layer is less than an order of magnitude.

The power in the lower wave number range reflects the change of the mean values with depth. Therefore when the mean salinity profiles are compared with those of temperature, the former has similar magnitudes of variation with depth between the upper 600 m and lower 600 m depths, but the latter shows a strong and very weak vertical gradient in the upper and lower layer, respectively. The salinity spectra have the second maximum at the log wave number of 2.1 to 2.15 in the lower layer at all stations and in the upper layer at some stations. Salinity perturbations plotted in Fig. 9 indicate presence of peaks at much smaller depth intervals than in those of temperature plotted in Fig. 8.

Spectra of sigma-t without and with correction for high-pass filter are plotted in Figs. 15-1 to 15-10 and in Figs. 16-1 to 16-10, respectively. A striking feature of sigma-t spectra is that the slope of their power against wave number in the high wave number range is less steep than the one of temperature and salinity spectra. Spectra in the lower layer have a slope between k^{-1} (dashed line) and k^{-2}. The upper layer spectra have a slope between k^{-2} and k^{-3} instead of a slope k^{-3} as the temperature and salinity spectra. Less steep slopes of the sigma-t spectra can be interpreted as effects of internal waves and dependency of sigma-t values on temperature and salinity. In the lower wave number side of the high wave number range, the perturbations of temperature and salinity may be generated by random internal waves, particularly in the upper layer where the density gradient is large. Spectra of temperature and salinity perturbations show a slope k^{-3} which represents a power spectrum of turbulence dominated by stratification

as discussed below. However, it is seen from smoothed profiles of temperature (Fig. 5) and salinity (Fig. 6) that both temperature and salinity decrease with depth below 200 m. Therefore when temperature and salinity perturbations are caused by internal waves, they contribute to the density change in opposite ways and thus the density perturbations are reduced from those caused by temperature or salinity change only. This may have happened in the lower wave number part of the high wave number range, whereas those in the higher wave number part may be caused mainly by turbulence and thus are dependent separately on temperature or salinity perturbations.

Slopes of temperature, salinity and sigma-t spectra are generally steeper in the upper layer than in the lower layer. This can be explained by a model on power spectrum of a passive scalor quantity in a field of turbulence with vertical stratification. Kolmogorov's model of turbulence in an inertial subrange can be generalized to a passive quantity s with stratification (buoyancy-subrange) (Ichiye, 1972; Phillips, 1968; Roden, 1971). Then the power spectrum of s is given by

$$S(k) = D N \varepsilon_c^{-1/3} \left\{ 1 + (k_f/k)^{4/3} \right\} k^{-5/3} \qquad (9)$$

where k is a wave number, D is a numerical constant, ε_c is the rate of viscous dissipation at a neutral stability, and N is the rate of dissipation of s by diffusivity and expressed by

$$N = 2\varkappa \overline{(\nabla s)^2} \qquad (10)$$

where $\varkappa$ is diffusivity and ∇s is vectorial gradient of s. The characteristic wave number k_f is dependent on Väisälä frequency N and ε_o and dimensional consideration yields

$$k_f = CN^{3/2} \varepsilon_o^{-1/2} \tag{11}$$

where C is a numerical constant. It is seen from equation (9) and (11) that the spectrum $S(k)$ behaves like $k^{-5/3}$ when N is small but like k^{-3} when N is large.

Since the value of constant C and ε_o are not determined definitely and also N varies with depth, it is of no use to fit theoretical curves from equation (9) to spectra determined in this work. However, this equation can explain steeper slopes against wave number of the upper layer spectra. The average Väisälä frequency N is about 7.6×10^{-3} sec^{-1} in the upper layer (0-600 m) but about 2.8×10^{-3} sec^{-1}, in the lower layer yielding the value of k_f in the upper layer larger by almost one order of magnitude than in the low layer.

In order to verify equations (9) and (11), it is more suitable to determine power spectra against horizontal wave numbers with a towed sensor at different depth, since in this way spectra with different values of N can be compared. It is also preferable to determine ε_c by measuring current fluctuations, although this is admittedly more difficult than to measure the spectra of passive quantities. Spectra against both horizontal and vertical wave numbers

should be used to determine geometrical structures of turbulence responsible for temperature, salinity and density microstructures, since turbulence may be highly anisotropic when internal waves have a dominant role.

6. Scattering of Sound by Microstructures

Tatarski (1961) derived the flux density vector $\vec{S}$ of waves which are generated by scattering of a plane wave with temperature irregularities in the ocean as

$$\vec{S} = \vec{m} \frac{\rho c k^6 A_o^2 V}{8\pi^2 r^2 T^2} \Phi_T (k(\vec{n} - \vec{m})) \tag{12}$$

where $\vec{n}$ and $\vec{m}$ are unit vectors in the direction of plane waves and scattered waves, respectively, k is the wave number of sound wave, ρ and c are water density and sound speed, respectively, A_o is the amplitude of the plane wave, r is the distance between the wave source and the receiver, V is the total volume of the scattering medium between the source and the receiver, and $\Phi_T(\vec{k})$ is spectrum of the temperature structure. Sound speed in the ocean $c(T)$ is expressed as a function of temperature T as

$$c(T) = c(\overline{T}, S, Z)\ (1 + T'/T_o) \tag{13}$$

where T_o is the reference temperature for sound speed, $T = \overline{T} + T'$ is the water temperature, $\overline{T}$ and T' are are the mean and perturbation temperature, respectively, S and Z are the mean salinity and depth, respectively.

In the temperature range 6 - 17°C, the empirical formula of Wood on the sound speed in the ocean is

$$c = 1410 + 4.21T - 0.037T^2 + 1.14S + 0.018Z \qquad (14)$$

where c = speed in m/sec, T = temperature in °C, S = salinity in ppt and Z = depth in m (Tucker and Gazey, 1966). For $T = 20°C$, $S = 36.5$ °/oo, $Z = 250$ m and for $T = 5°C$, $S = 35.0$ °/oo and $Z = 1000$ m, equation (14) gives $c = 1526$ and 1488 m/sec, respectively. When these two speeds are taken as the reference speed $c(\overline{T}, S, Z)$, then the reference temperature T_o becomes 362 (°K) and 353 (°K), respectively.

Equation (12) represents scattering by temperature irregularities only. There are other effects causing sound scattering. The effect of currents on sound scattering can be expressed in terms of $(u/c)^2$ in contrast to $(T'/T_o)^2$ of the scattering by temperature irregularities, where u is the current speed. Except in a strong current like the Gulf Stream, u is less than 1 m/sec, thus u/c is less than 1/1500. The ratio (T'/T_o) is of the order of 1/350 because the temperature perturbations T' is about 1°K from Fig. 8 and $T_o = 350°$ K as discussed before. The effect of salinity perturbations is about 1/40 of the temperature perturbations, since the salinity perturbations ΔS is about 0.2 °/oo from Fig. 9 and causes sound speed deviation of 0.2 m/sec whereas the temperature perturbation of 1°K causes 8 m/sec deviation. Therefore the energy flux of scattered waves can

be expressed by equation (12) within an error of 5% at the most.

Equation (12) is derived under an assumption that the temperature perturbations are homogeneous but may be either isotropic or anisotropic. In the ocean the temperature perturbation spectra are anisotropic except in a high wave number range which corresponds to the inertial subrange of turbulence. In such a range the local isotropicity may be valid and the wave number spectra is proportional to $k^{-5/3}$. As indicated in Section 5, the observed power spectra of temperature, salinity and sigma-t against the vertical wave number (k) are strongly influenced by stratification and are not generally proportional to $k^{-5/3}$ in a range of wave number lower than about 5×10^{2} cycles p km and they are deviated from this form particularly in the upper 600 m. Also the power of a spectrum increases as the wave number decreases further and does not decrease at least up to the wave number of 8 cycles p km as shown in Figs. 12, 14 and 16. Therefore the temperature spectrum Φ_T seems to be anisotropic in the real ocean.

In case of anisotropic spectra, Φ_T can be expressed by

$$\Phi_T [k(\vec{n} - \vec{m})] = \Phi_v (k_v) \Phi_h (k_h) \qquad (15)$$

where Φ_v and Φ_h are the vertical and horizontal spectral function, respectively, and k_v and k_h are the vertical and horizontal projection of the vector $k(\vec{n} - \vec{m})$, respectively. In this expression the horizontal isotropy is assumed.

The effective cross section for scattering $d\sigma$ is defined as the ratio of acoustic power scattered into a solid angle $d\Omega$ to the power flux of the incident wave in the same angle and is expressed by

$$d\sigma = \frac{2\pi k^4 V}{T_o^2} \Phi_v(k_v)\, \Phi_h(k_h) \tag{16}$$

In order to express k_v and k_h in terms of k and relative directions of $\vec{n}$ and $\vec{m}$, the x, y, z coordinate system is taken with the x-axis parallel to $\vec{n}$ and with z-axis in the plane consisting of $\vec{n}$ and the vertical unit vector $\vec{j}$ (Fig. 17). The unit vectors $\vec{j}$ and $\vec{m}$ can be expressed in this coordinate system as

$$\vec{j} = (\sin\theta_0,\ 0,\ \cos\theta_0) \tag{17}$$

$$\vec{m} = (\sin\theta\cos\phi,\ \sin\theta\sin\phi,\ \cos\theta) \tag{18}$$

Then k_v projection of $k(\vec{m} - \vec{n})$ on the vertical direction can be given by

$$k_v = k\left[\sin\theta_0 \sin\theta\cos\phi + \cos\theta_0\,(\cos\theta - 1)\right] \tag{19}$$

The horizontal wave number k_h is projection of $k(\vec{m} - \vec{n})$ on the horizontal plane and is given by

$$k_h = k\left[2(1-\cos\theta) - \left\{\sin\theta_0 \sin\theta\sin\phi + \cos\theta_0(\cos\theta - 1)\right\}^2\right]^{\frac{1}{2}} \tag{20}$$

The effective cross section (16) can be computed for any direction of $\vec{m}$ by using (19) or (20) as an argument of the spectral function $\Phi_v(k_v)$ or $\Phi_h(k_h)$, respectively.

Equations (19) and (20) become simpler when the incident plane wave propagates in a horizontal plane. Then $\theta_0 = 0$ and

$$k_v = k(1 - \cos\theta) \tag{21}$$

and

$$k_h = k \sin^2\theta \tag{22}$$

Thus the effective cross section depends only on θ, the angle of scattering direction from the vertical. Since the right hand sides of (21) and (22) are symmetrical about $\theta = \pi/2$, the effective cross section is symmetrical about the horizontal plane, as it should be. When $\Phi_v \sim (k_v)^m$ and $\Phi_h \sim (k_h)^n$, equation (16) can be expressed by

$$d\sigma \sim k^{4+m+n} \sin^{2m}(\theta/2) \sin^{2n}\theta \tag{23}$$

For instance, the spectra of temperature perturbations yields $m = n = -3$ when stratification has a strong effect. Then $d\sigma$ is proportional to k^{-2}. When dependency of $d\sigma$ both on the azimuth angle θ and on the wave number is known by experiments, the values of m and n can be determined. Therefore data on sound scattering can be used to determine spectra of

temperature perturbations.

Ocean microstructures have other effects on sound propagation than scattering. Particularly they change amplitudes and phases of sound waves propagating in the deep sound (SOFAR) channel for a long distance (Brekhovskikh, 1968). Long range sound propagation is affected more by temperature and salinity perturbations with scales larger than those now usually defined as microstructures. The latter designates temperature or salinity perturbations within one meter in the vertical direction, though in this report "microstructure" is used as a synonym to perturbation.

There are two approaches to study theoretically effects on long range propagation in a sound channel. One is the W.K.B. method or geometrical optics method (Tatarski, 1961; Tolstoy and Clay, 1966). In this approach, the phase change due to the perturbations can be determined as line integral of sound speed perturbation along the path determined by geometrical optics for the mean field. The amplitude change can be computed as interaction among elementary waves of randomly different phases. The second approach is to determine perturbations of normal modes due to random perturbations in the vertical distributions of the sound speed (Tolstoy and Clay, 1966; Boyce, 1968; Brekhovskikh, 1968). This approach is more complicated mathematically, since random eigen functions must be determined.

These two approaches will be useful to interpret results from any long range sound propagation experiment in the future. As demonstrated in scattering problems treated above, sound propagation in the ocean is influenced not only by vertical structures but also horizontal distributions

of temperature and salinity perturbations. Therefore it will be necessary to determine horizontal wave number spectra of the perturbations by measuring temperature and salinity possibly with towed sensors.

7. Concluding Remarks

Although this study is of a preliminary nature, some interesting features of ocean microstructure (or perturbations) of temperature, salinity and density are determined by analyzing STD data in the Cayman Sea. Amplitudes of perturbations of these quantities are vertically distributed as almost proportional to the vertical gradient of smoothed values of corresponding quantities. The power spectra of these perturbations against vertical wave number k are rather proportional to k^{-3} of the buoyancy-subrange than to $k^{-5/3}$ of the inertial subrange of turbulence particularly in the upper 600 m. Further, the spectra in the upper 600 m have steeper slope about k and have powers larger by an order of magnitude than those in the lower 600 m. It is suggested theoretically that horizontal distributions of the perturbations and their spectra about horizontal wave number are important to determine scattering and amplitudes and phases change of sound waves propagating in a sound channel.

Acknowledgement:

Technicians and crew were very helpful during cruise 72-A-8. T. Sellers participated in the cruise, reduced data including STD data and prepared a program to obtain corrected temperature-salinity data from magnetic tapes. M. Carnes made spectral analysis and prepared the whole data printouts with a computer. The author is supported partly by a contract with Office of Naval Research N00014-68-A-0308(0002) and by a grant from the National Science Foundation GA-26498.

References

Boyce, W. E. (1968) Random eigen value probelms. Probabilistic Methods in Applied Mathematics (Edited by A. T. Bharucha-Reid) Vol. 1, Academic Press, 1-73.

Brekhovskikh, L. M. (1968) Some problems of oceanic acoustics. Izvestia, Atmospheric & Oceanic Phys. 4, English Translation, 739-746.

Cooper, J. W. and H. Stommel (1968) Regularly spaced steps in the main thermocline near Bermuda. J. Geophys. Res. 73(10), 5849-5854.

Frisch, U. (1968) Wave propagation in random media. Probabilistic Methods in Applied Mathematics (Edited by A. T. Bharucha-Reid) Vol. 1, Academic Press, 75-197.

Holloway Jr., J. L. (1958) Smoothing and filtering of time series and space fields. Advances in Geophysics (Edited by H. E. Landsberg and J. van Mieghem) Vol. 4, Academic Press, 351-391.

Ichiye, T. (1972) Power spectra of temperature and salinity fluctuations in the slope water off Cape Hatteras. Pure & Appl. Geophys. (PAGEOPH) 96, 205-216.

Ichiye, T. (1973) Ocean microstructure due to instability for different heat-salt diffusivity. Mémoire Société Royale des Sciences de Liège. 6th Ser., Vol. 4, 69-80.

Ichiye, T. and H. Sudo (1971) Mixing processes between shelf and deep sea waters off the Texas coast. Texas A&M Univ. Dept. of Oceanogr. Ref. 71-19-T (unpublished).

Phillisps, O. M. (1966) The Dynamics of the Upper Ocean. Cambridge Univ. Press, pp 261.

Roden, G. I. (1971) Spectra of North Pacific temperature and salinity perturbations in the depth domain. J. Phys. Oceanog. 1, 25-33.

Tait, R. I. and M. R. Howe (1968) Some observations of thermocline stratification in the deep ocean. Deep-Sea Res. 15, 275-280.

Tatarski, V. I. (1961) Wave Propagation in a Turbulent Medium. (Translated by R. A. Silverman) McGraw-Hill, 81-90, pp 285.

Tolstoy, I. and C. S. Clay (1966) Ocean Acoustics. McGraw-Hill, 222-232, pp 292.

Tucker and Gazey (1966) Applied Underwater Acoustics. Pergamon Press, 13-14, pp 244.

Weyl, P. K. (1964) On the change in electrical conductance of seawater with temperature. Limn. & Oceanog. 9, 75-78.

Worthington, L. V. (1966) Recent measurements in the Caribbean Sea. Deep-Sea Res. 13, 731-739.

Wüst, G. (1963) Stratification and circulation in the Antillean-Caribbean basins. Deep-Sea Res. 10, 165-187.

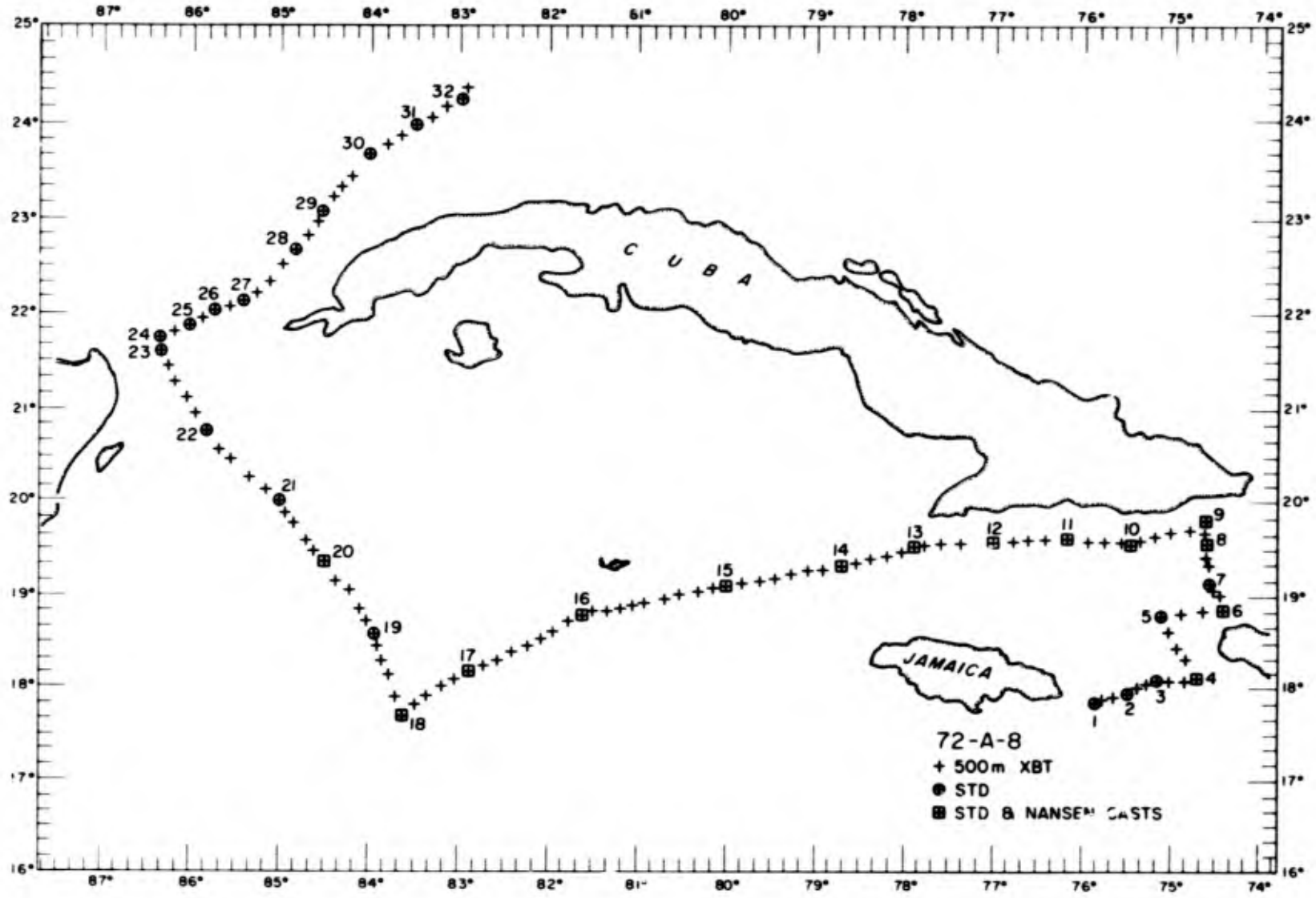

FIG. 1. Locations of XBT, STD and Nansen cast stations during Cruise 72-A-8.

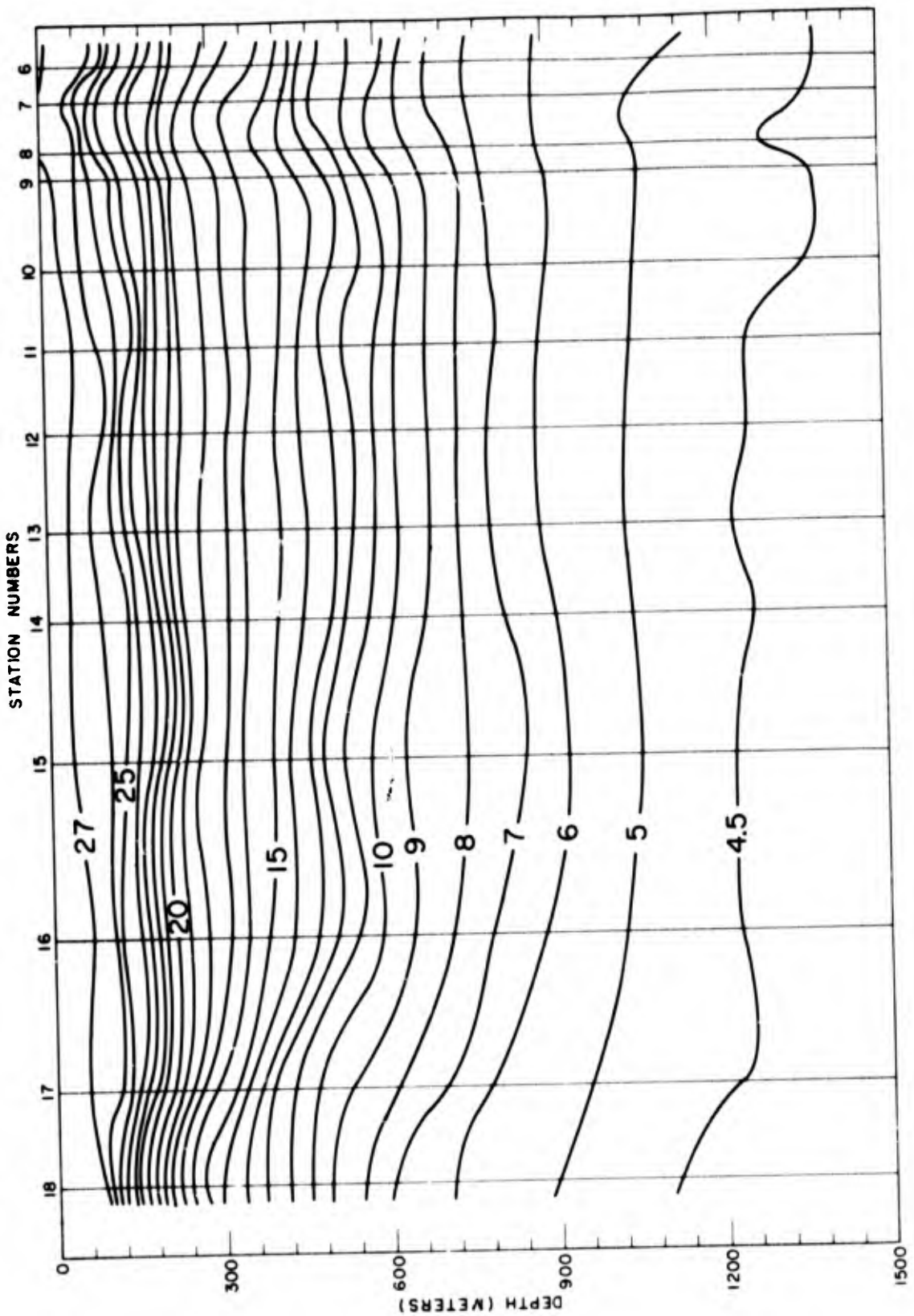

FIG. 2. Vertical section of temperature (°C).

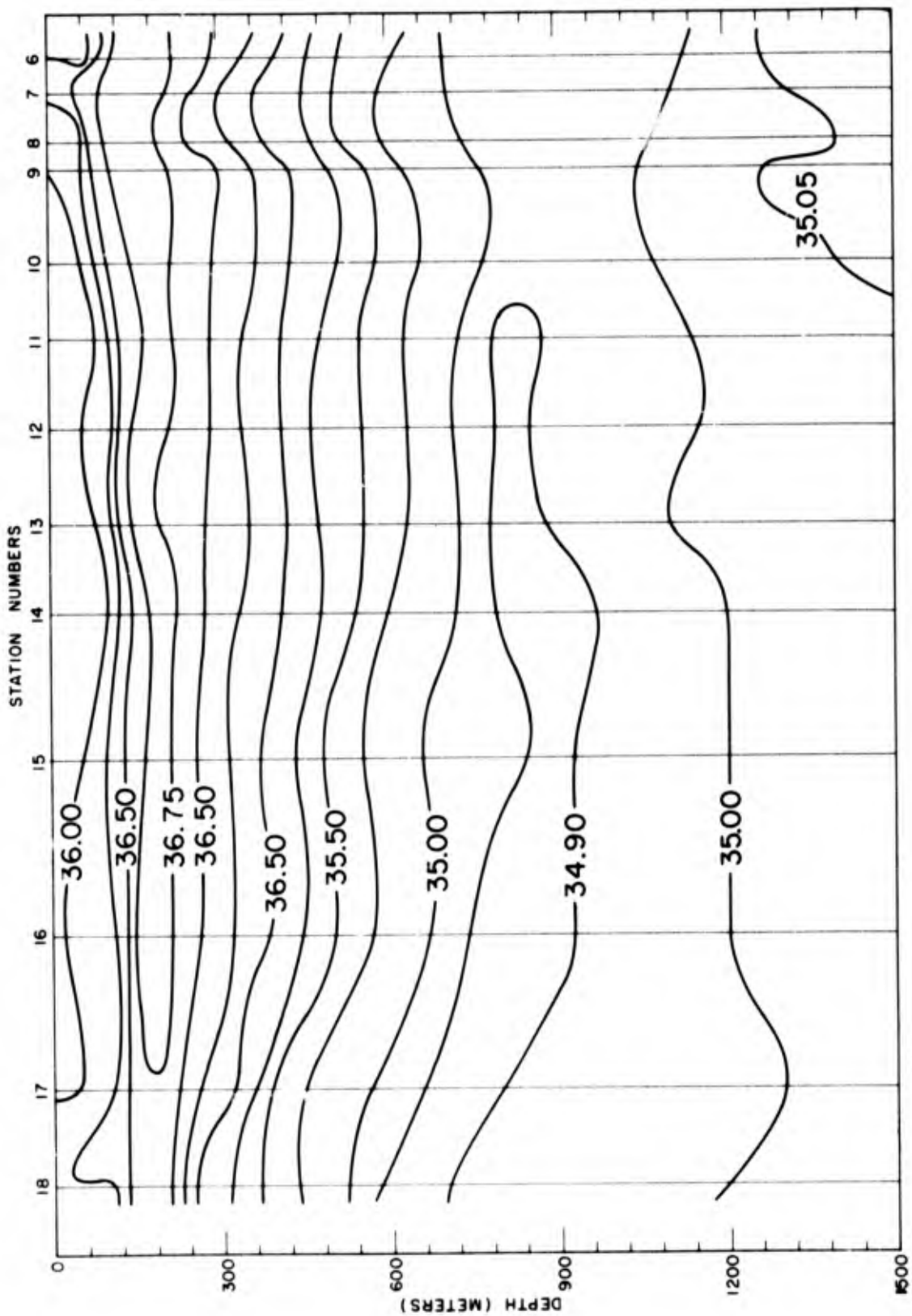

FIG. 3. Vertical section of salinity ($^{o}/_{oo}$).

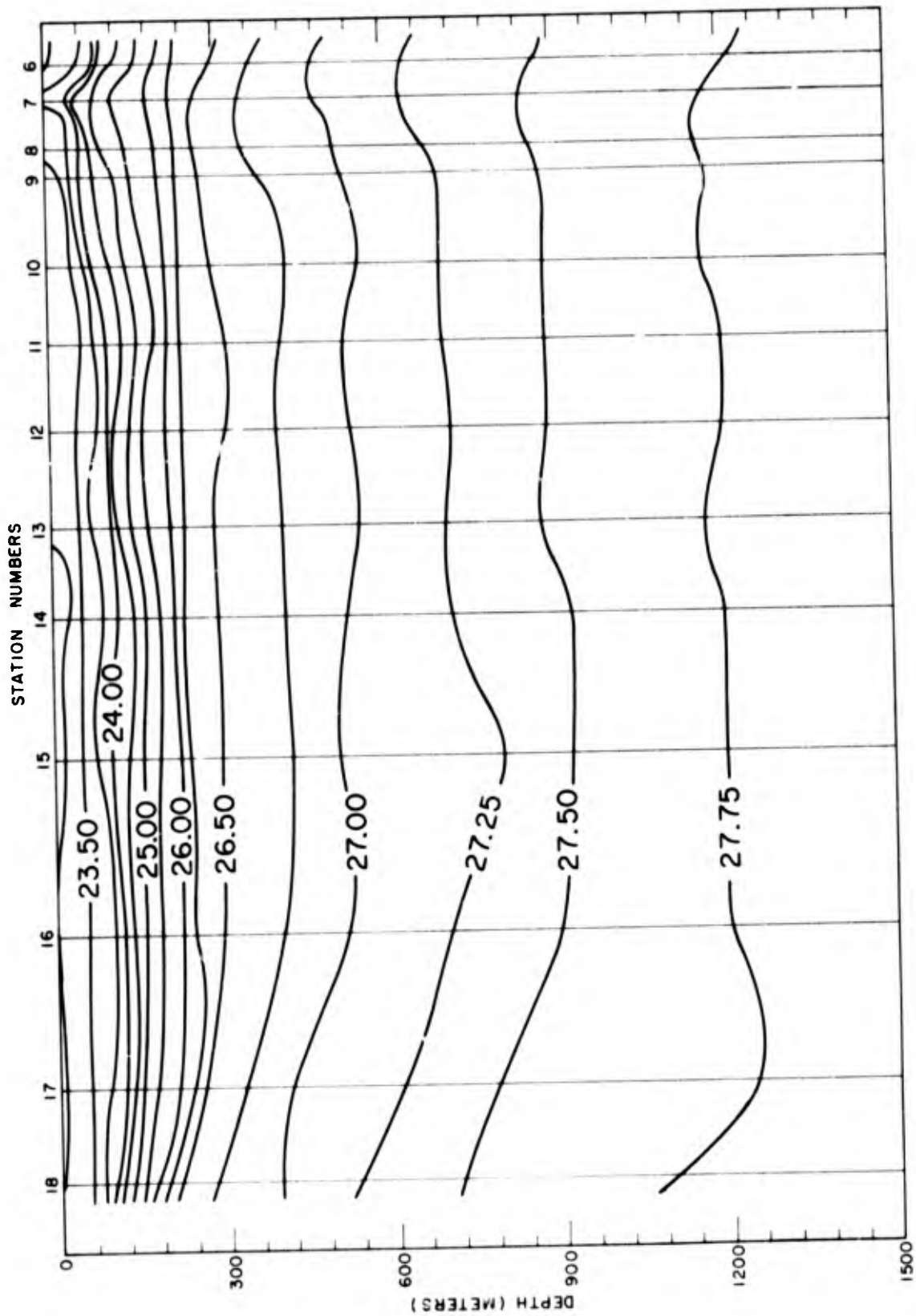

FIG. 4. Vertical section of sigma-t (10^3 gcm^{-3}).

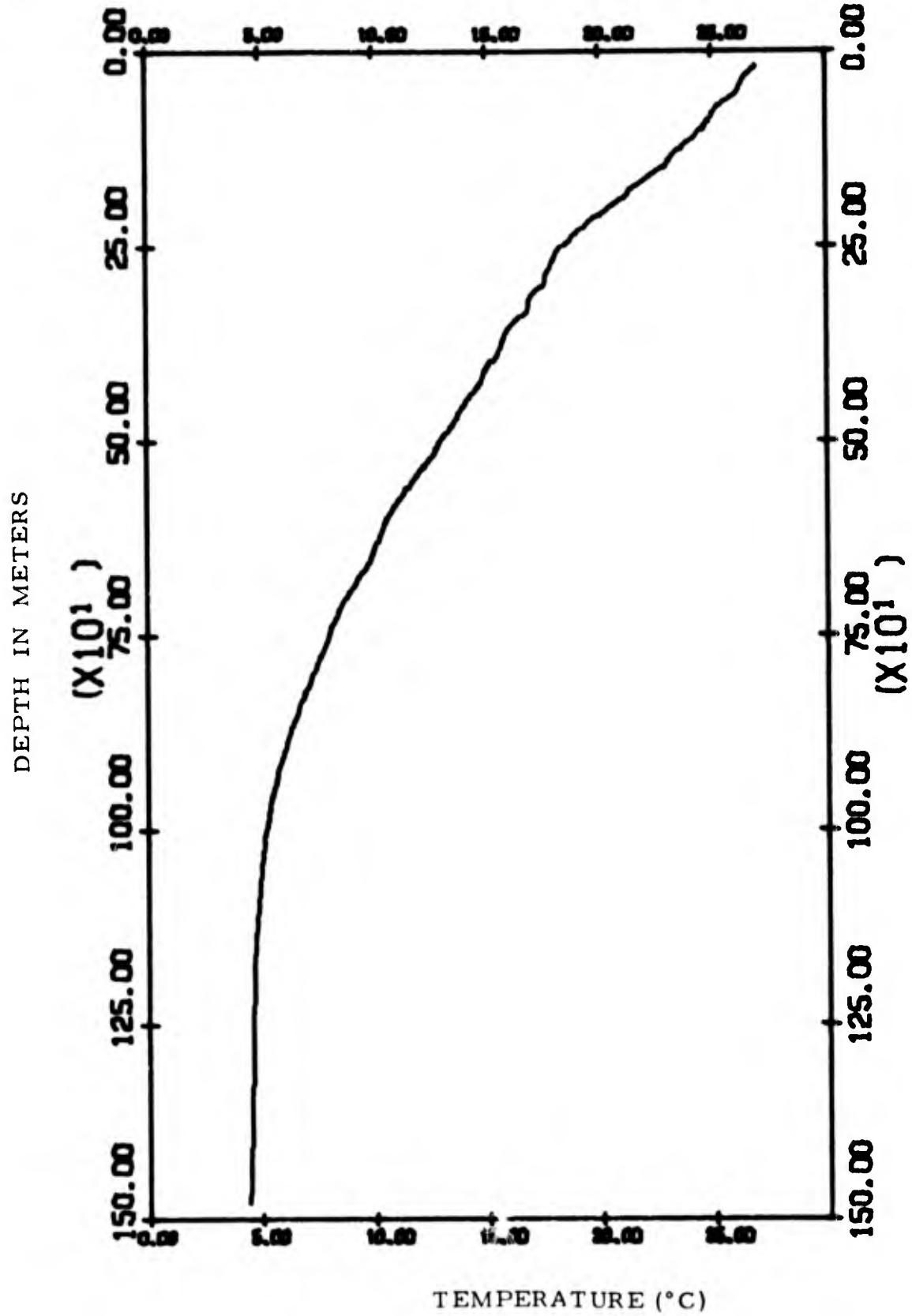

FIG. 5-1. Smoothed profile of temperature versus depth obtained by binomial filtering.
Station 9.

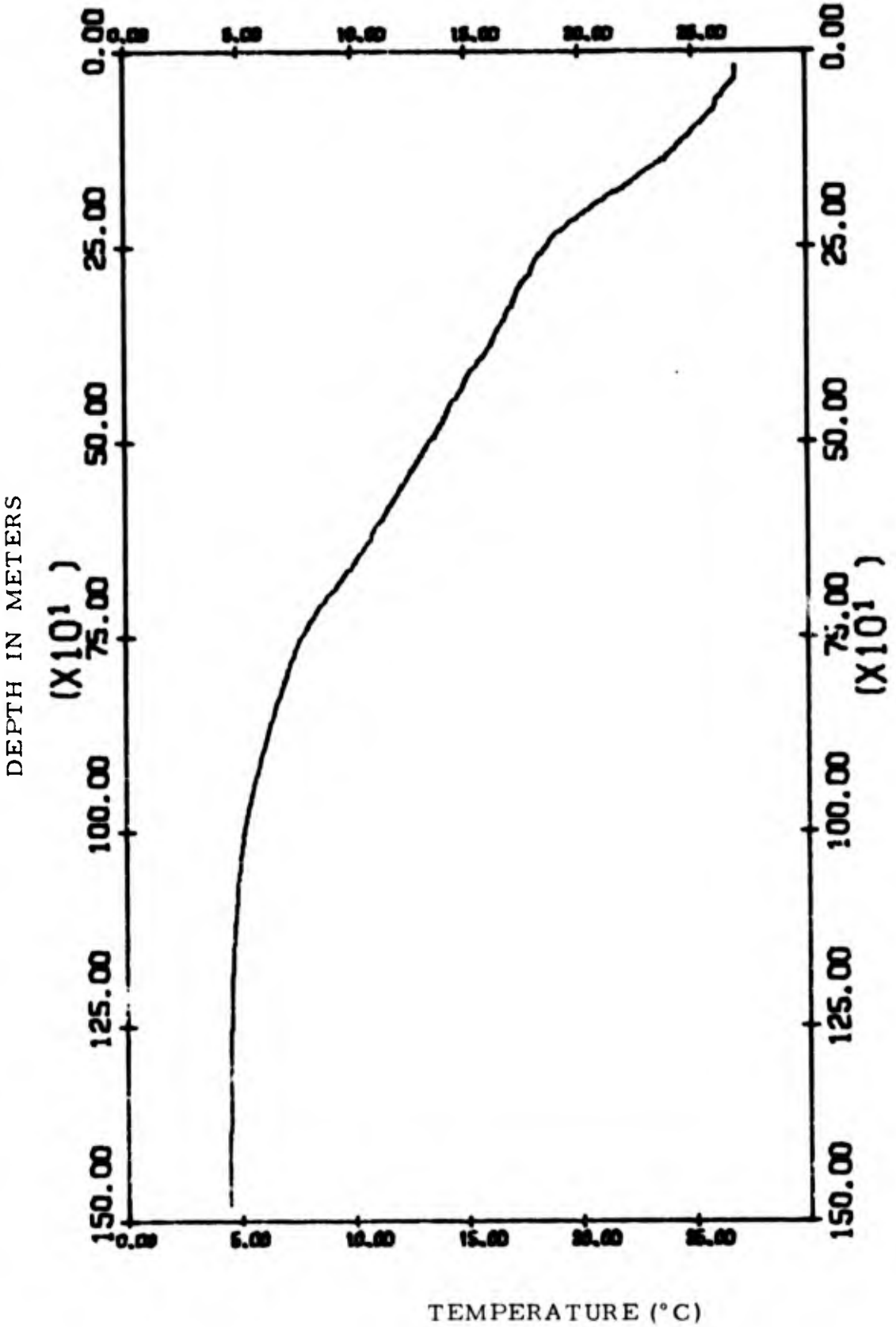

FIG. 5-2. Smoothed profile of temperature versus depth obtained by binomial filtering.
Station 10.

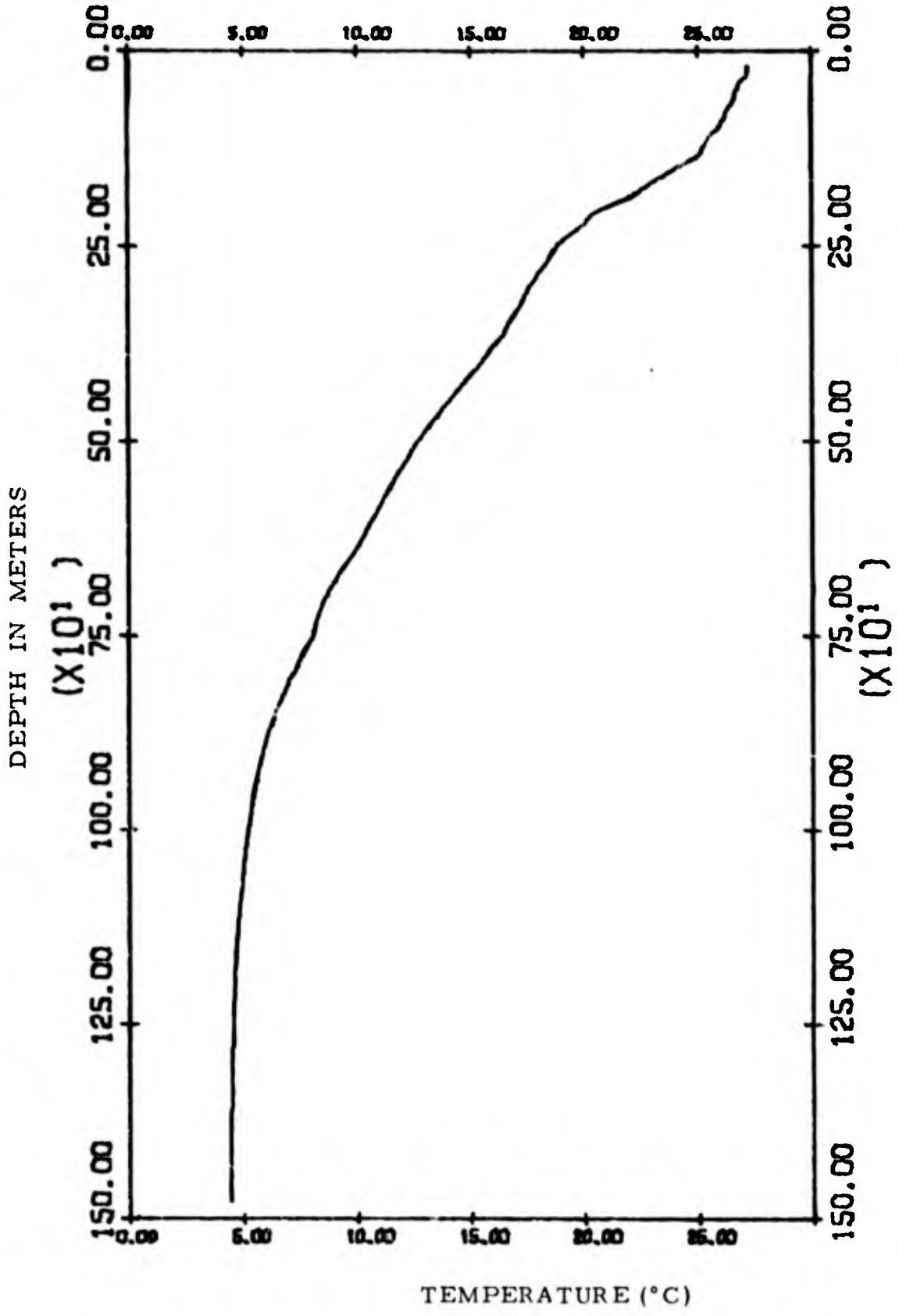

FIG. 5-3. Smoothed profile of temperature versus depth obtained by binomial filtering.
Station 11.

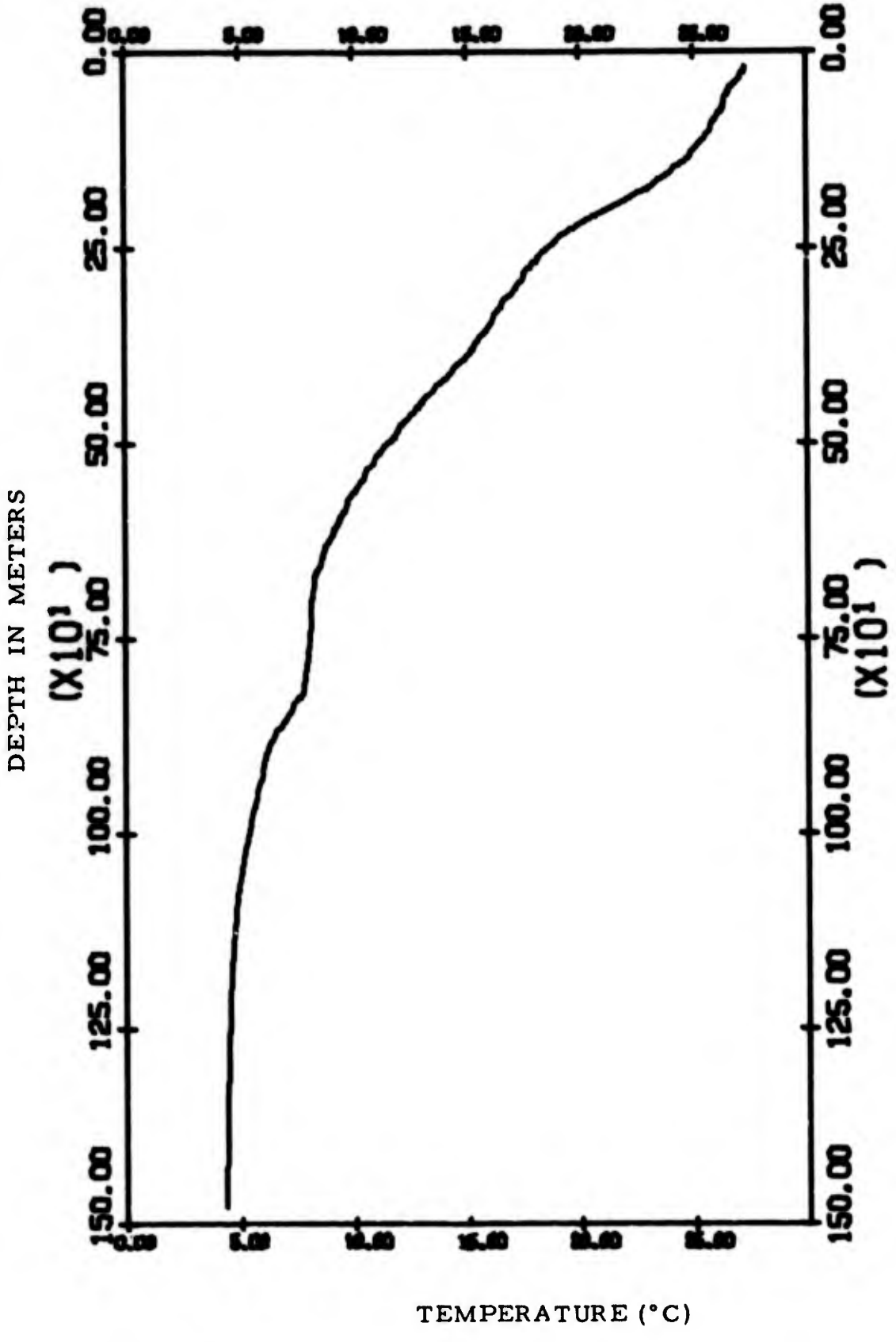

FIG. 5-4. Smoothed profile of temperature versus depth obtained by binomial filtering.
Station 15.

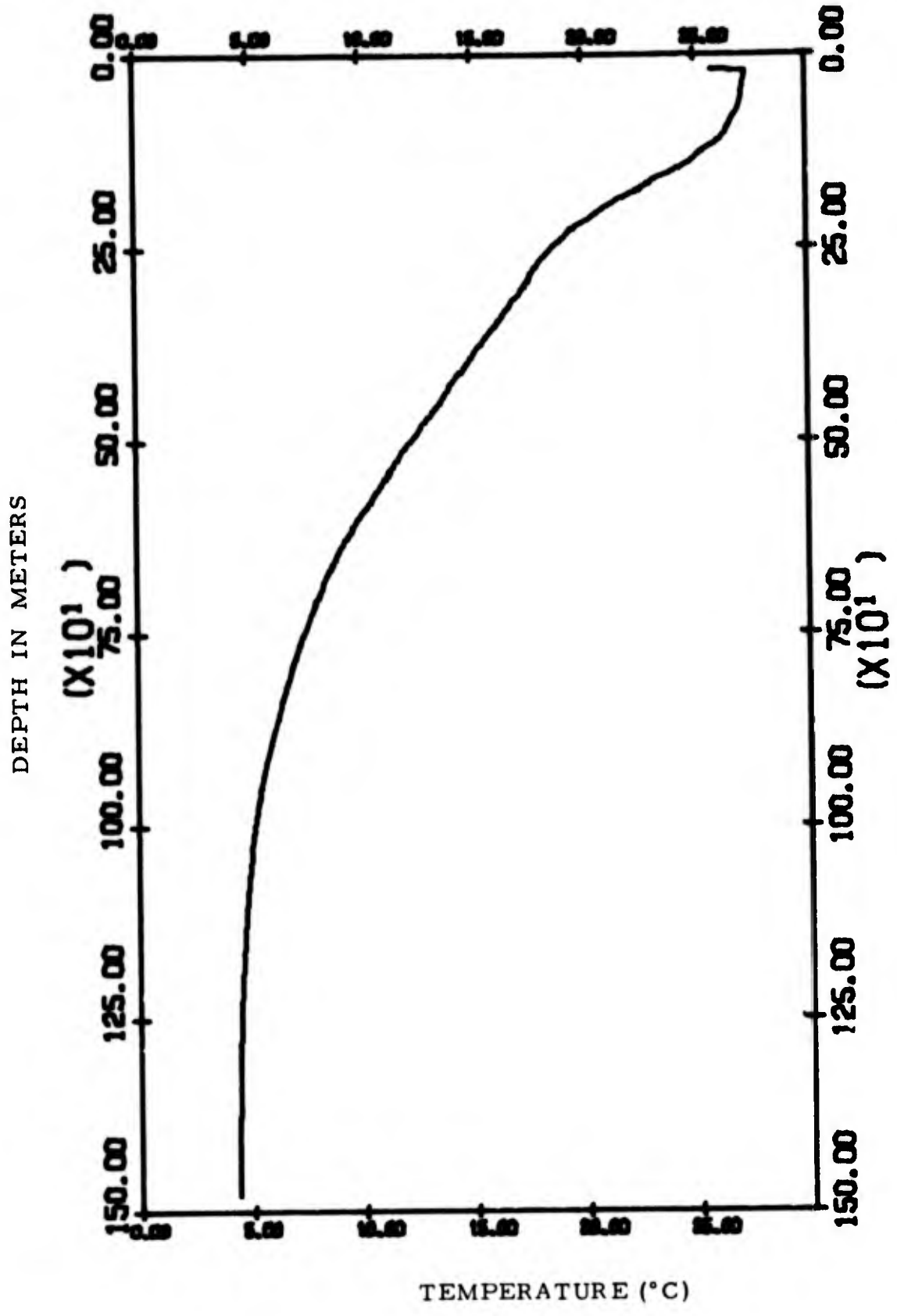

FIG. 5-5. Smoothed profile of temperature versus depth obtained by binomial filtering.
Station 16.

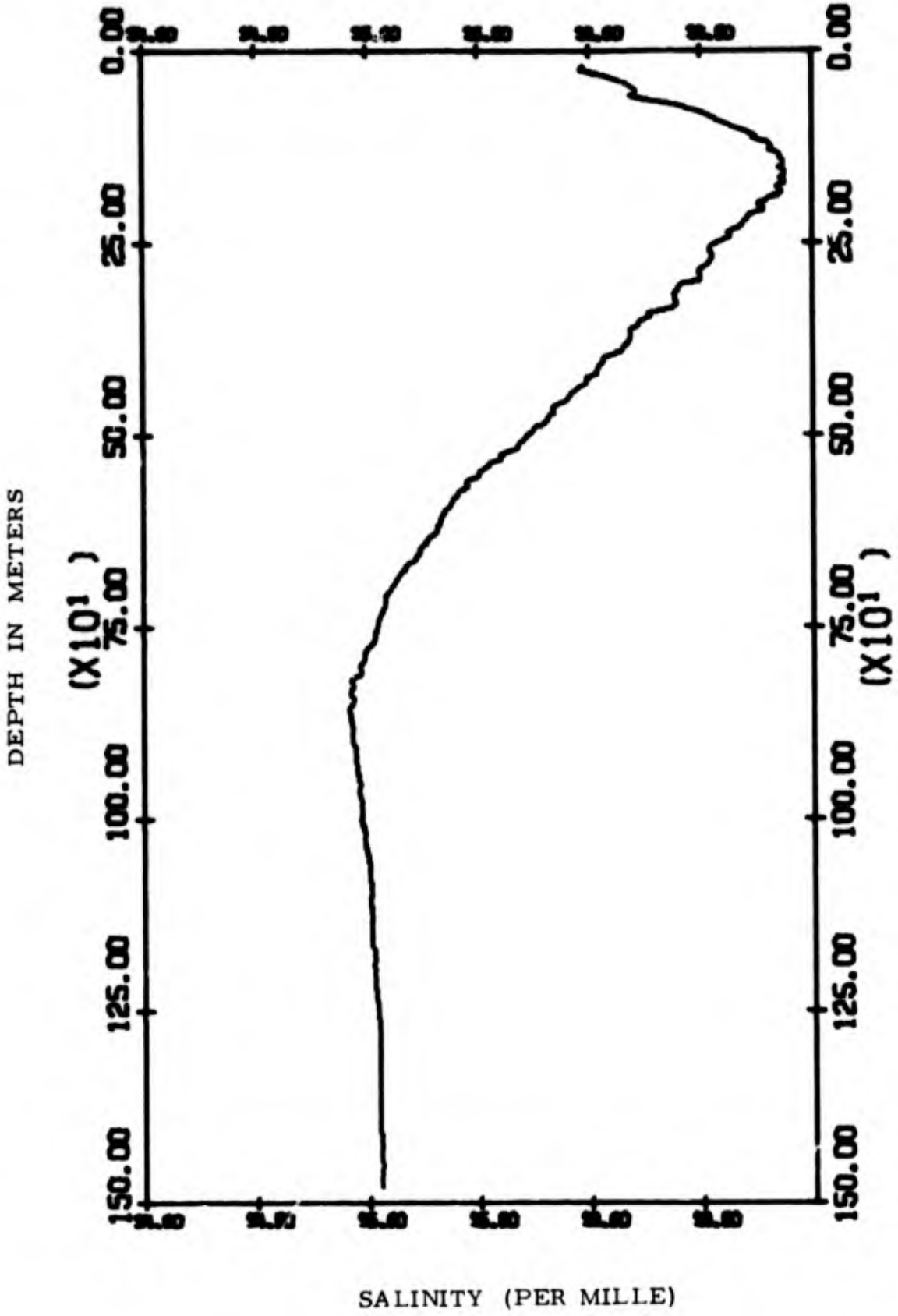

FIG. 6-1. Smoothed profile of salinity versus depth obtained by binomial filtering.
Station 9.

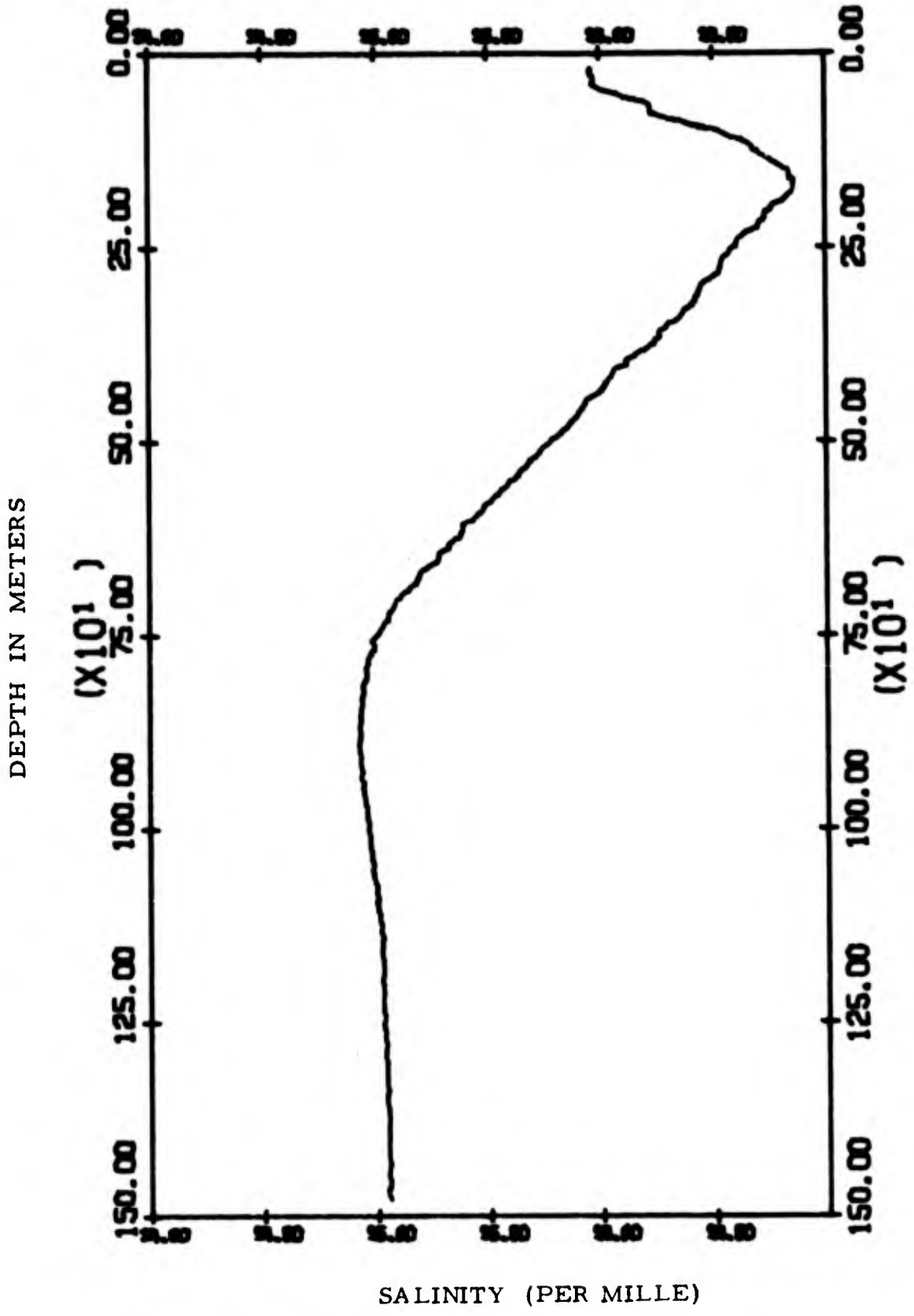

FIG. 6-2. Smoothed profile of salinity versus depth obtained by binomial filtering.
Station 10.

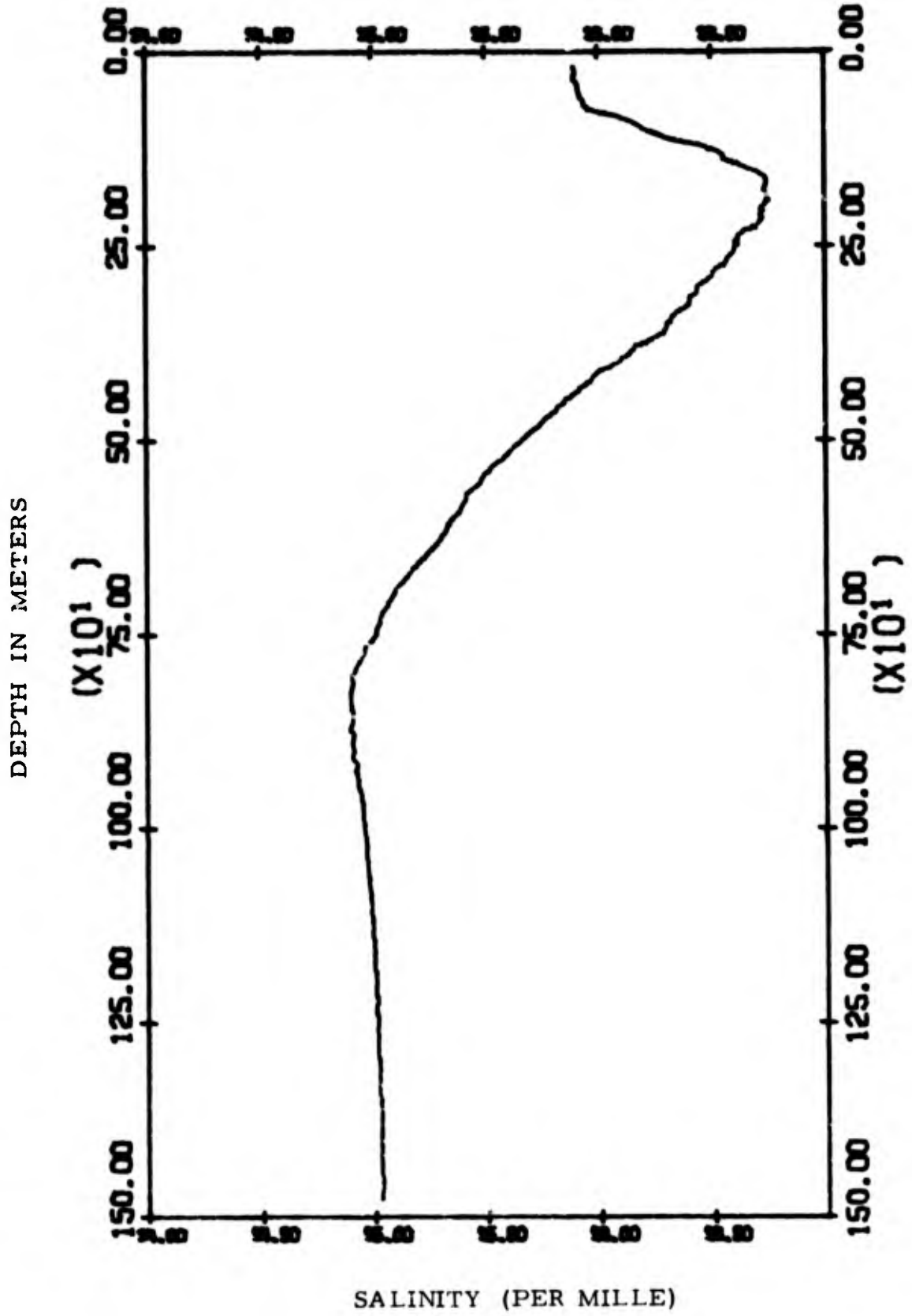

FIG. 6-3. Smoothed profile of salinity versus depth obtained by binomial filtering.
Station 11.

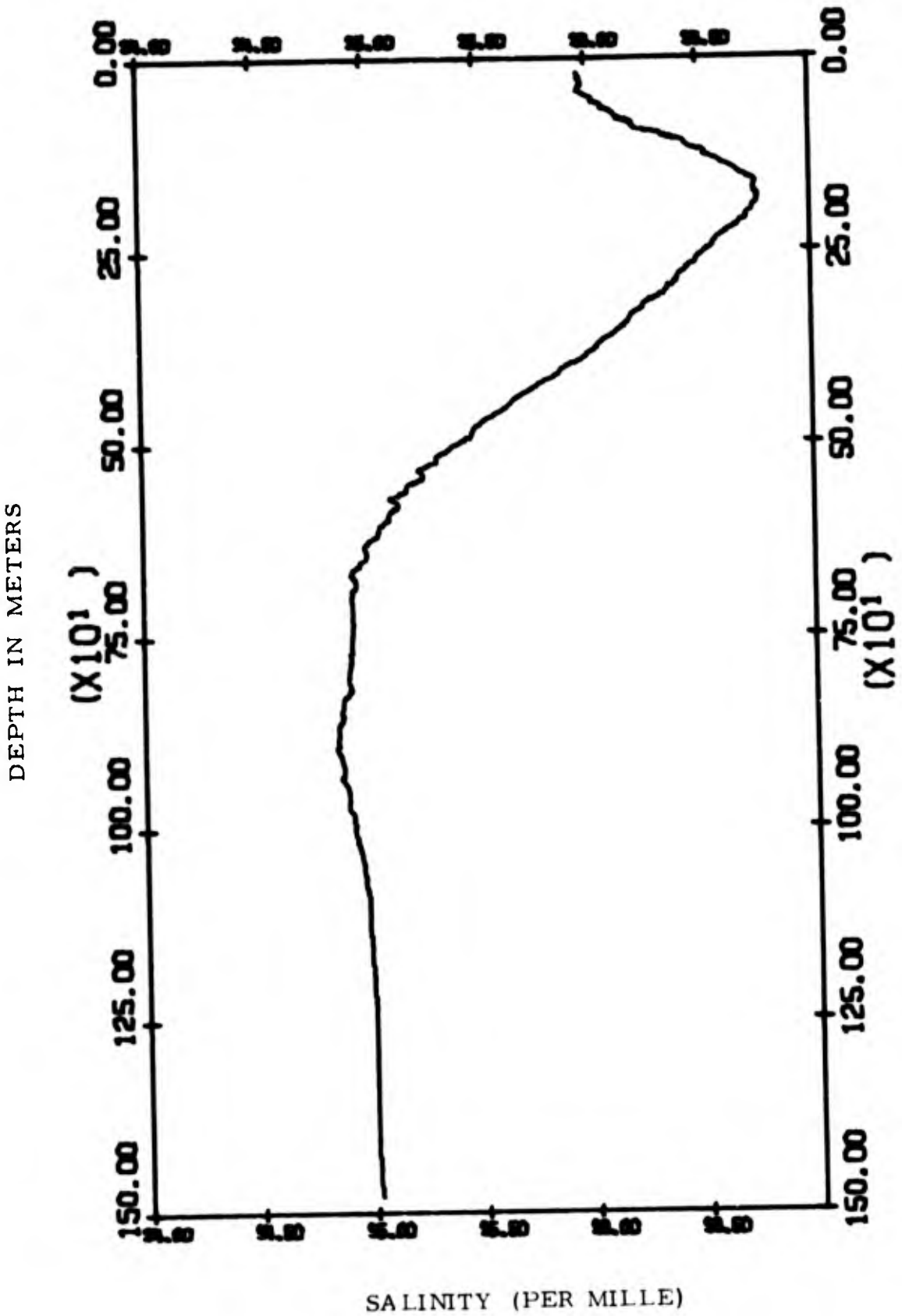

FIG. 6-4. Smoothed profile of salinity versus depth obtained by binomial filtering.
Station 15.

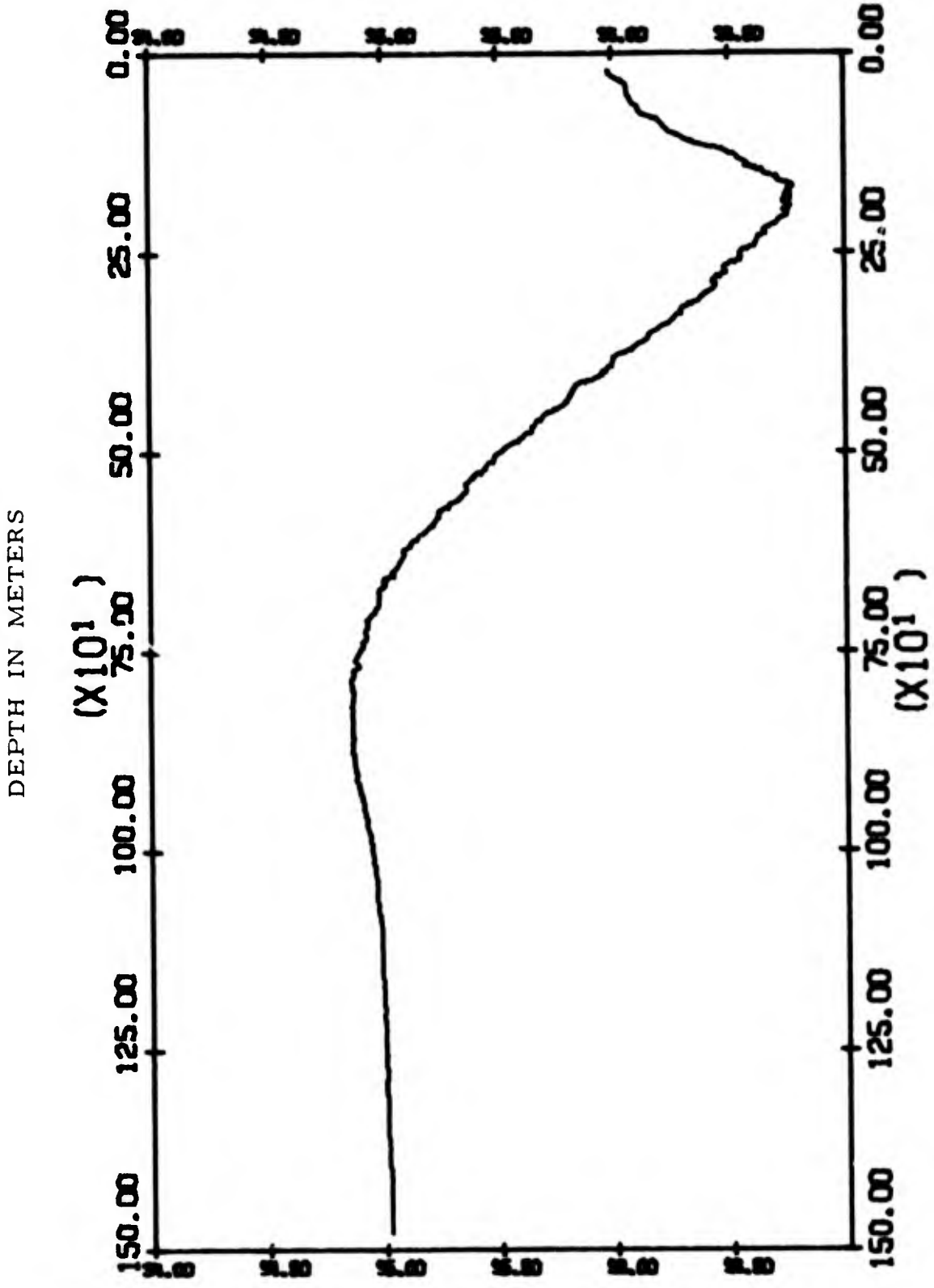

FIG. 6-5. Smoothed profile of salinity versus depth obtained by binomial filtering.
Station 16.

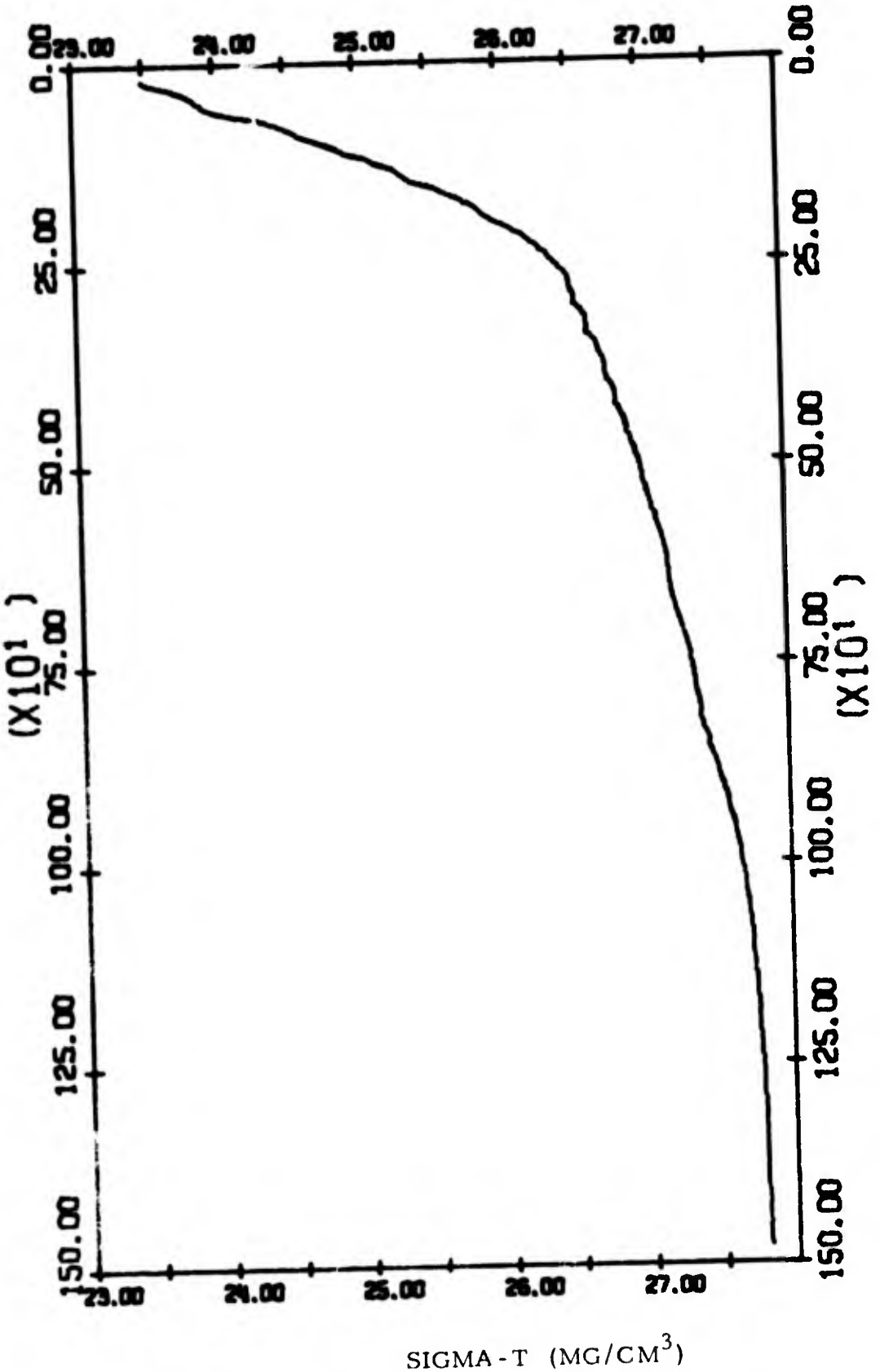

FIG. 7-1. Smoothed profile of sigma-t versus depth obtained by binomial filtering.
Station 9.

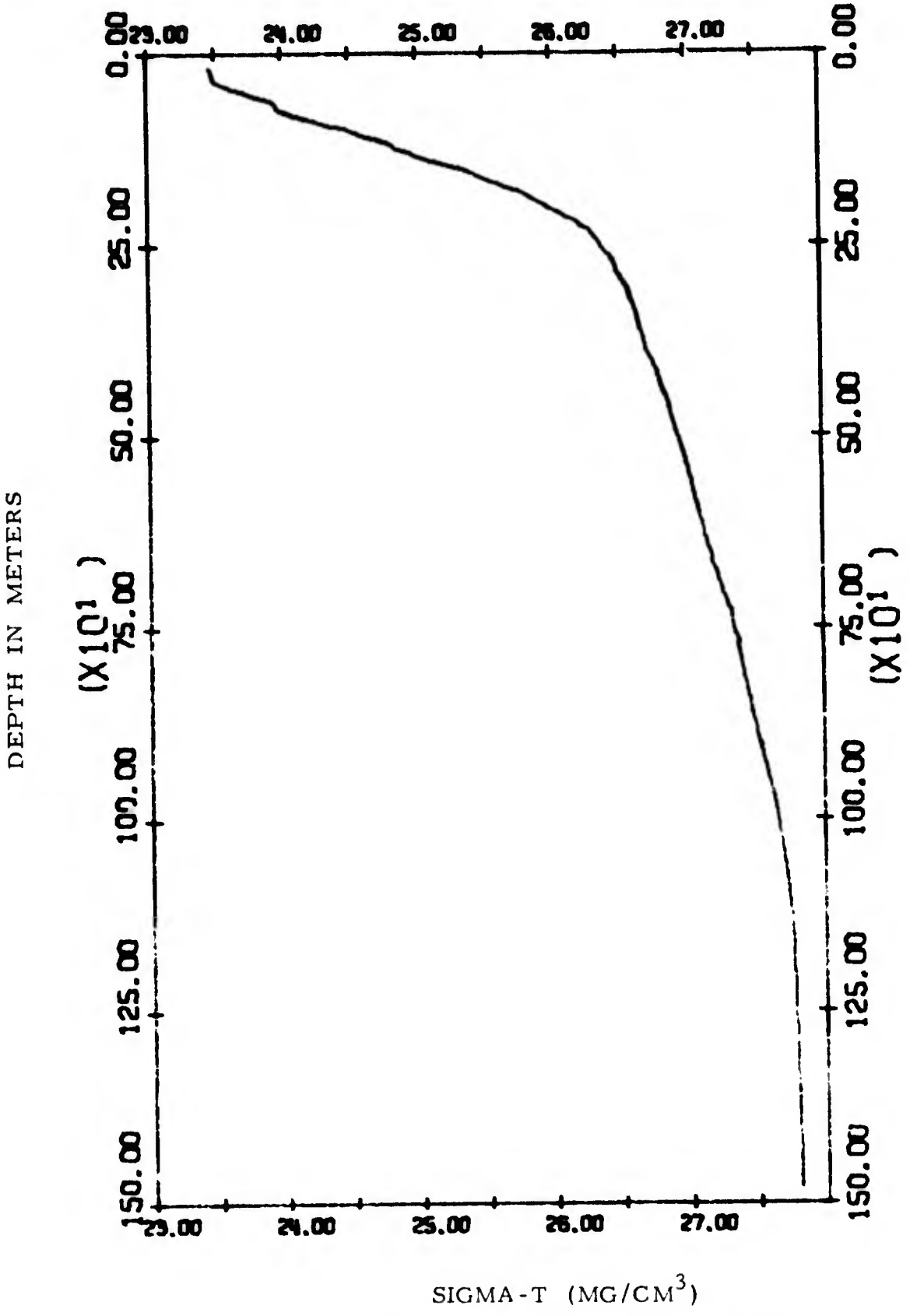

FIG. 7-2. Smoothed profile of sigma-t versus depth obtained by binomial filtering.
Station 10.

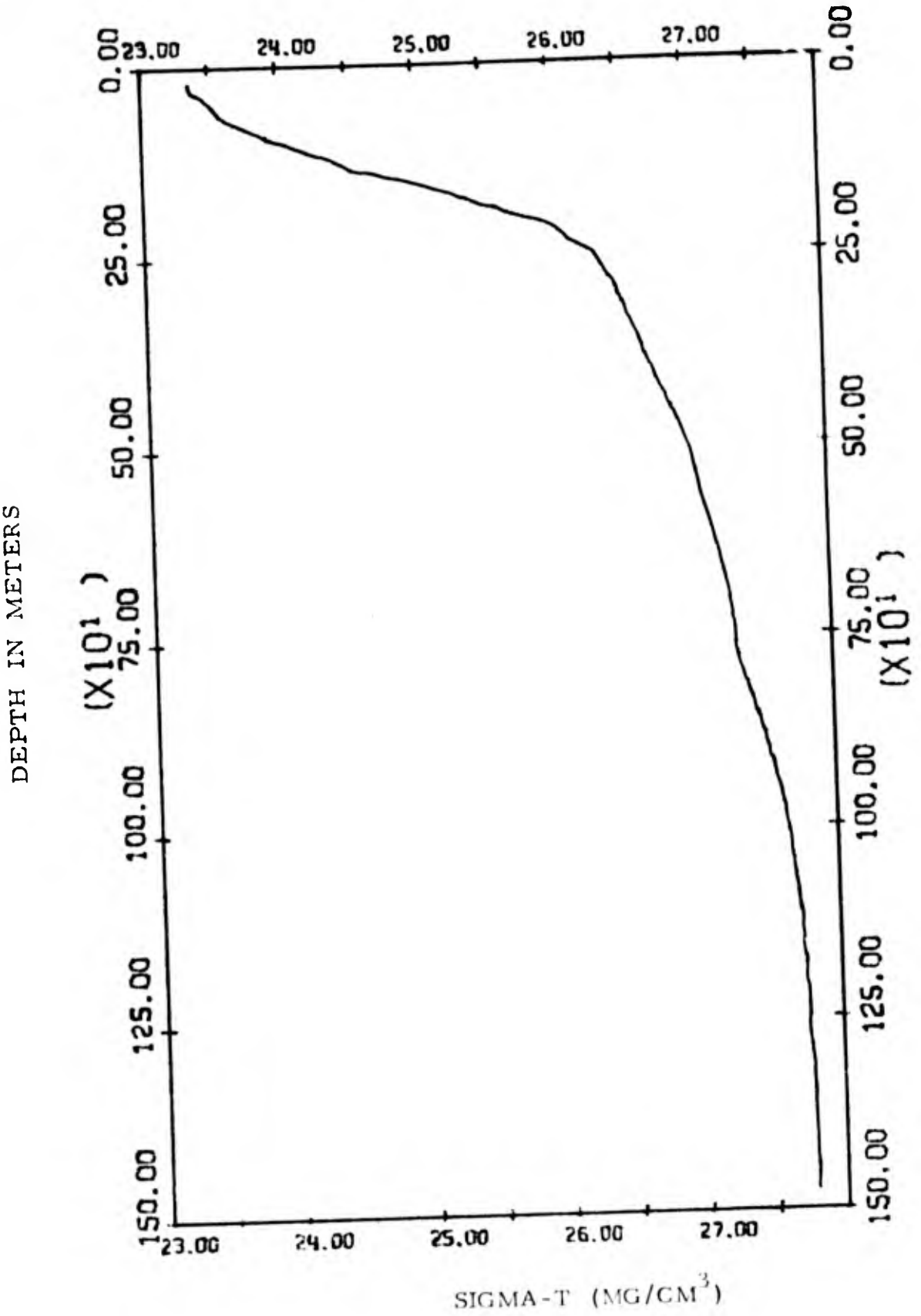

FIG. 7-3. Smoothed profile of sigma-T versus depth obtained by binomial filtering.
Station 11.

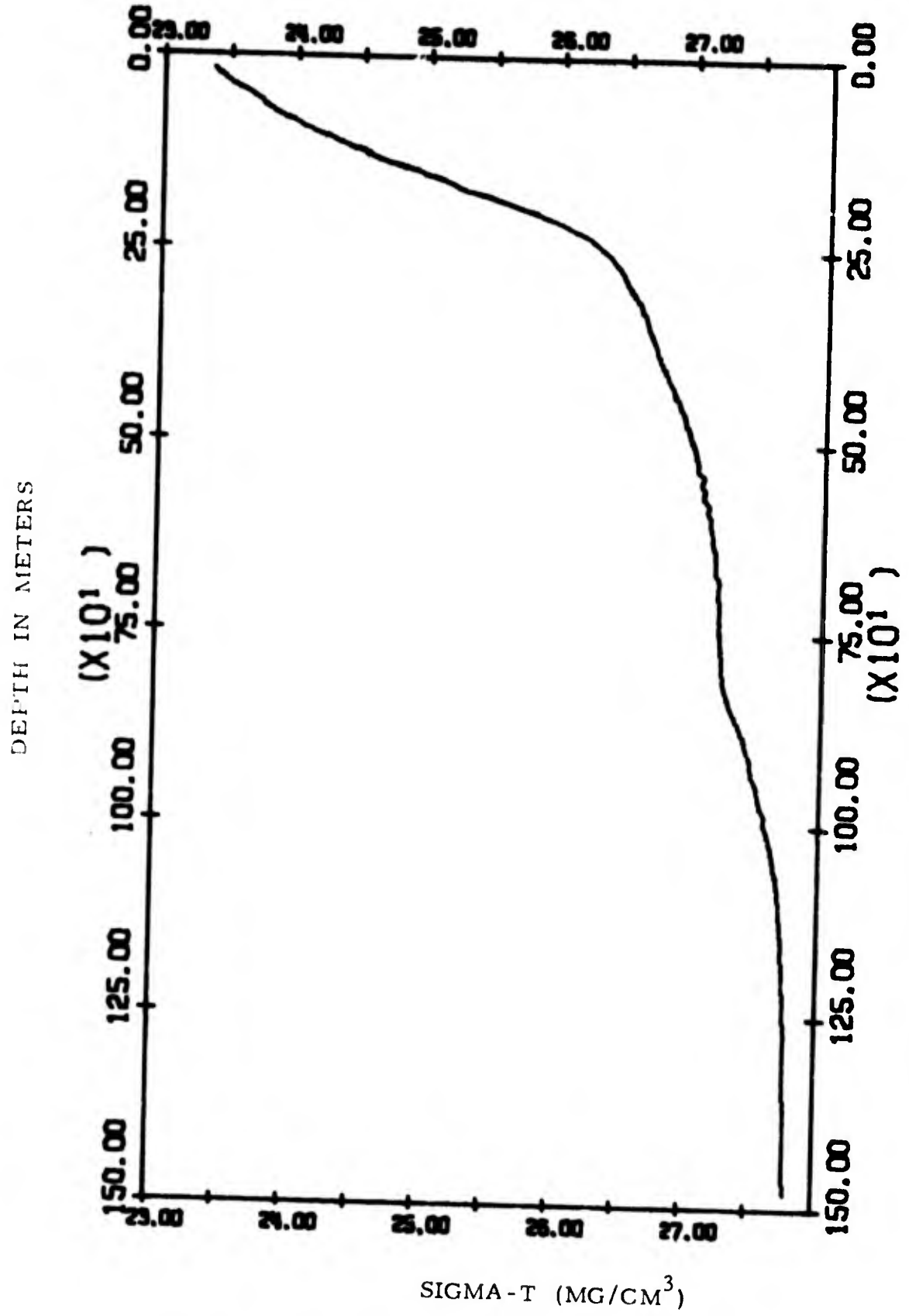

FIG. 7-4. Smoothed profile of sigma-t versus depth obtained by binomial filtering.
Station 15.

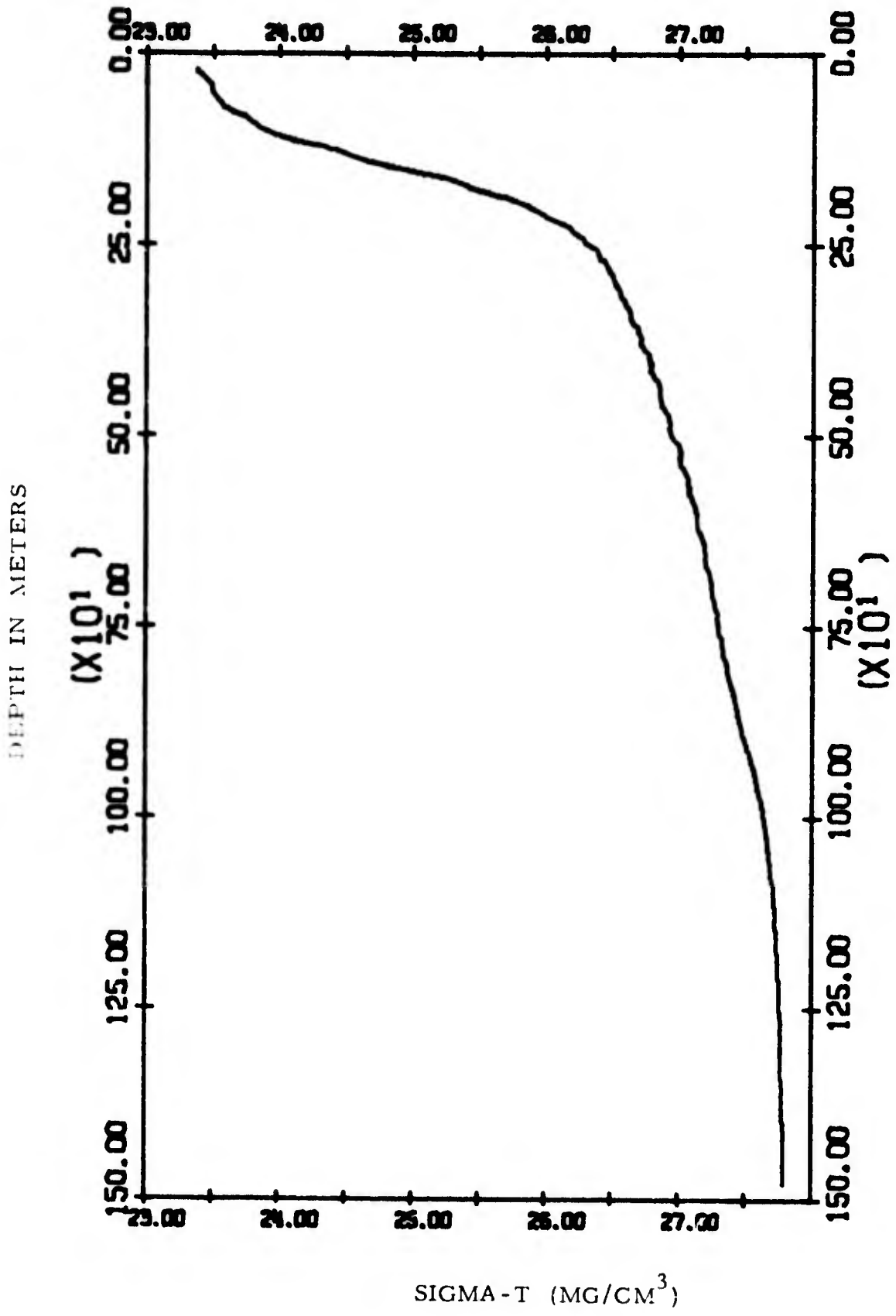

FIG. 7-5. Smoothed profile of sigma-t versus depth obtained by binomial filtering.
Station 16.

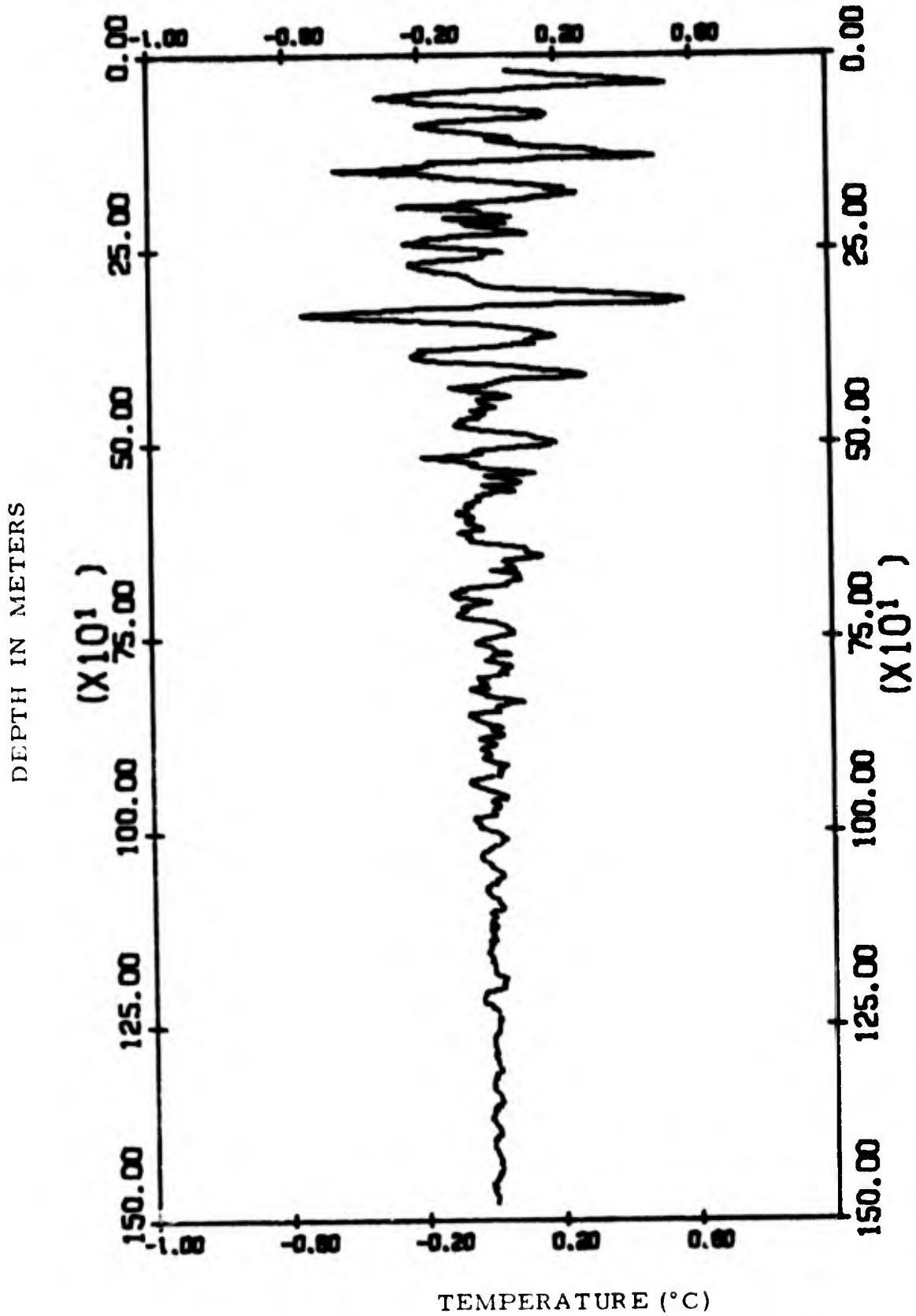

FIG. 8-1. Temperature perturbations from the mean as a function of depth obtained by binomial filtering. Station 9.

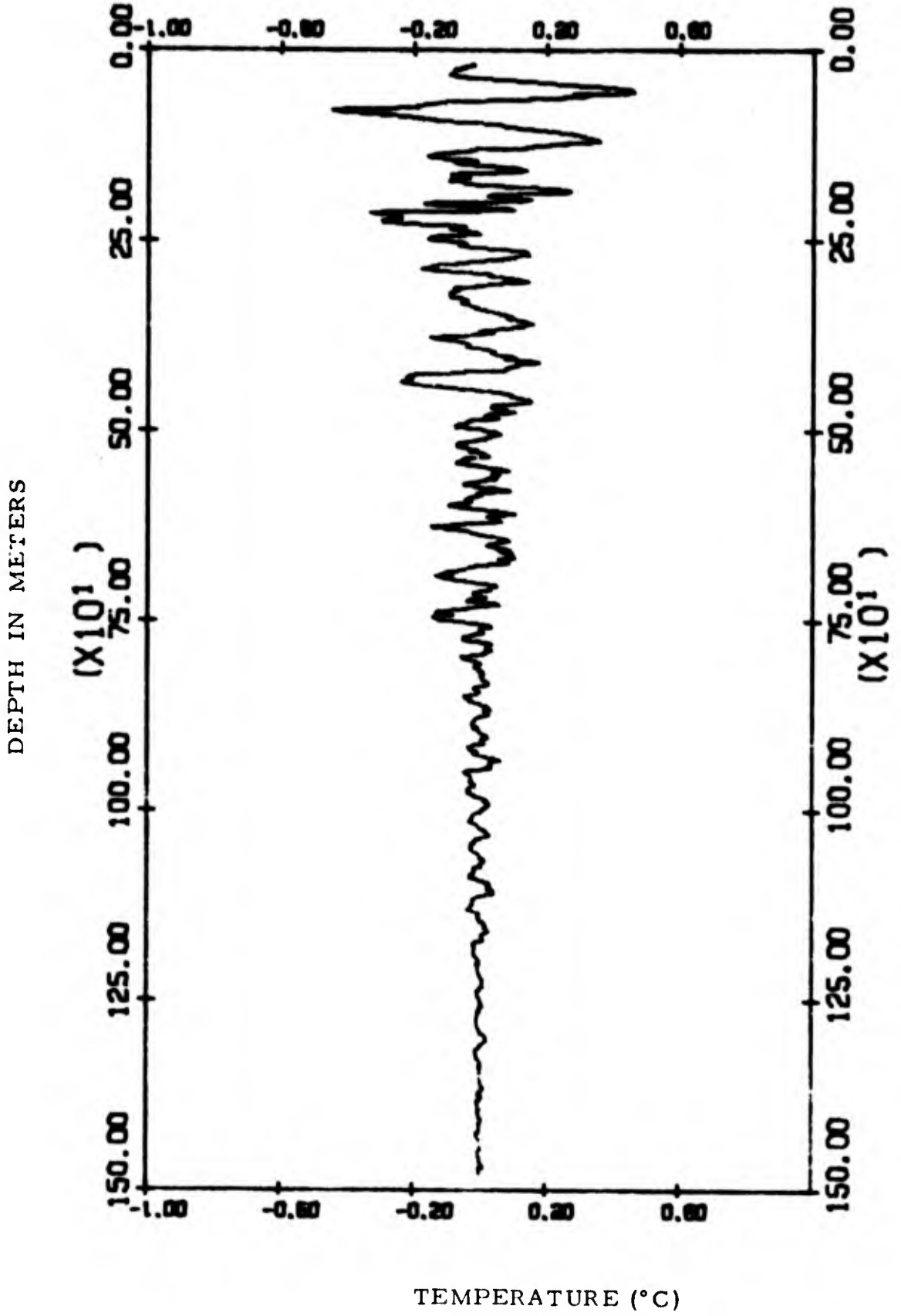

FIG. 8-2. Temperature perturbations from the mean as a function of depth obtained by binomial filtering. Station 10.

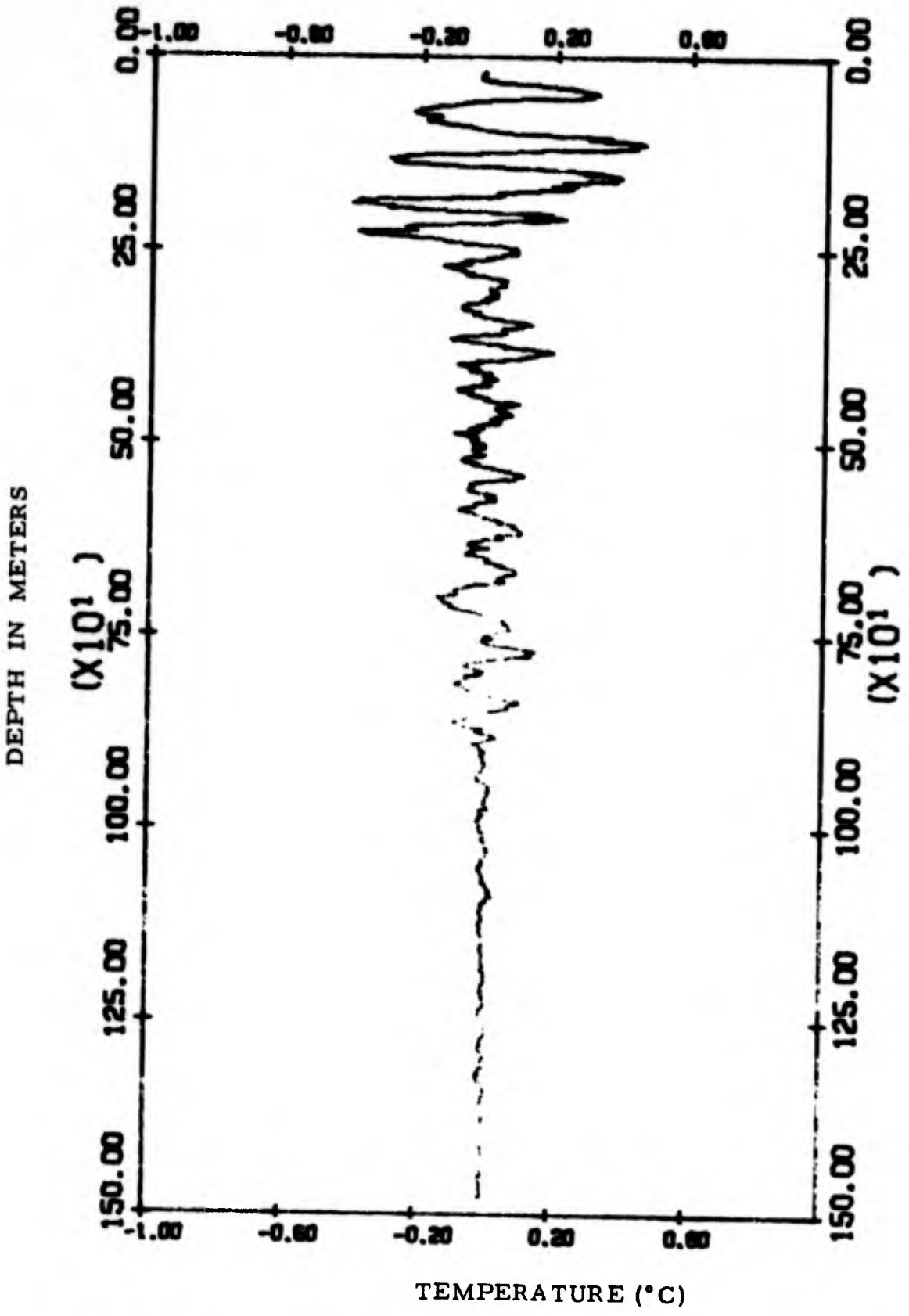

FIG. 8-3. Temperature perturbations from the mean as a function of depth obtained by binomial filtering. Station 11.

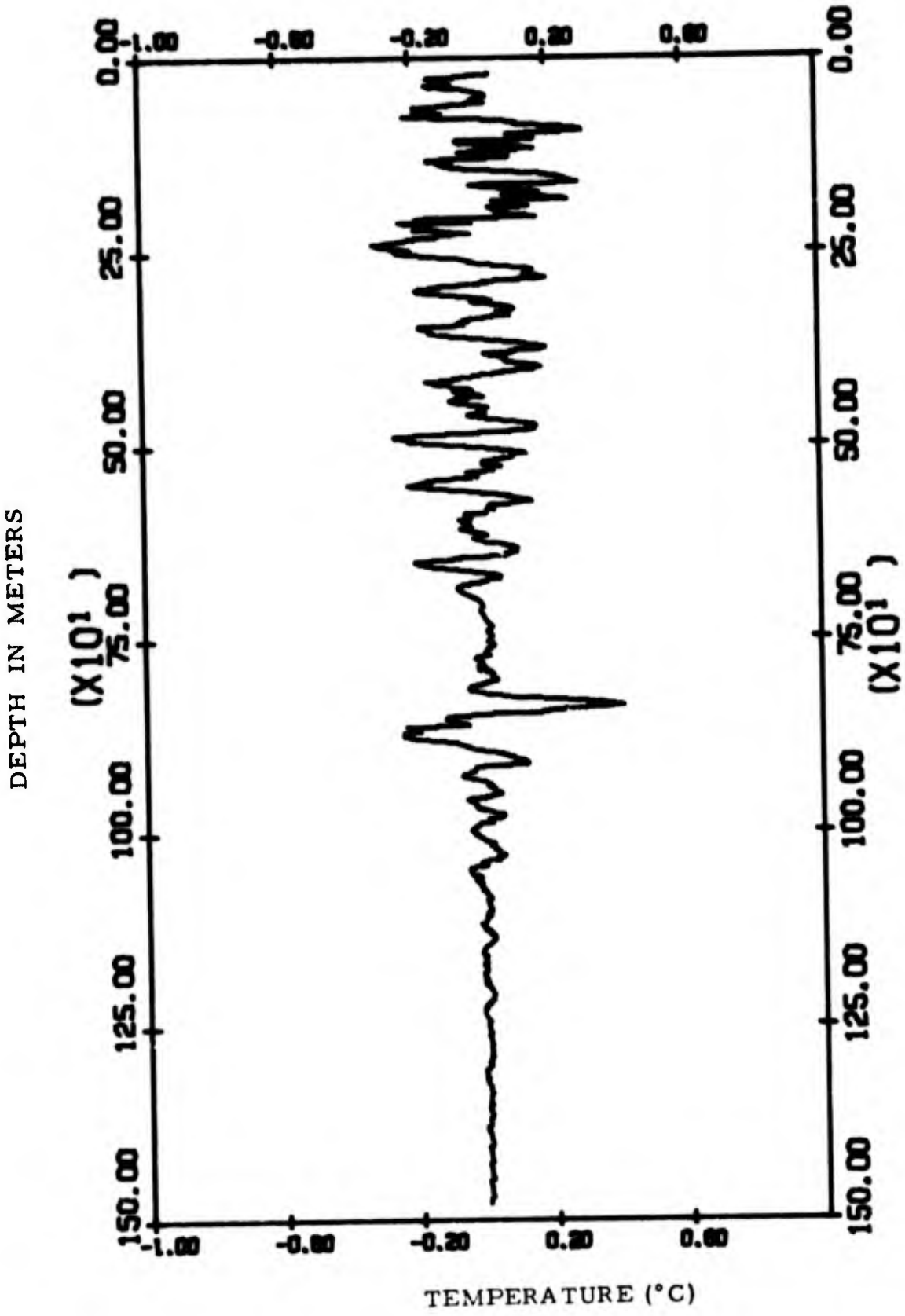

FIG. 8-4. Temperature perturbations from the mean as a function of depth obtained by binomial filtering. Station 15.

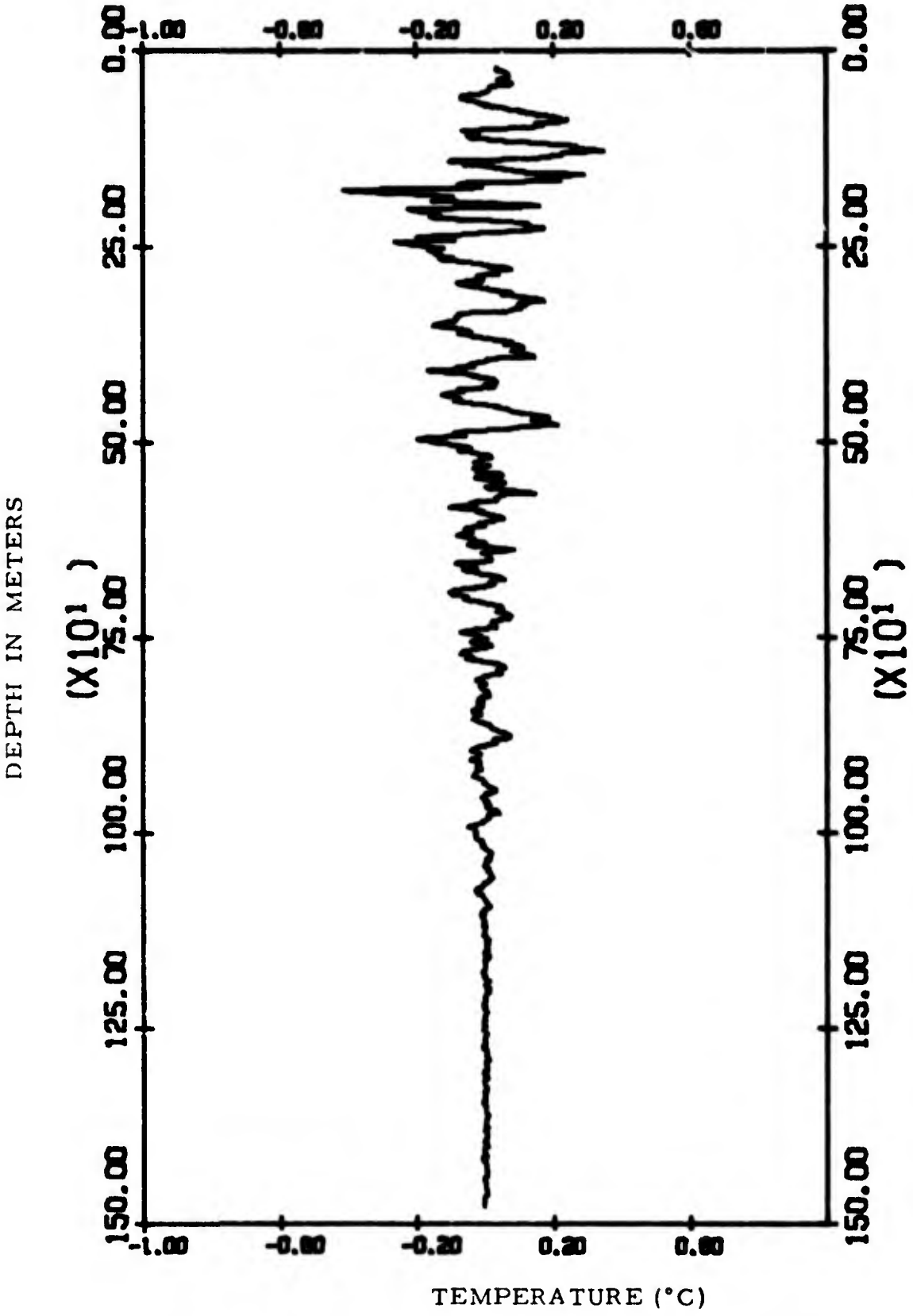

FIG. 8-5. Temperature perturbations from the mean as a function of depth obtained by binomial filtering. Station 16.

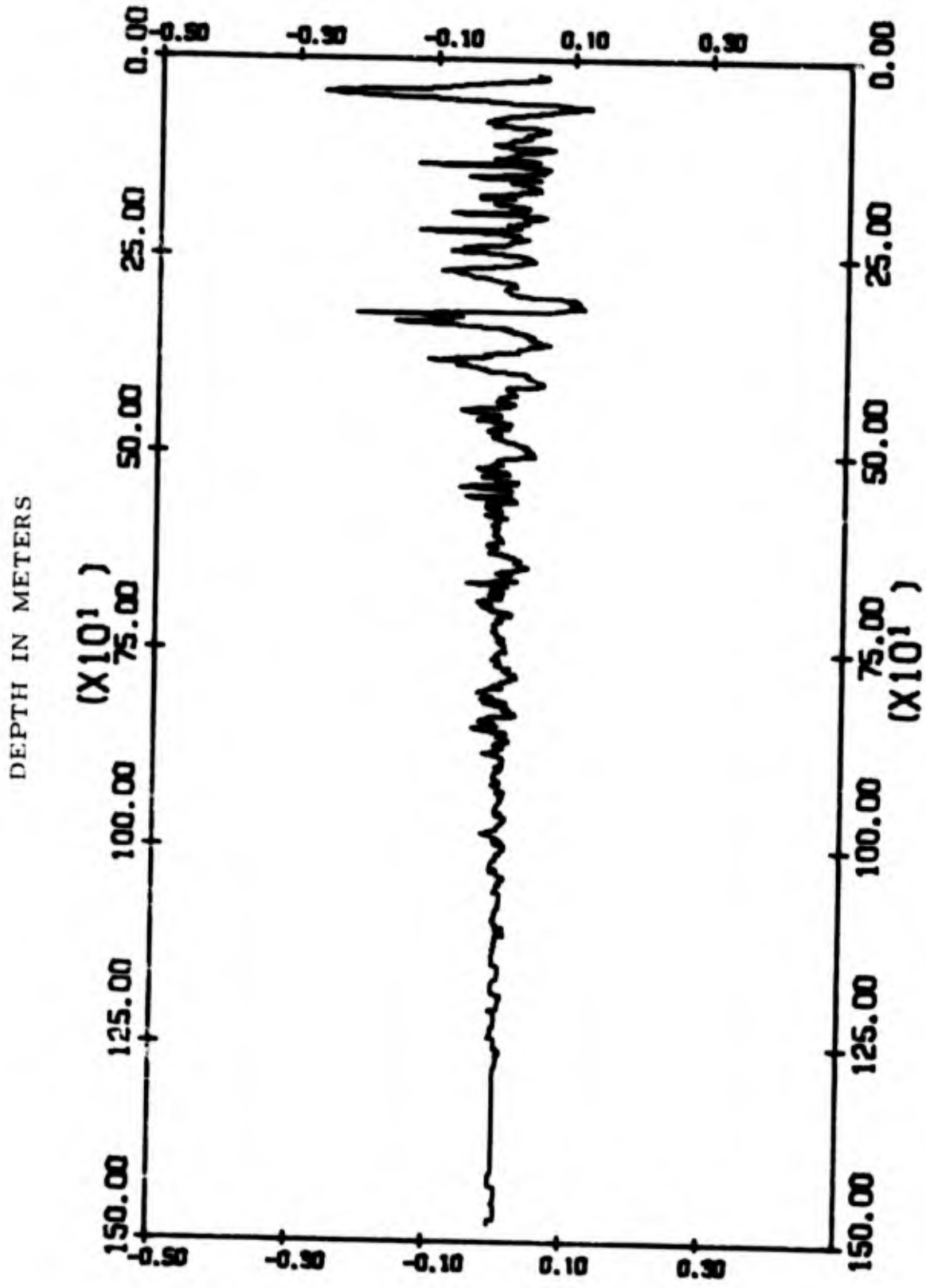

FIG. 9-1. Salinity perturbations from the mean as a function of depth obtained by binomial filtering. Station 9.

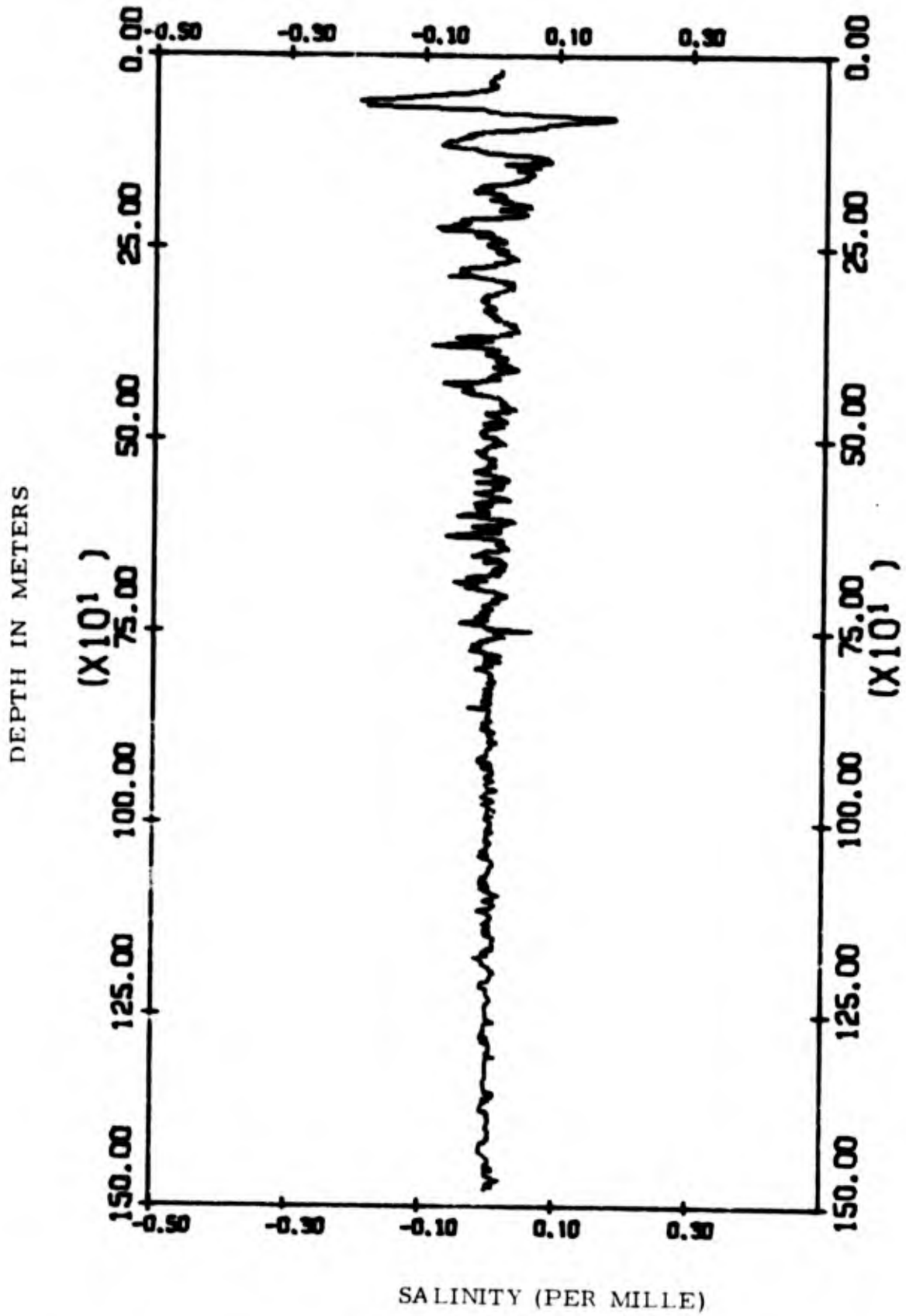

FIG. 9-2. Salinity perturbations from the mean as a function of depth obtained by binomial filtering. Station 10.

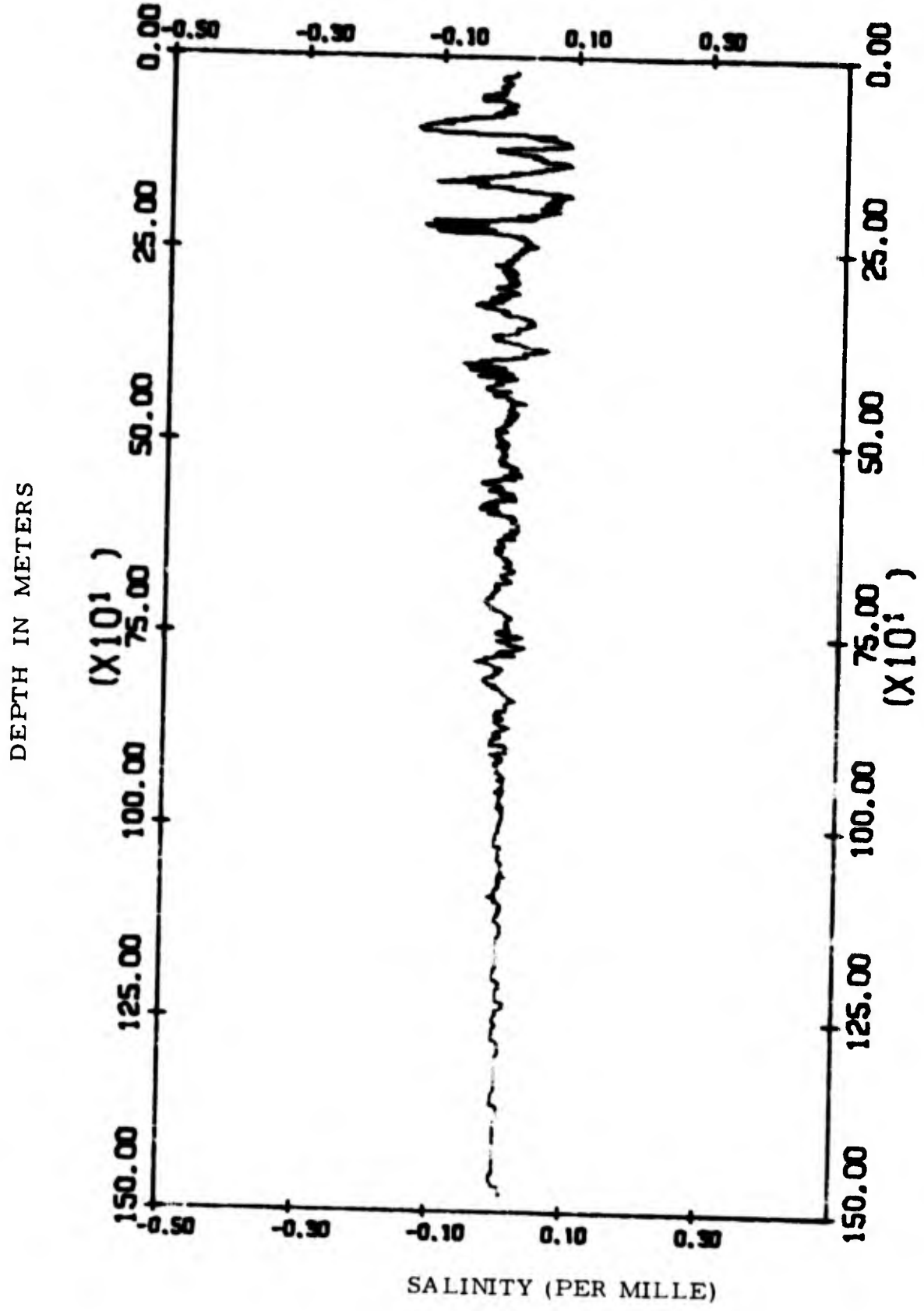

FIG. 9-3. Salinity perturbations from the mean as a function of depth obtained by binomial filtering. Station 11.

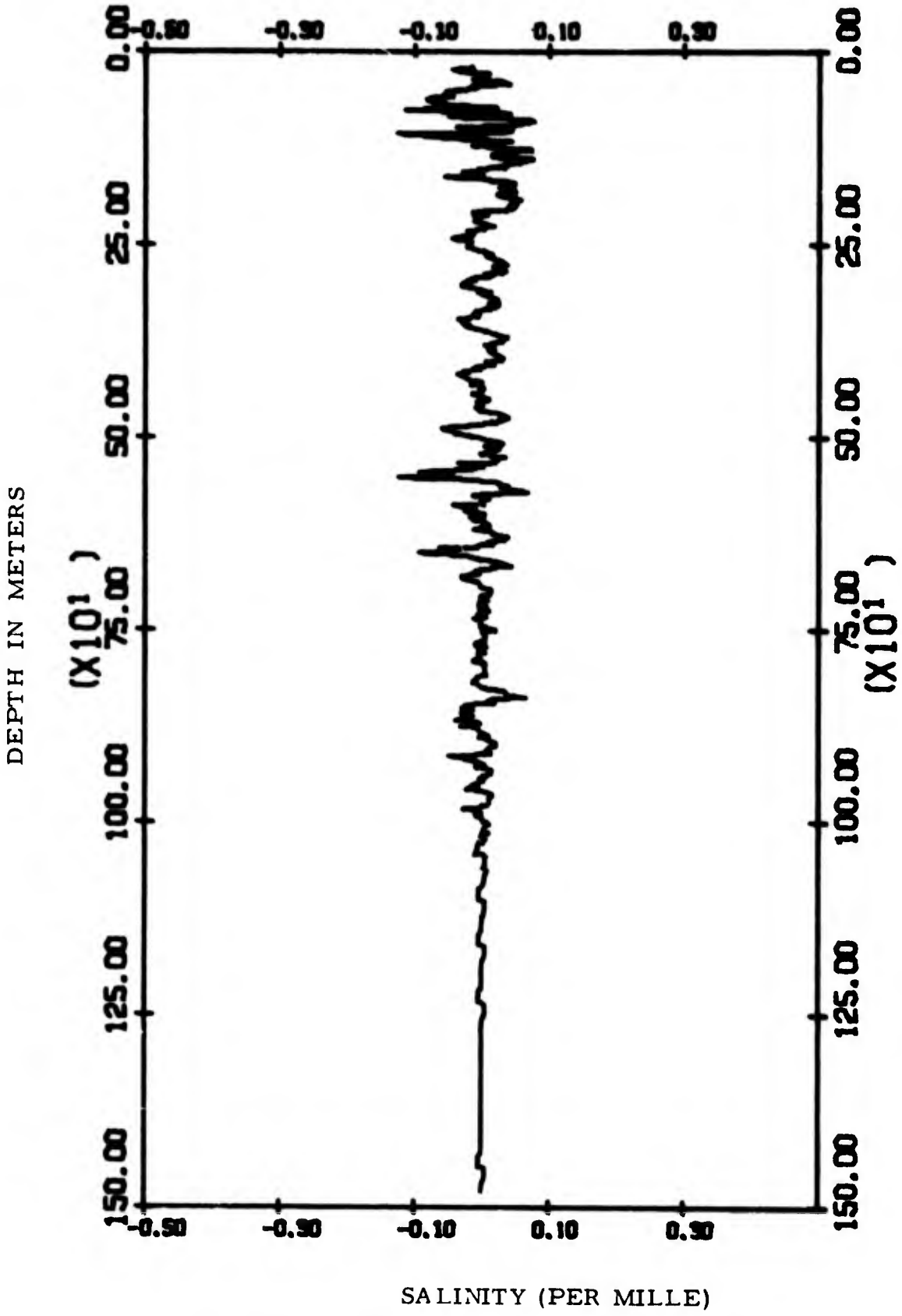

FIG. 9-4. Salinity perturbations from the mean as a function of depth obtained by binomial filtering. Station 15.

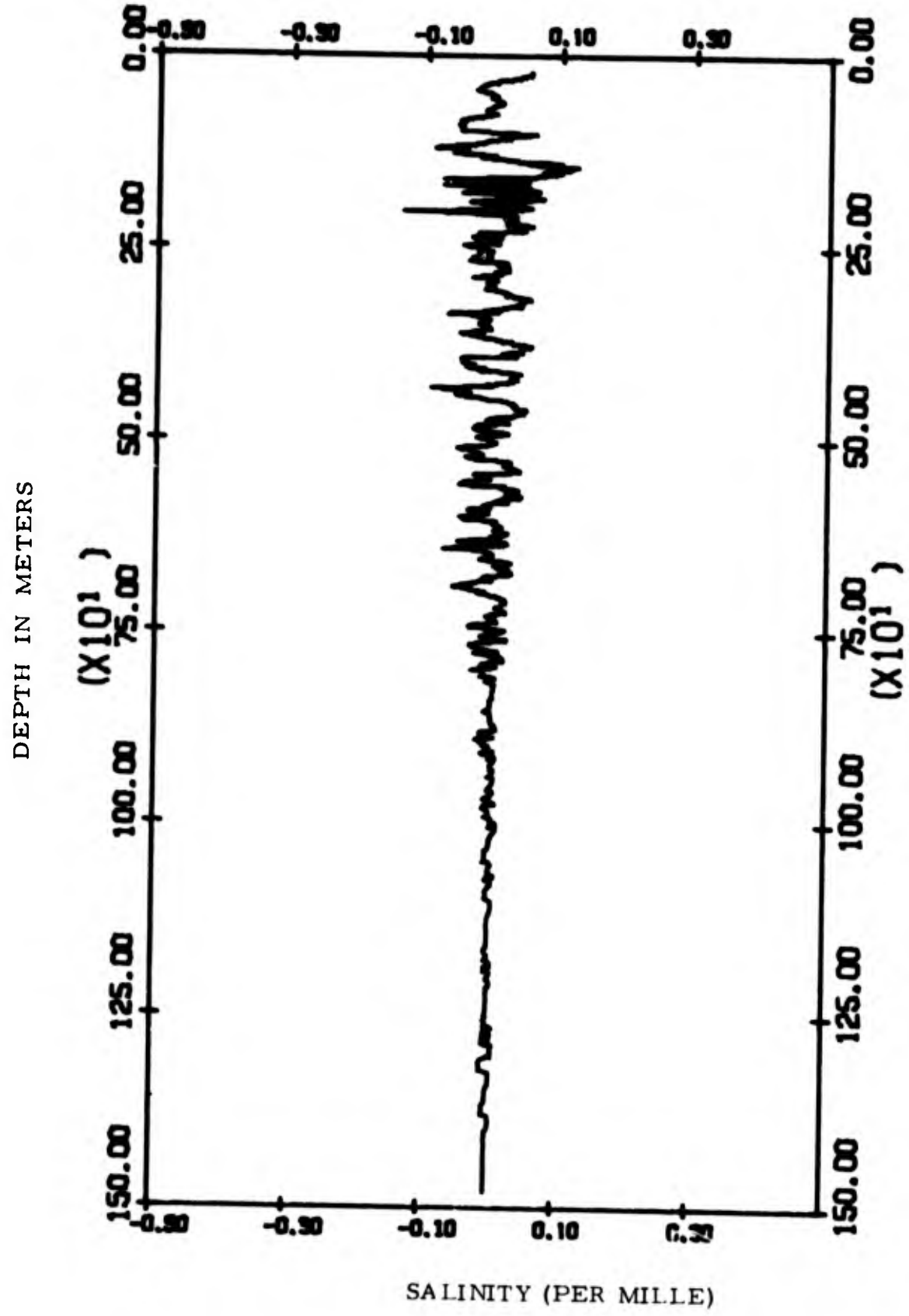

FIG. 9-5. Salinity perturbations from the mean as a function of depth obtained by binomial filtering. Station 16.

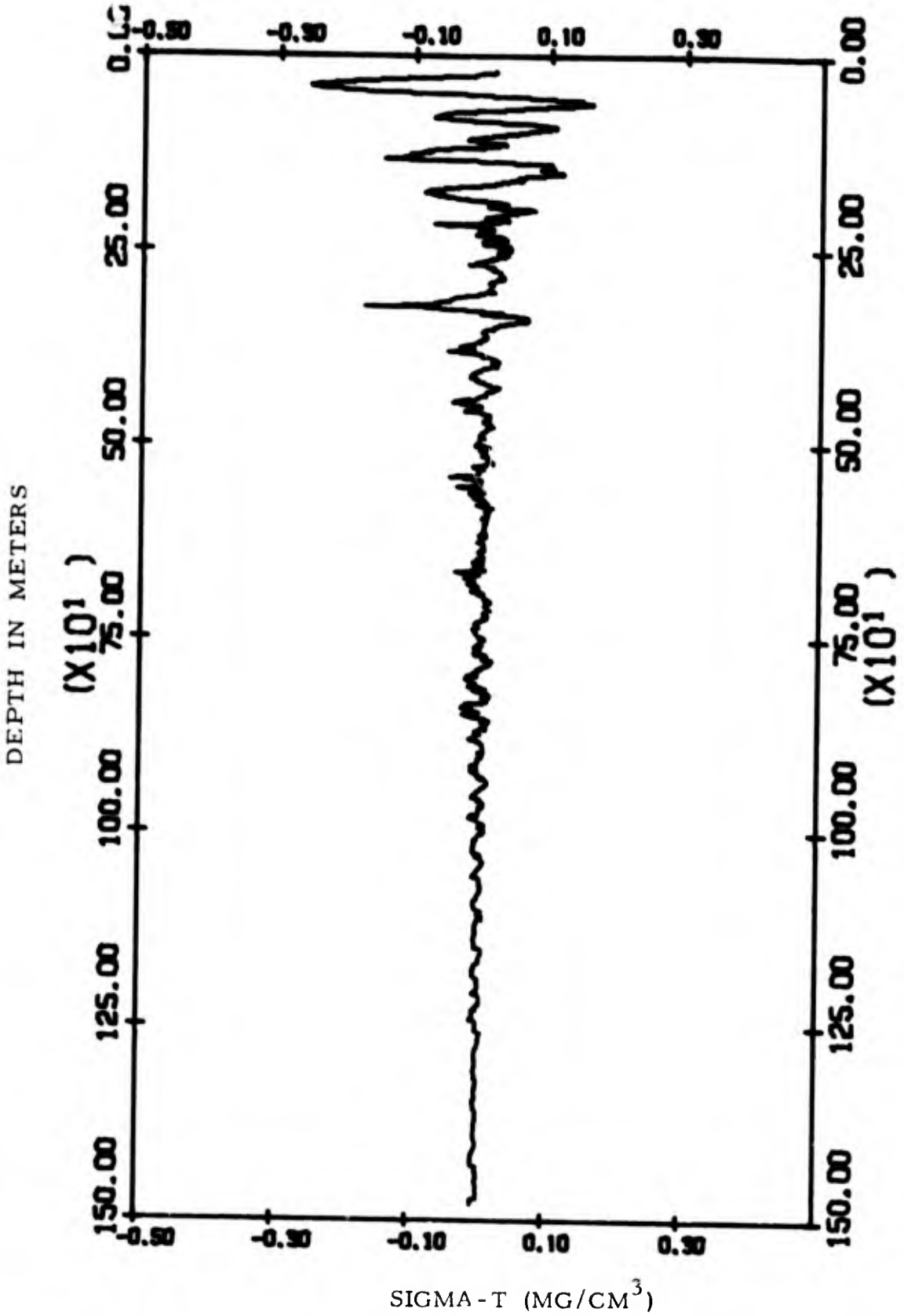

FIG. 10-1. Sigma-t perturbations from the mean as a function of depth obtained by binomial filtering. Station 9.

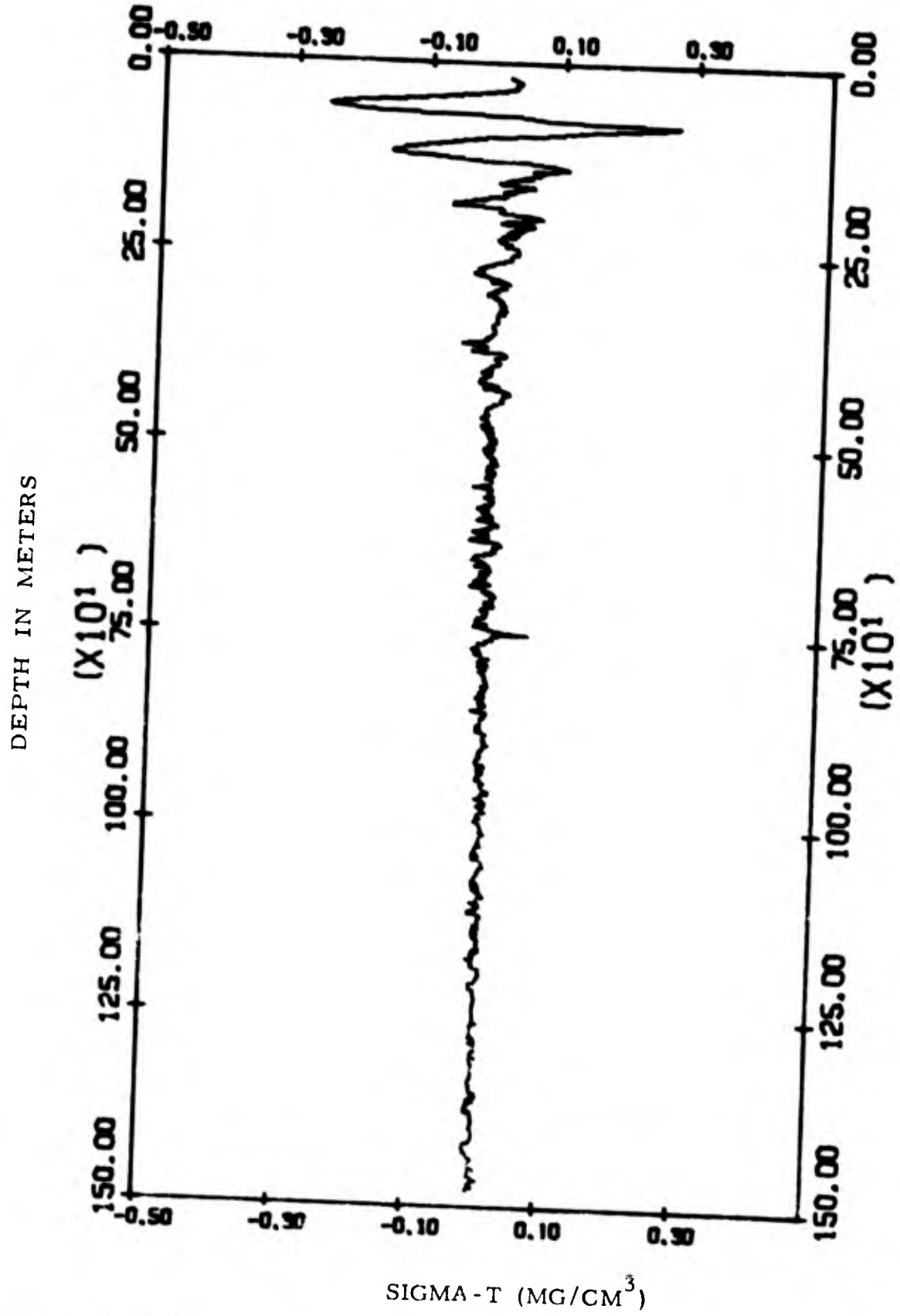

FIG. 10-2. Sigma-t perturbations from the mean as function of depth obtained by binomial filtering. Station 10.

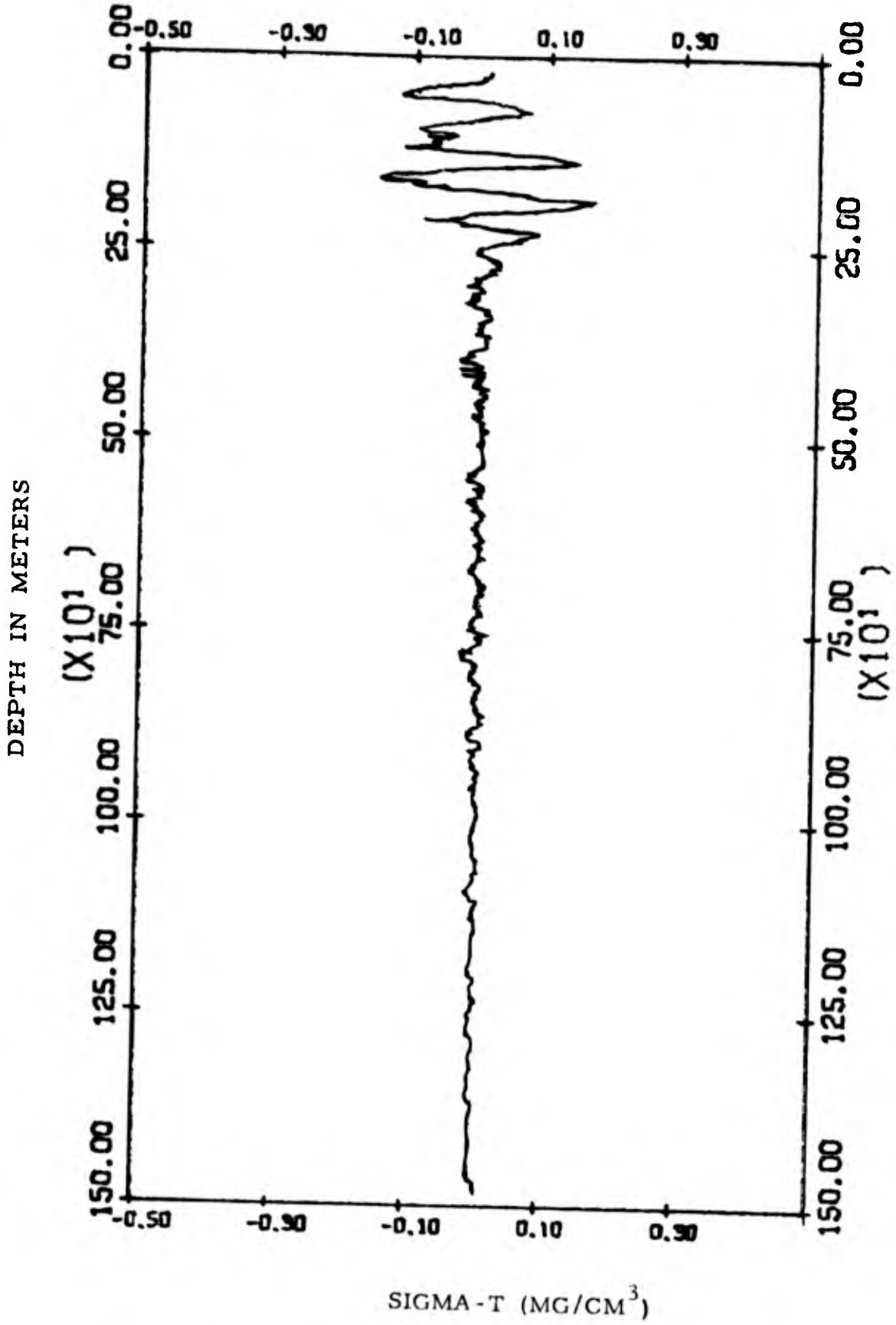

FIG. 10-3. Sigma-T perturbations from the mean as a function of depth obtained by binomial filtering. Station 11.

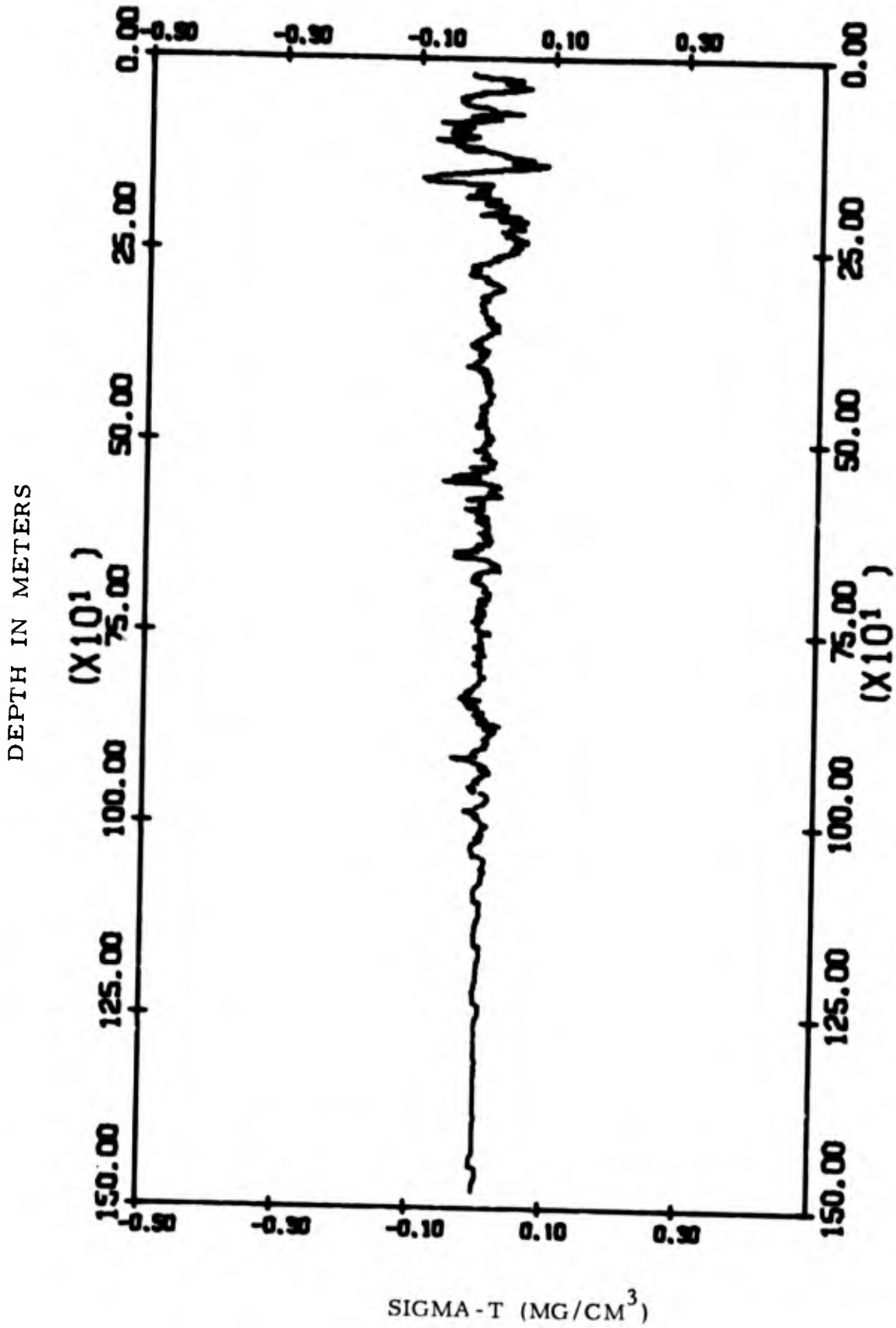

FIG. 10-4. Sigma-t perturbations from the mean as a function of depth obtained by binomial filtering. Station 15.

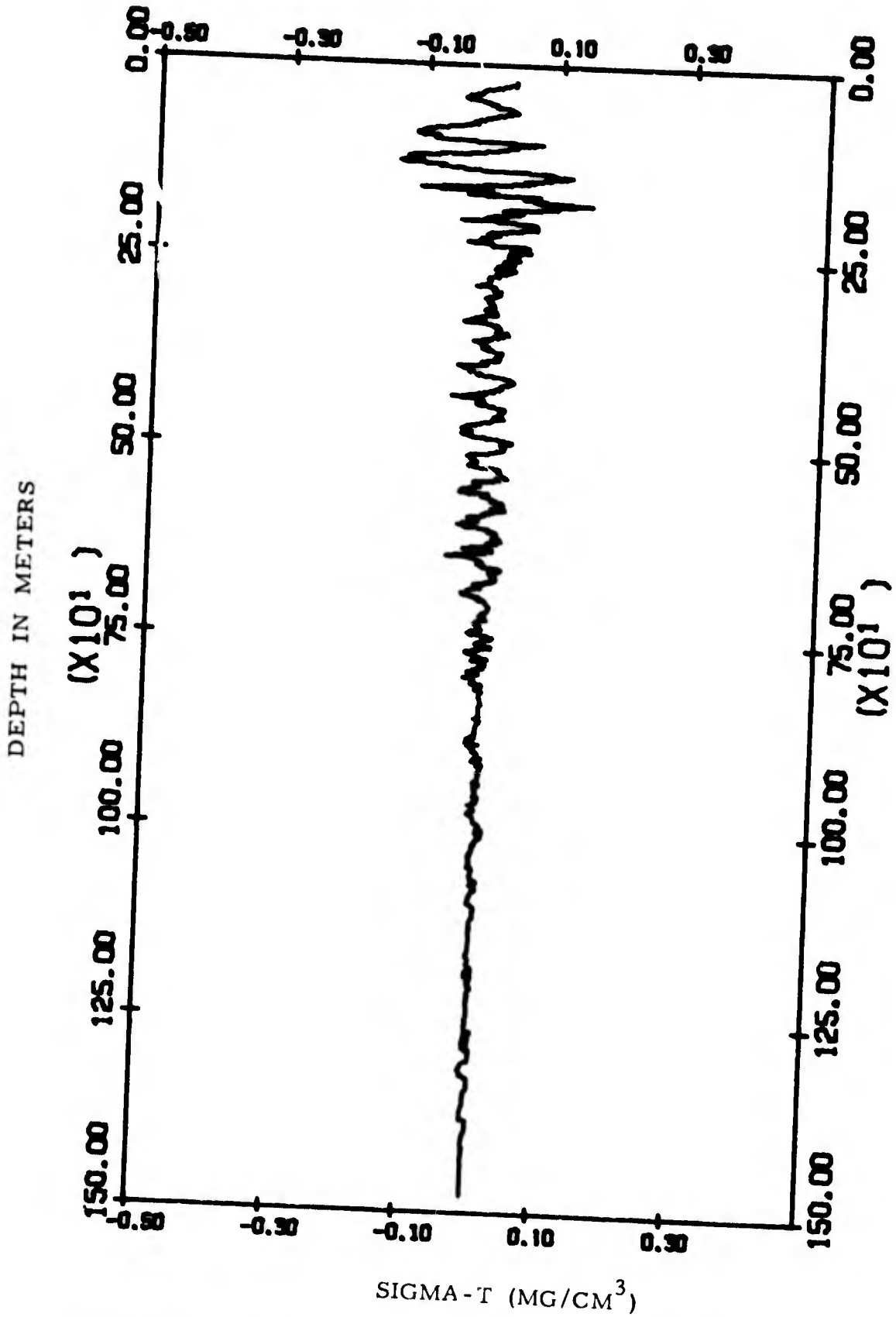

FIG. 10-5. Sigma-t perturbations from the mean as a function of depth obtained by binomial filtering. Station 16.

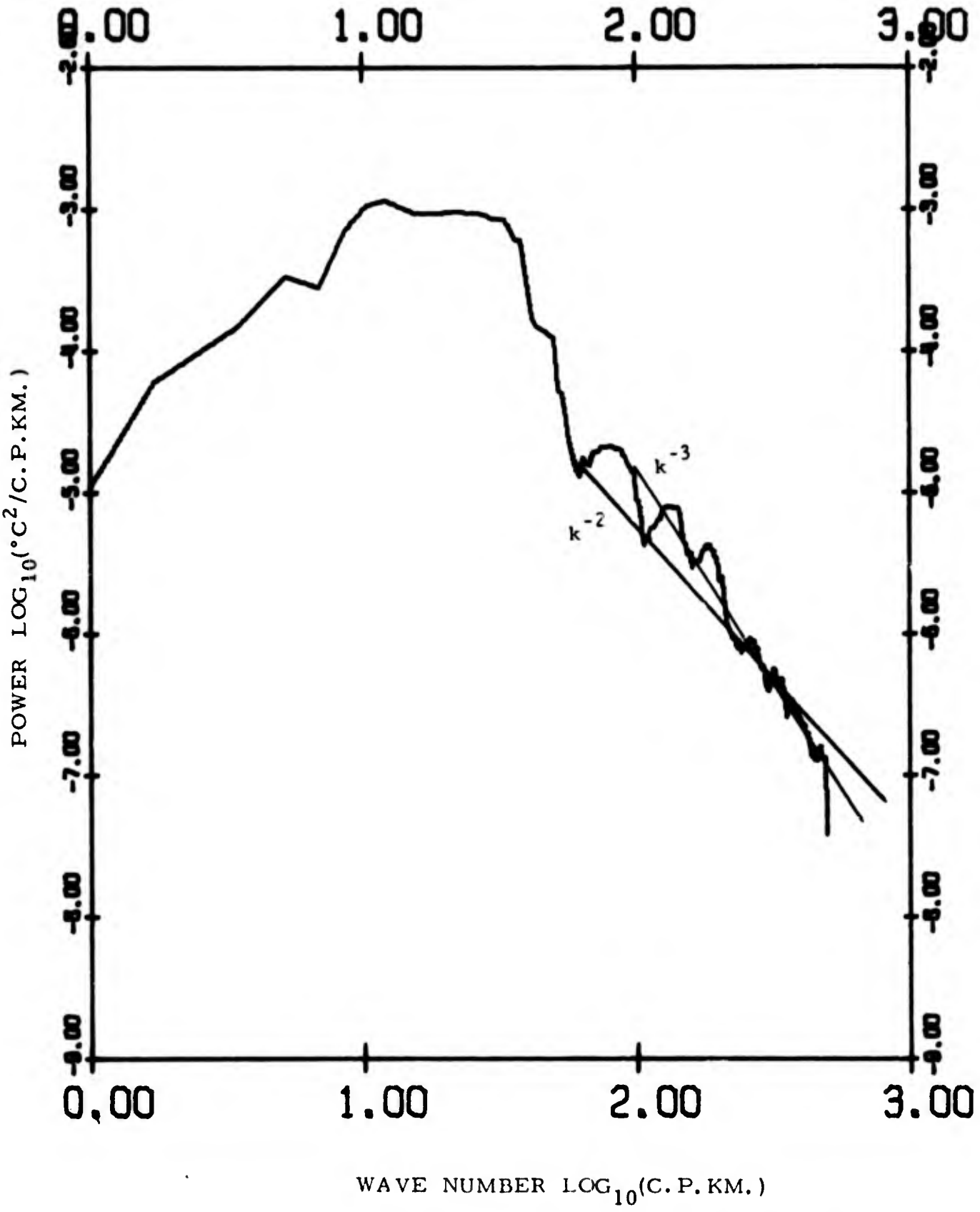

FIG. 11-1. Wave number spectra of temperature perturbations.
Depth interval 0-600 meters.
Station 9.

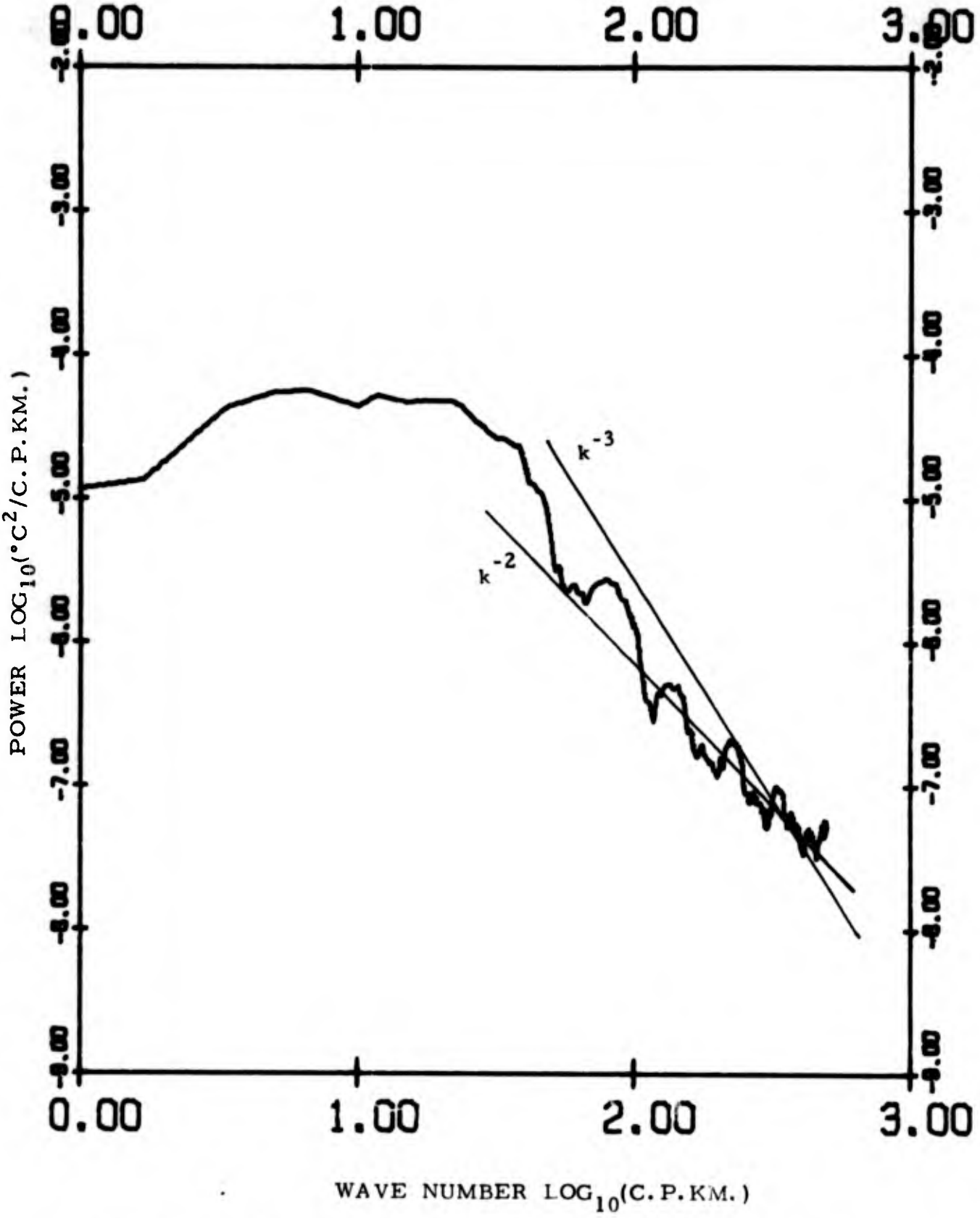

FIG. 11-2. Wave number spectra of temperature perturbations.
Depth interval 600-1200 meters.
Station 9.

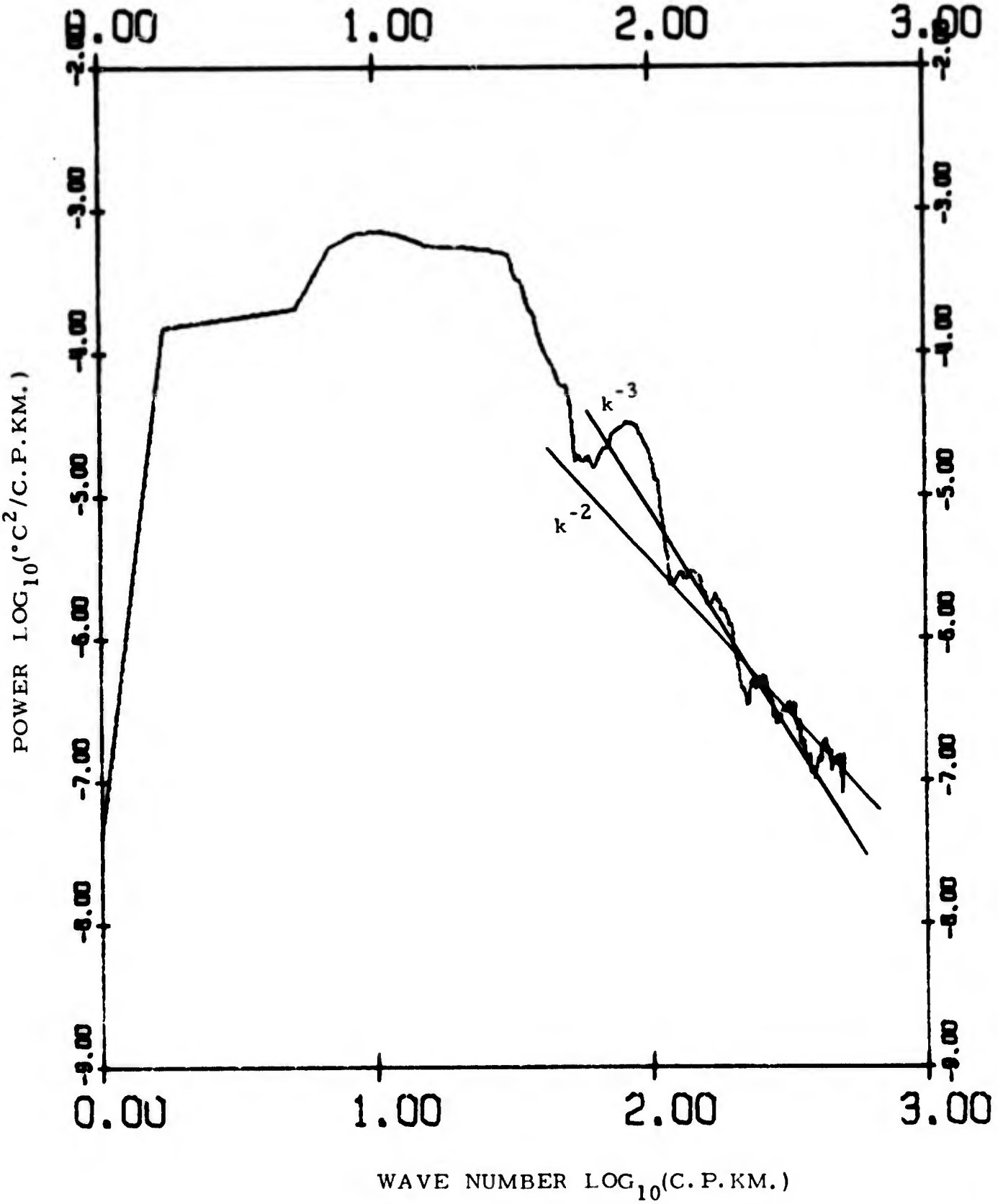

FIG. 11-3. Wave number spectra of temperature perturbations.
Depth interval 0-600 meters.
Station 10.

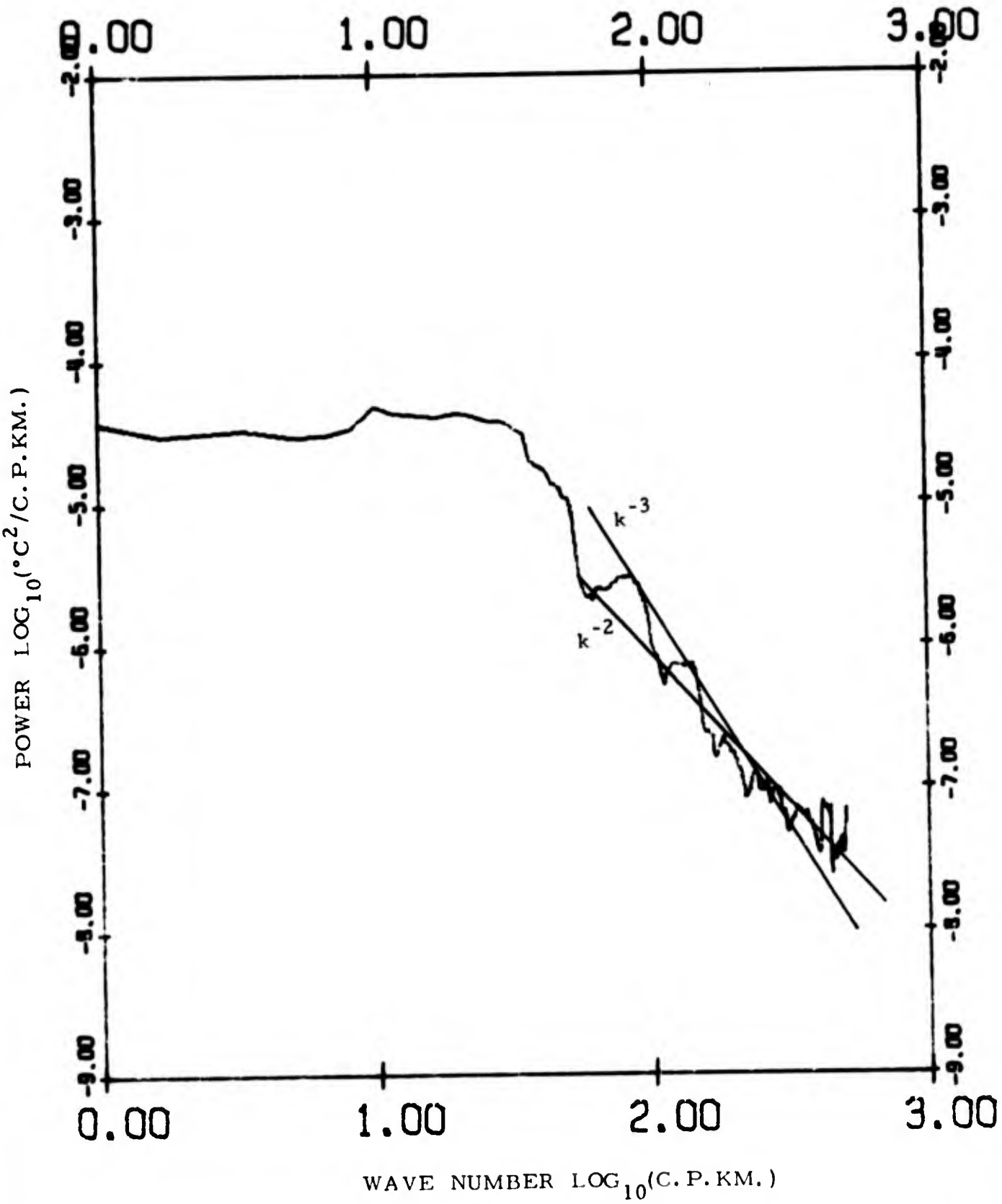

FIG. 11-4. Wave number spectra of temperature perturbations.
Depth interval 600-1200 meters.
Station 10.

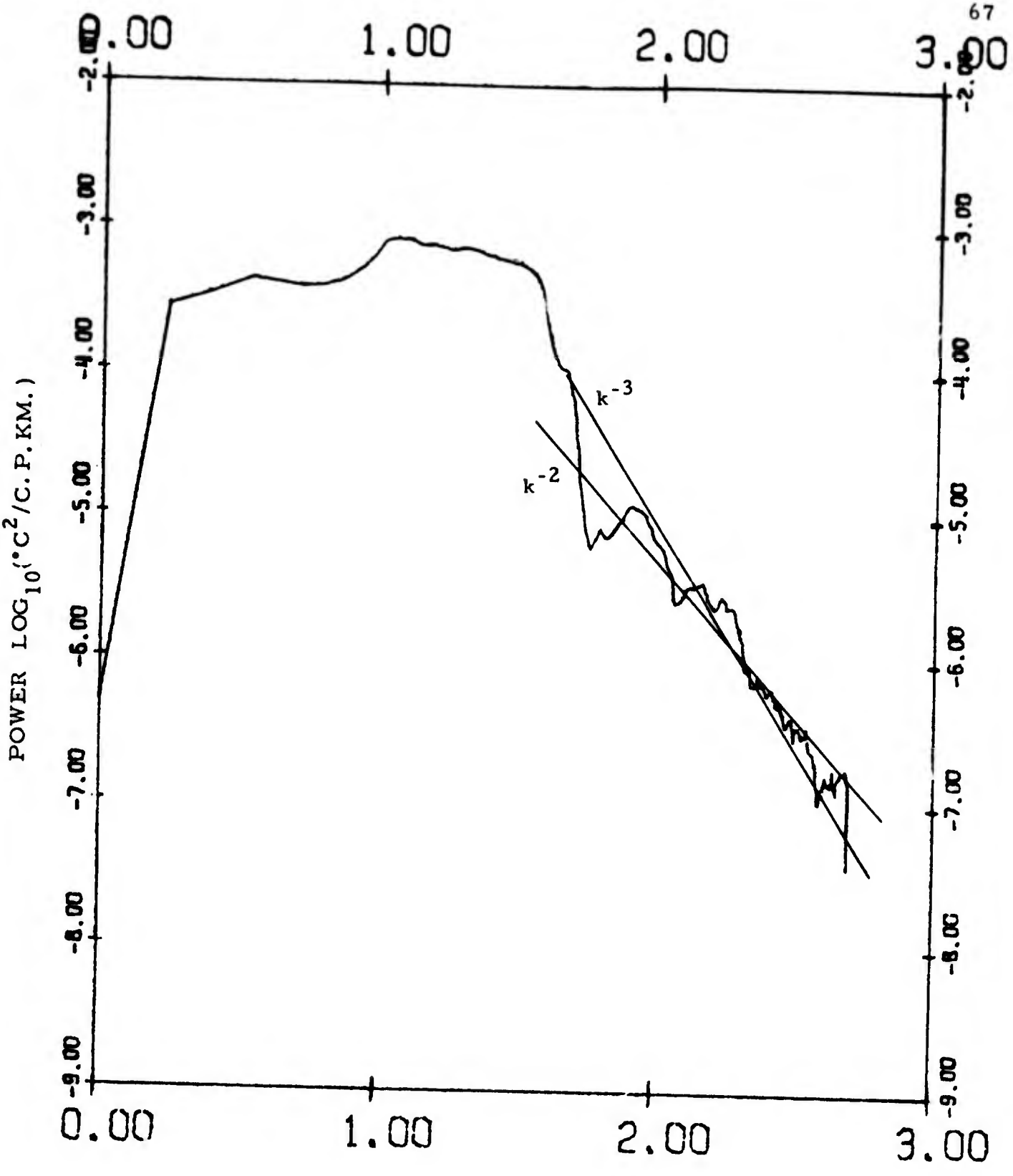

FIG. 11-5. Wave number spectra of temperature perturbations.
Depth interval 0-600 meters.
Station 11.

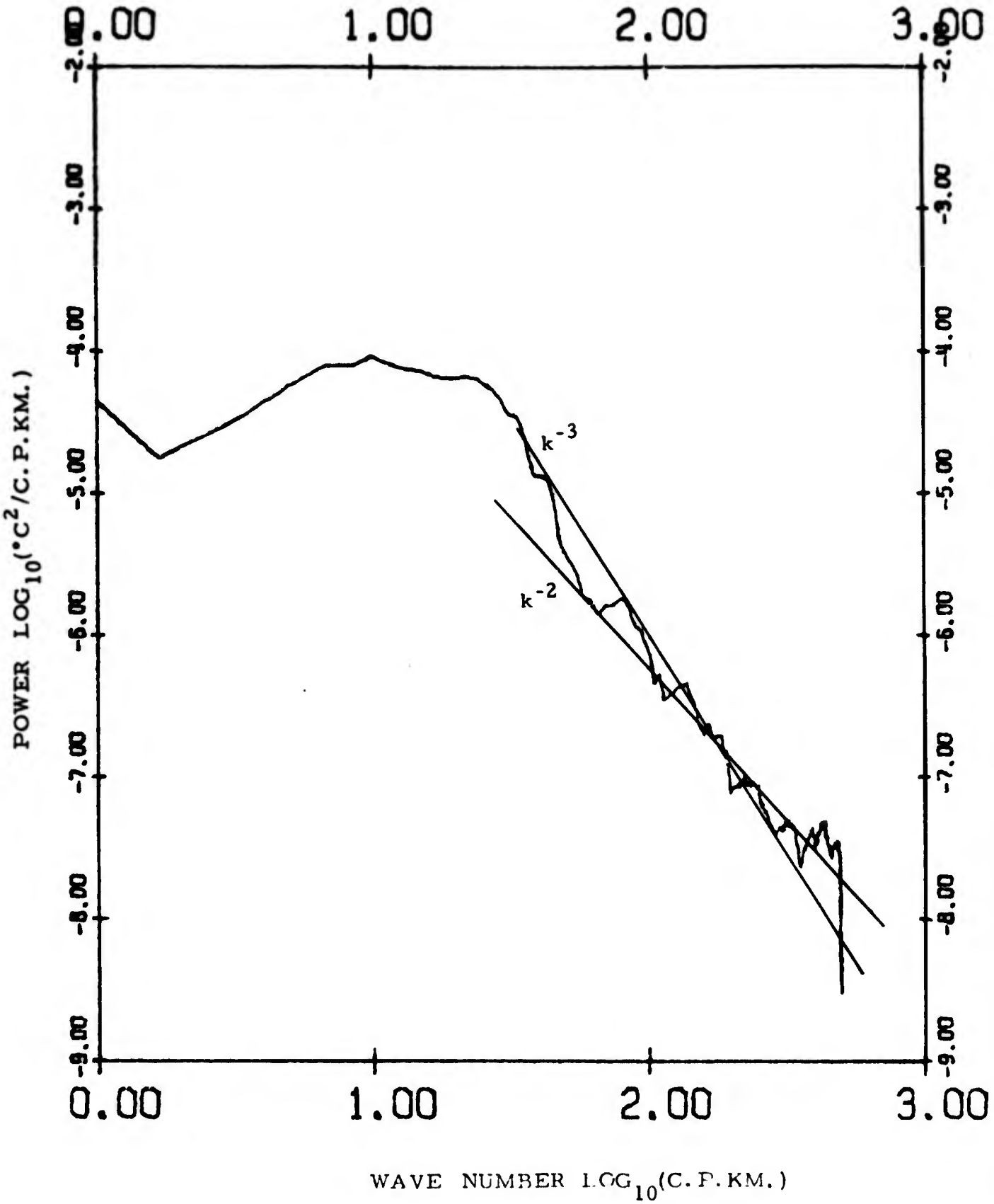

FIG. 11-6. Wave number spectra of temperature perturbations.
Depth interval 600-1200 meters.
Station 11.

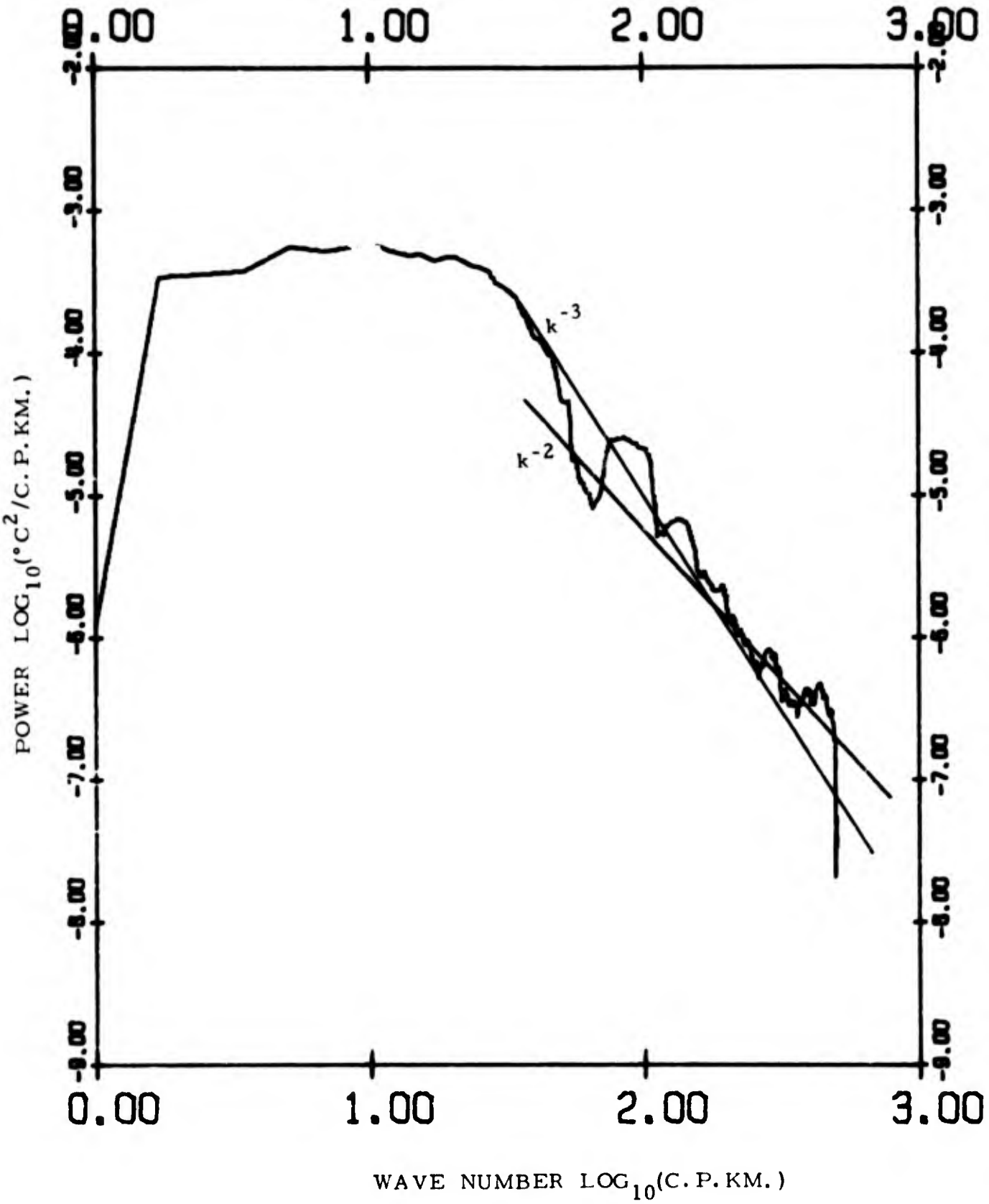

FIG. 11-7. Wave number spectra of temperature perturbations.
Depth interval 0-600 meters.
Station 15.

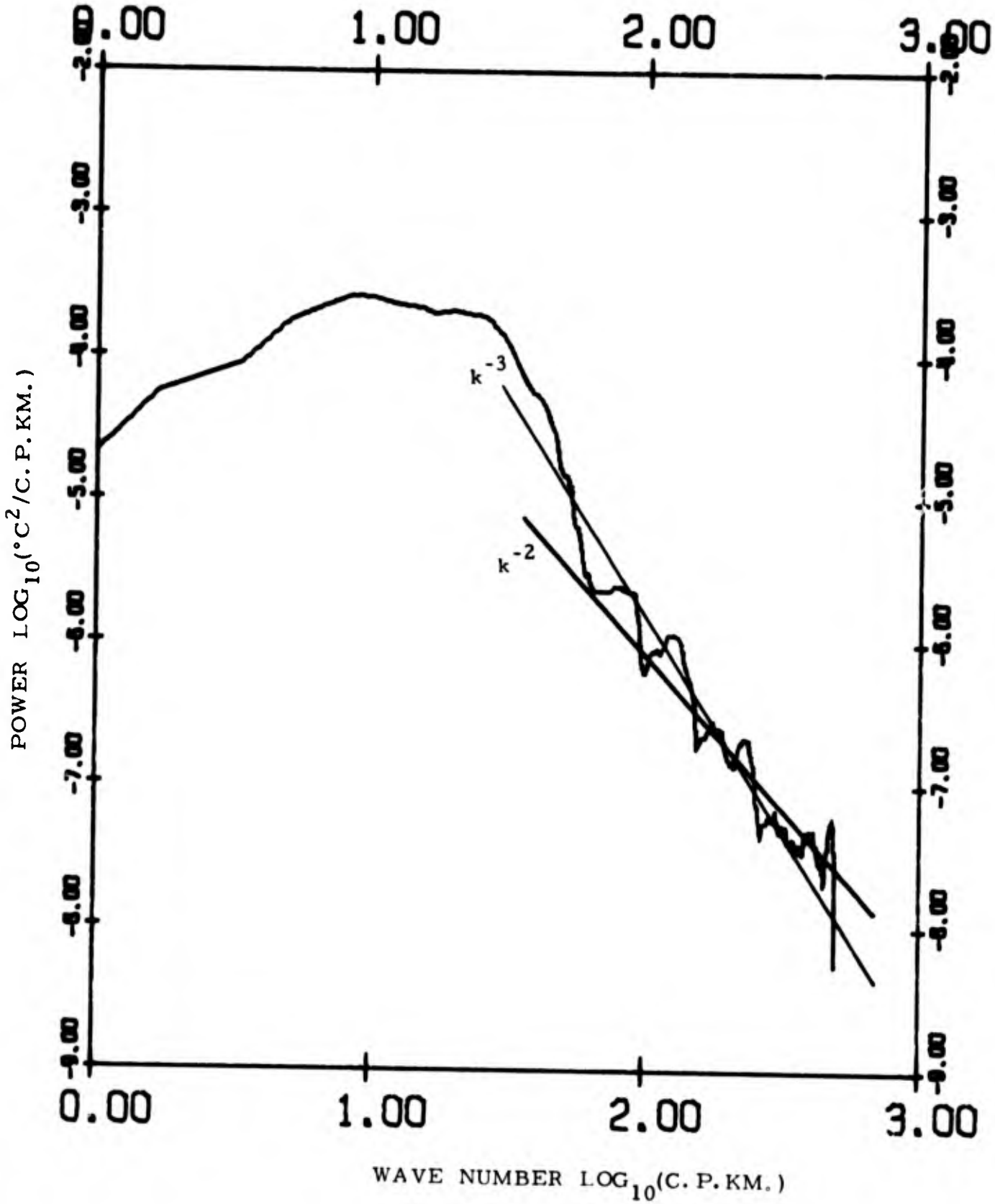

FIG. 11-8. Wave number spectra of temperature perturbations.
Depth interval 600-1200 meters.
Station 15.

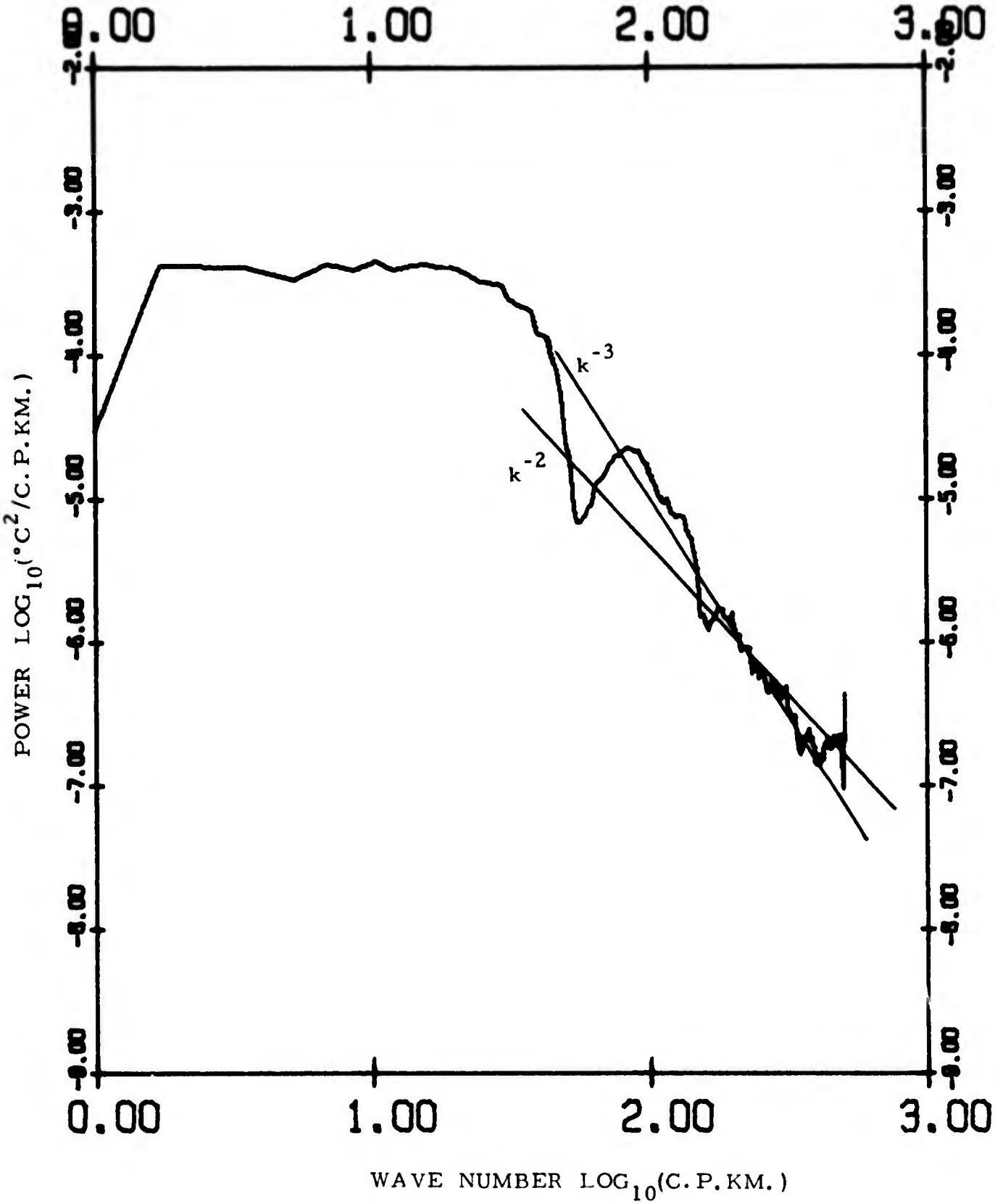

FIG. 11-9. Wave number spectra of temperature perturbations.
Depth interval 0-600 meters.
Station 16.

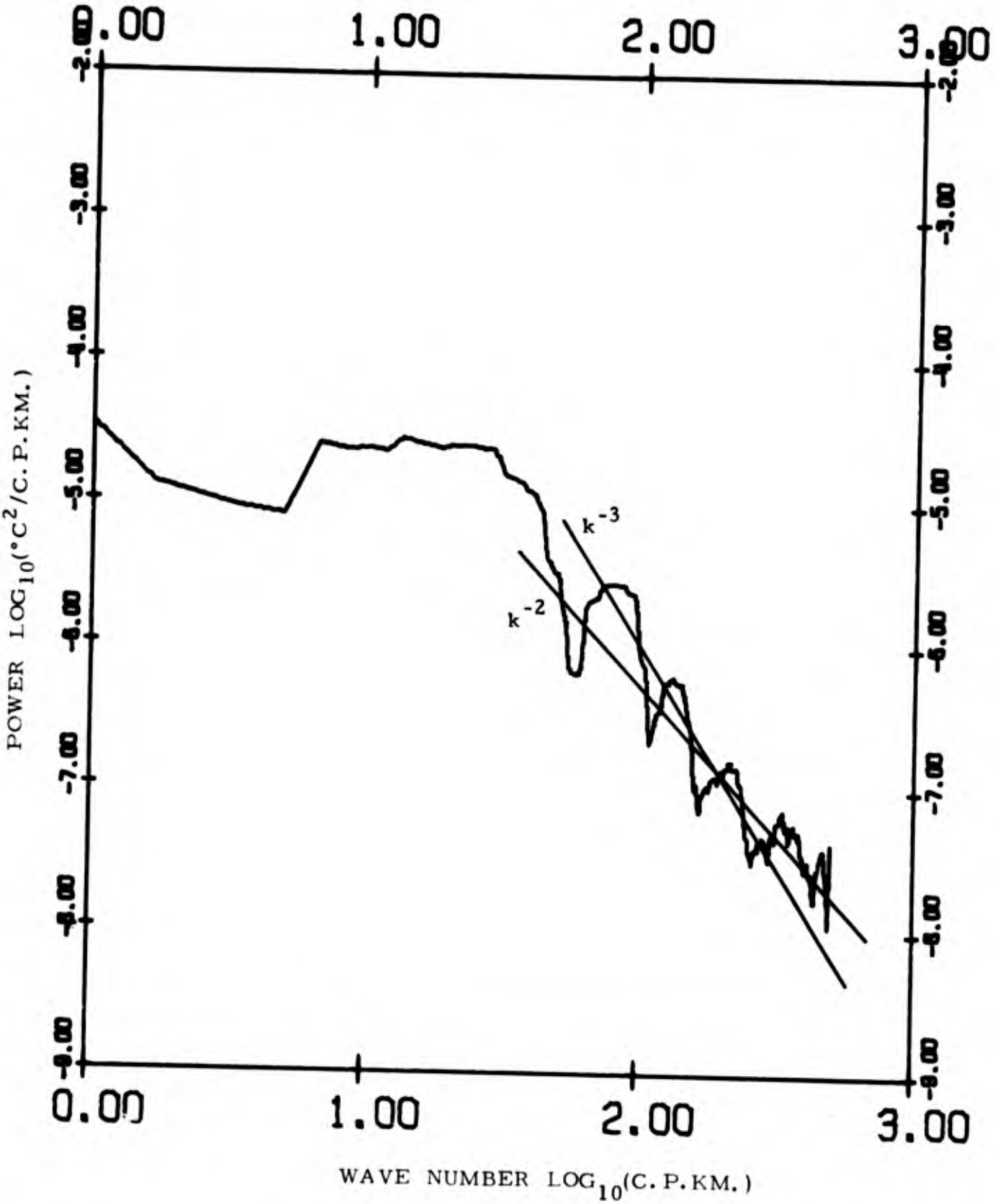

FIG. 11-10. Wave number spectra of temperature perturbations.
Depth interval 600-1200 meters.
Station 16.

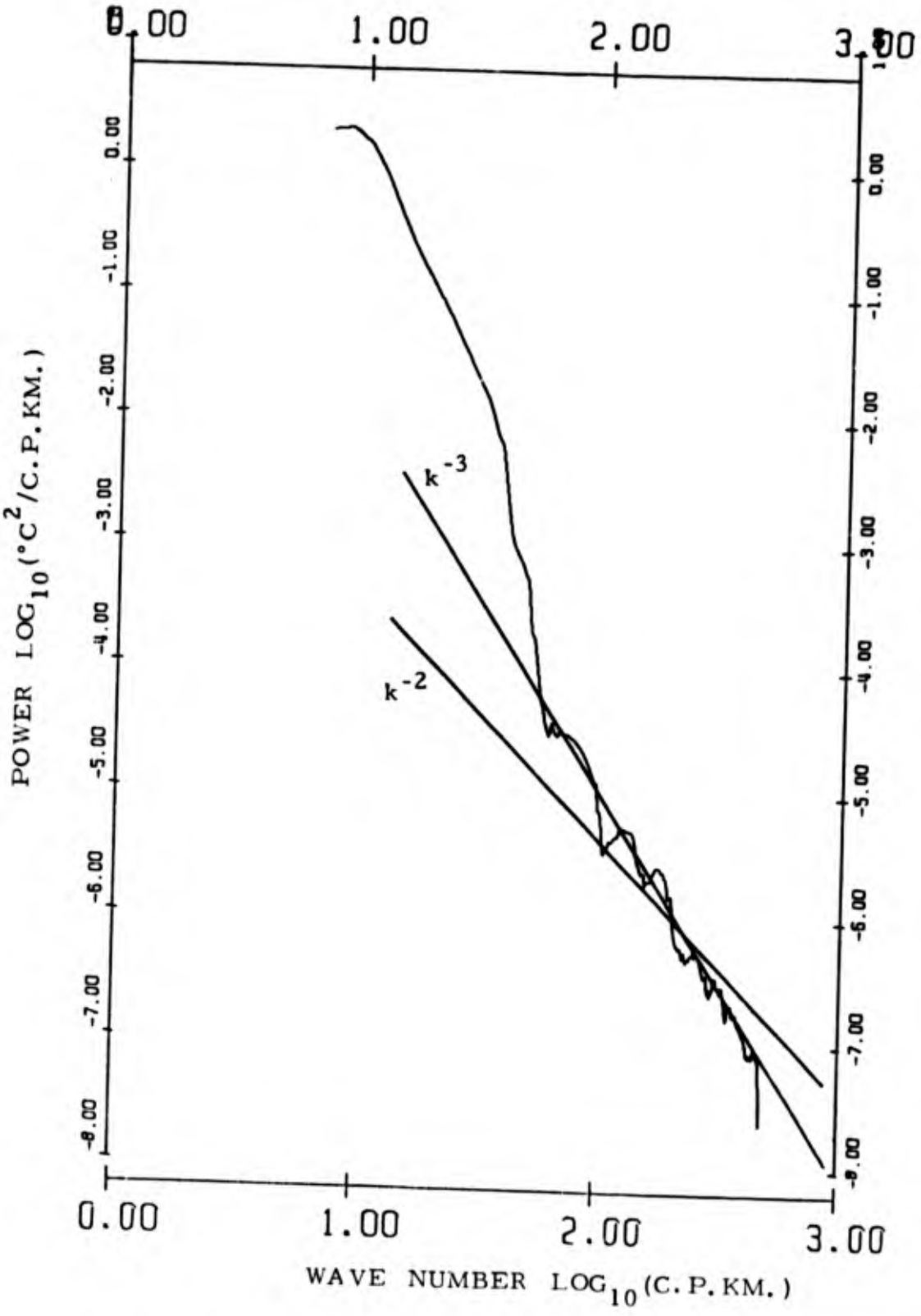

FIG. 12-1. Wave number spectra of temperature perturbations corrected for binomial filtering.
Depth interval 0-600 meters.
Station 9.

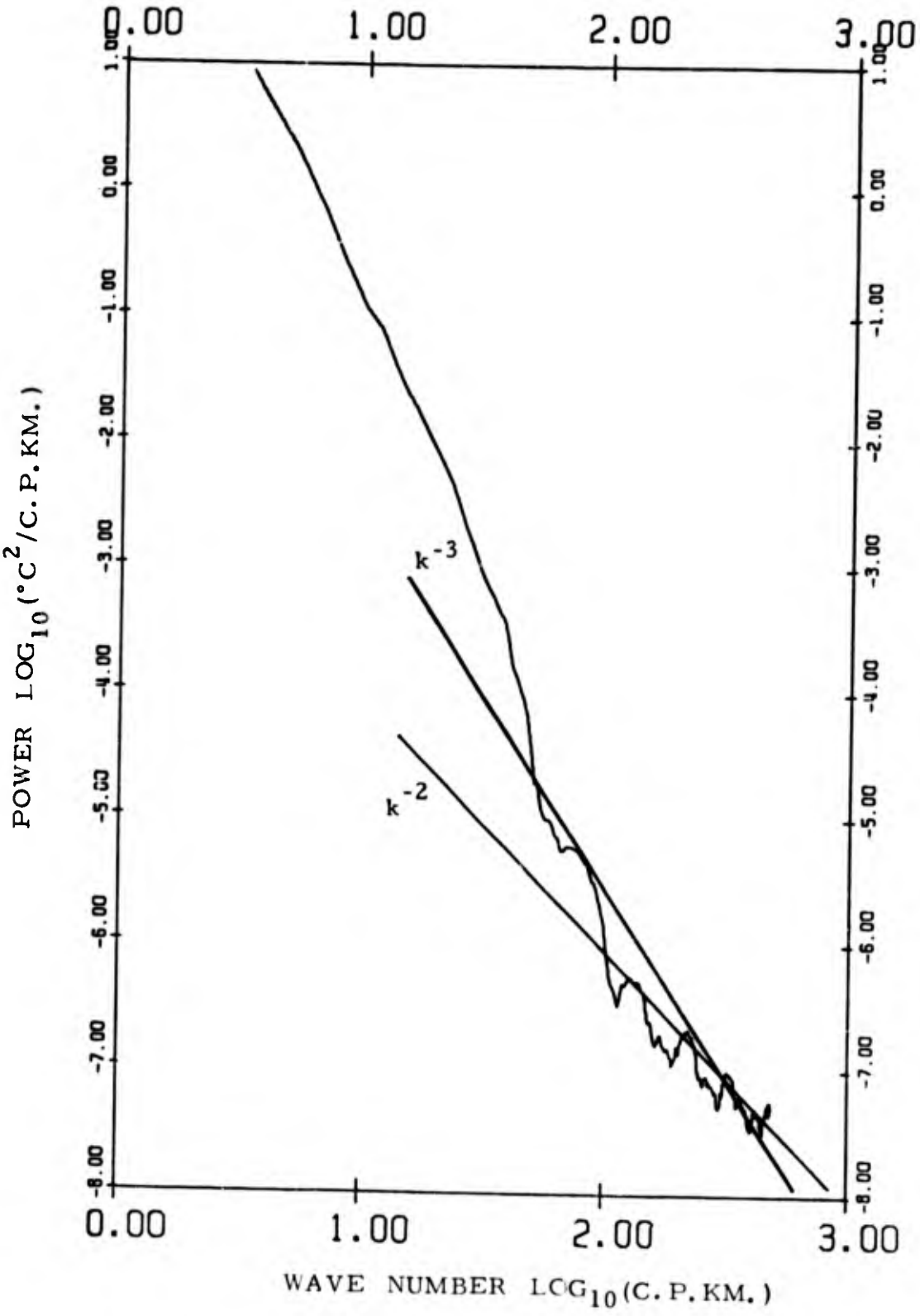

FIG. 12-2. Wave number spectra of temperature perturbations corrected for binomial filtering. Depth interval 600-1200 meters. Station 9.

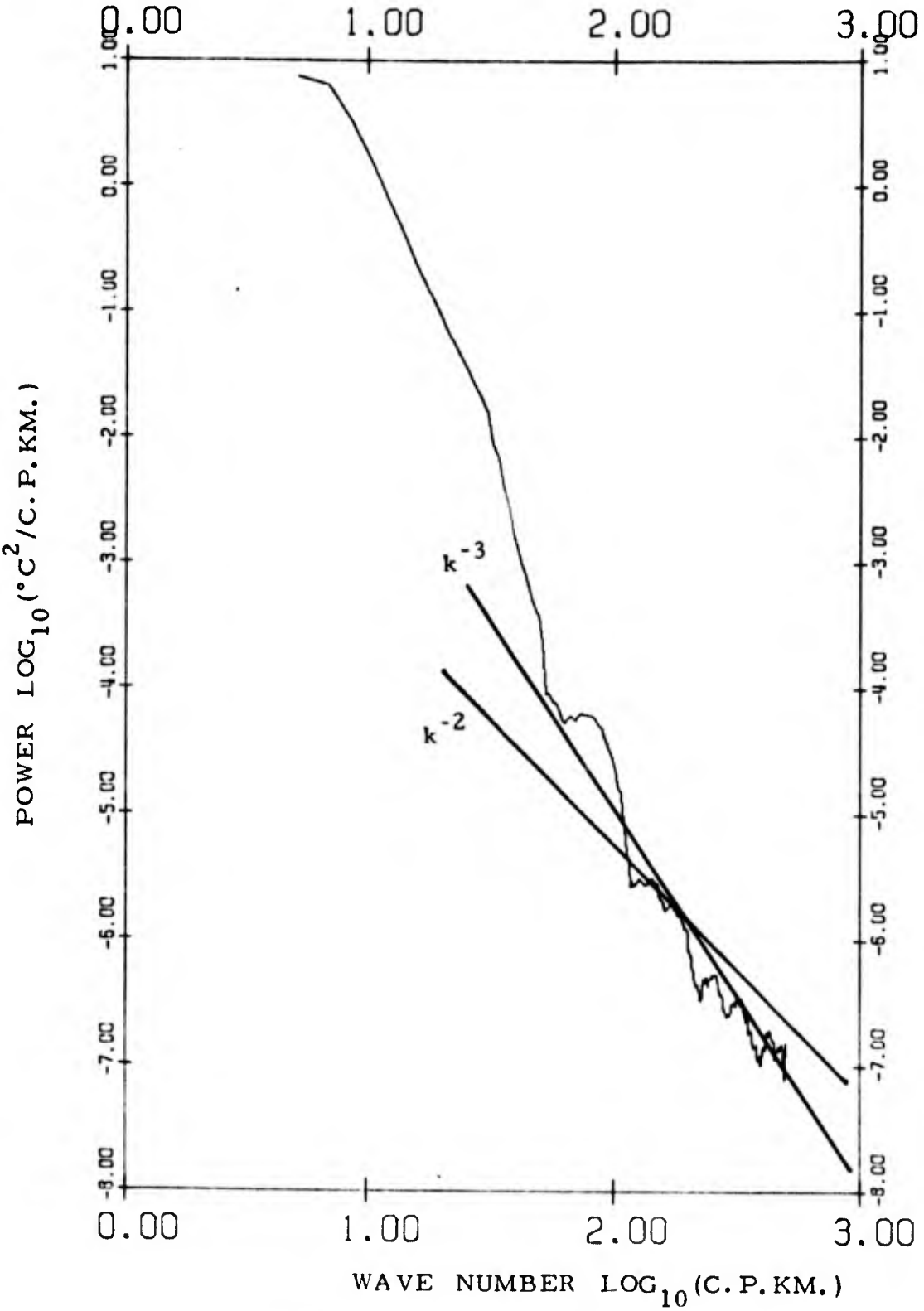

FIG. 12-3. Wave number spectra of temperature perturbations corrected for binomial filtering.
Depth interval 0 - 600 meters.
Station 10.

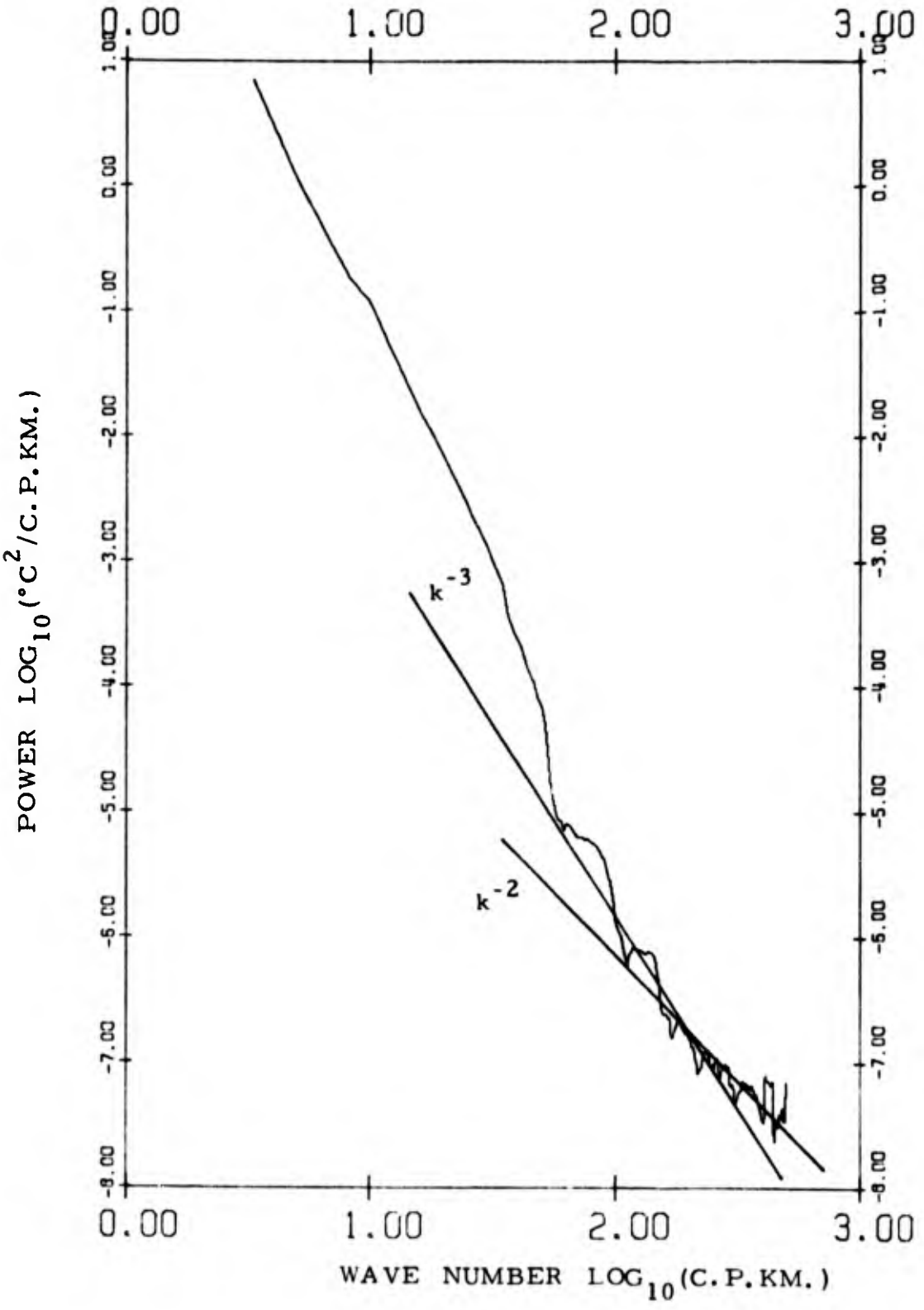

FIG. 12-4. Wave number spectra of temperature perturbations corrected for binomial filtering.
Depth interval 600-1200 meters.
Station 10.

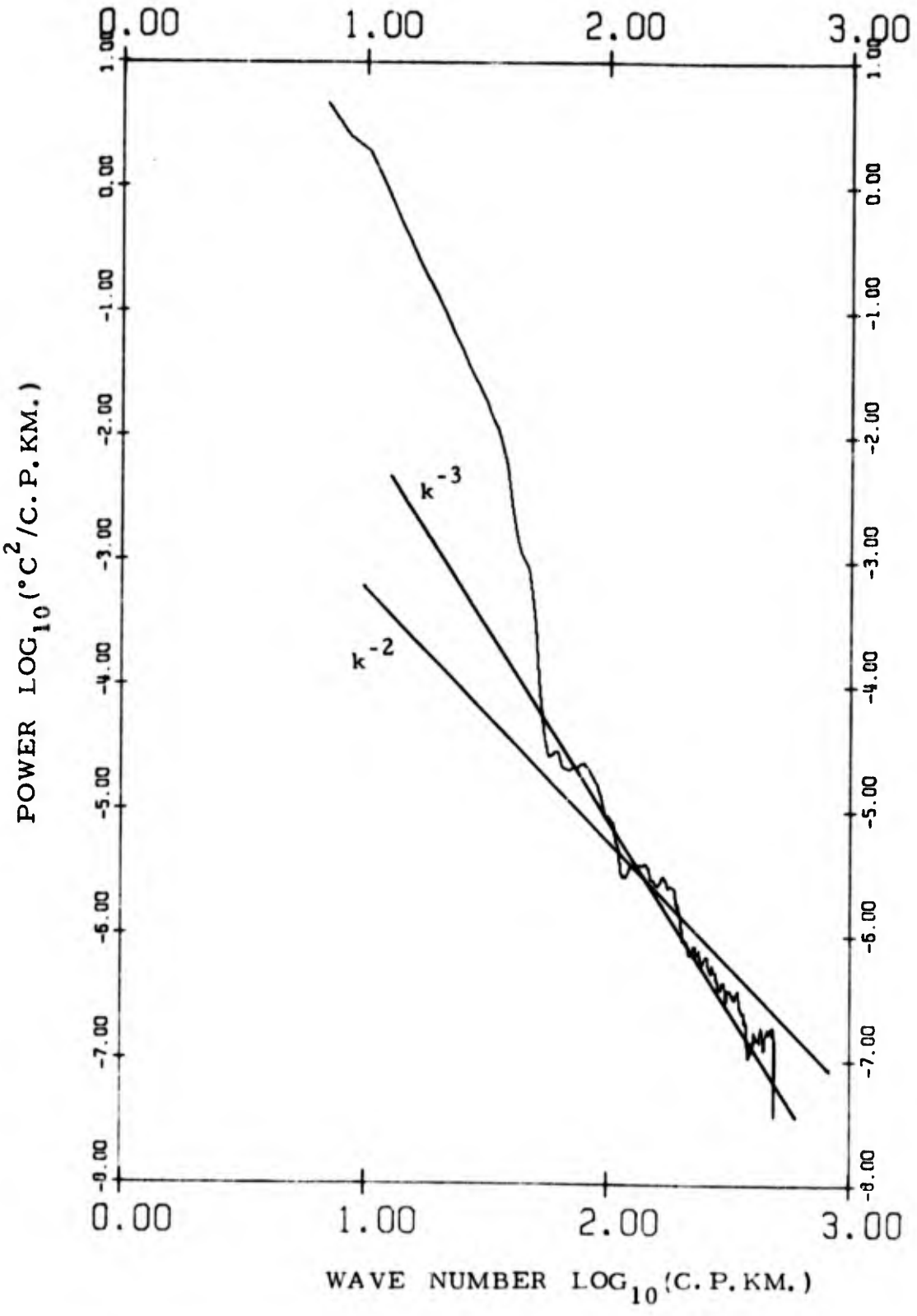

FIG. 12-5. Wave number spectra of temperature perturbations corrected for binomial filtering.
Depth interval 0 - 600 meters.
Station 11.

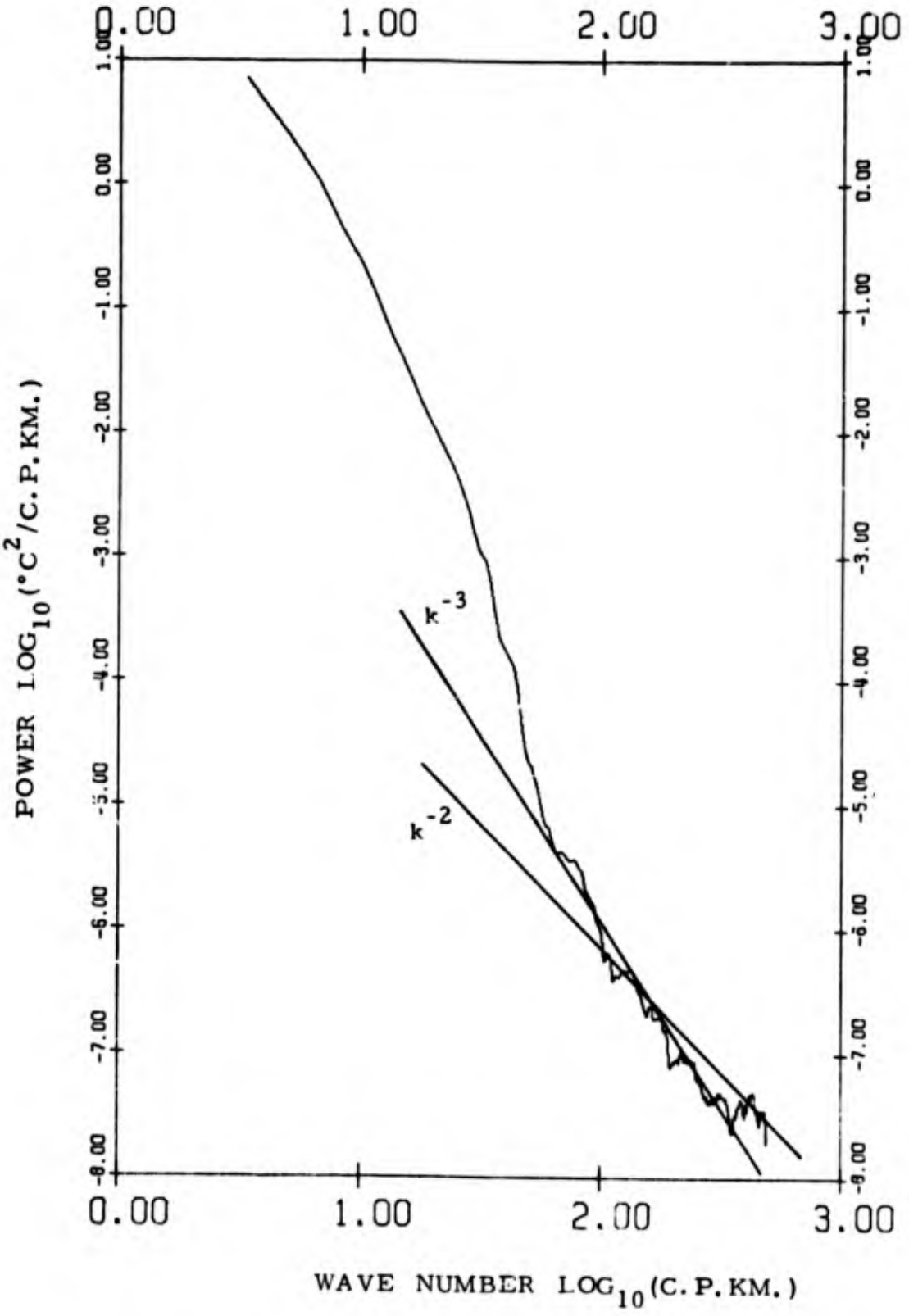

FIG. 12-6. Wave number spectra of temperature perturbations corrected for binomial filtering.
Depth interv.l 600-1200 meters.
Station 11.

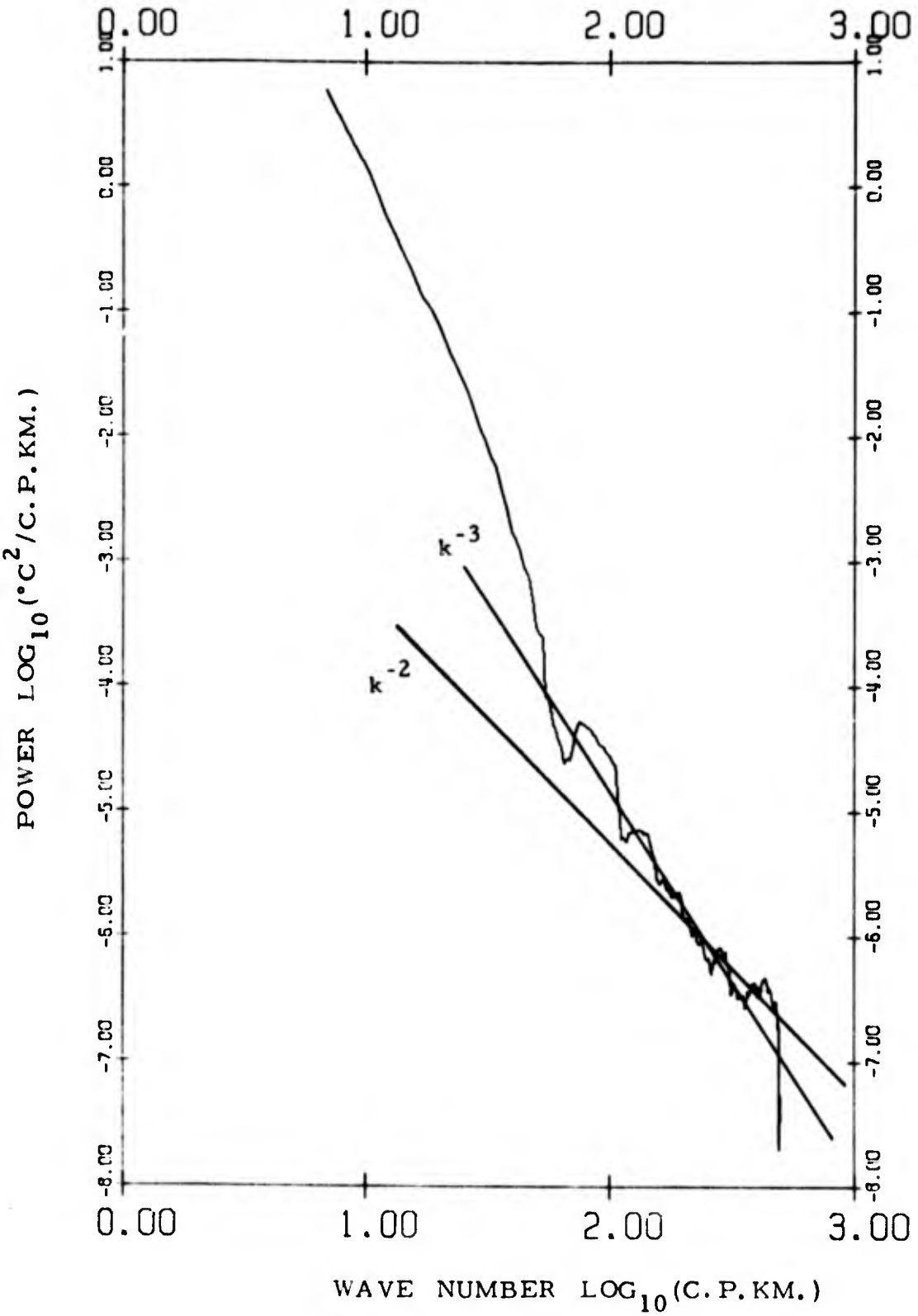

FIG. 12-7. Wave number spectra of temperature perturbations corrected for binomial filtering.
Depth interval 0 - 600 meters.
Station 15.

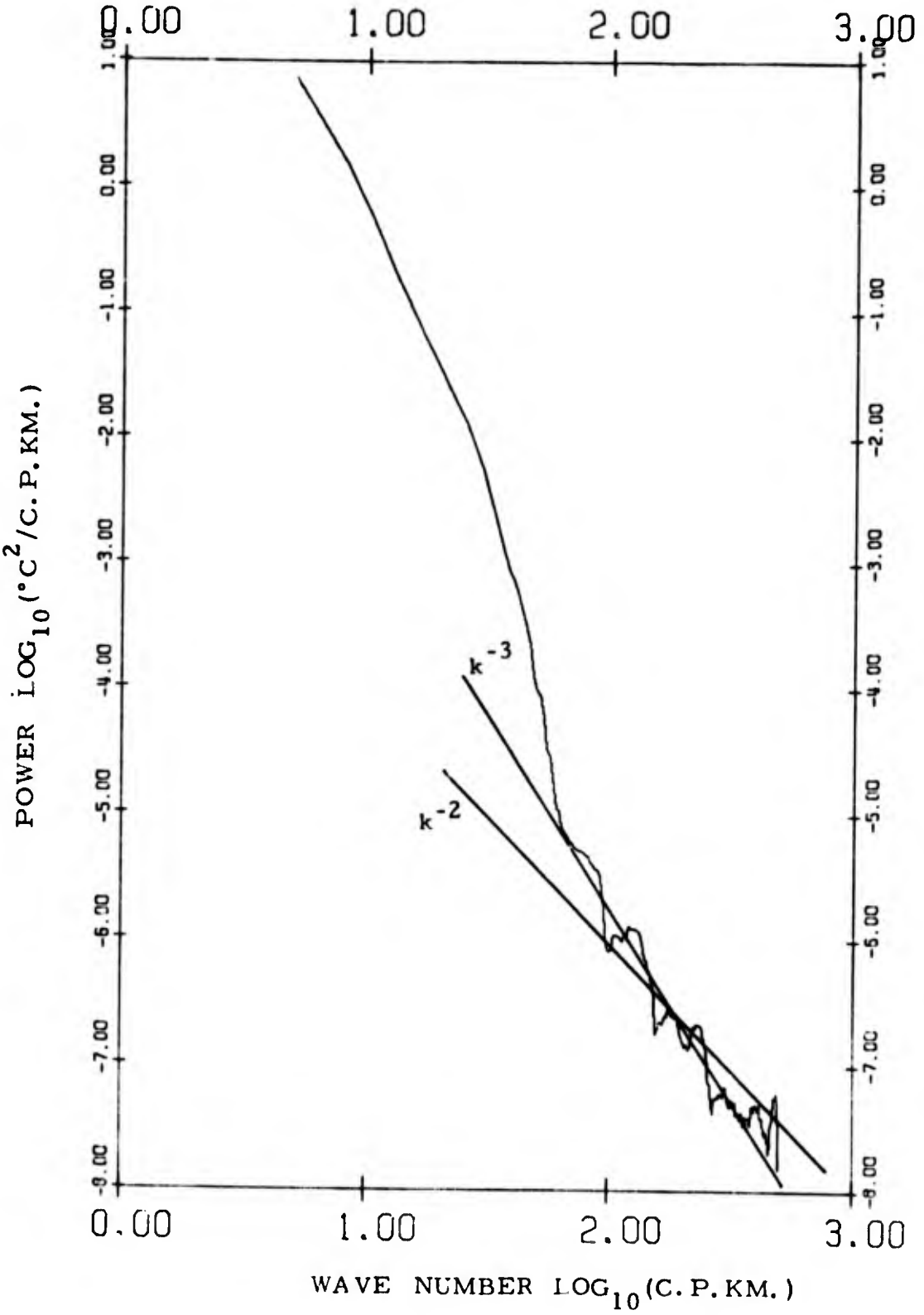

FIG. 12-8. Wave number spectra of temperature perturbations corrected for binomial filtering. Depth interval 600-1200 meters. Station 15.

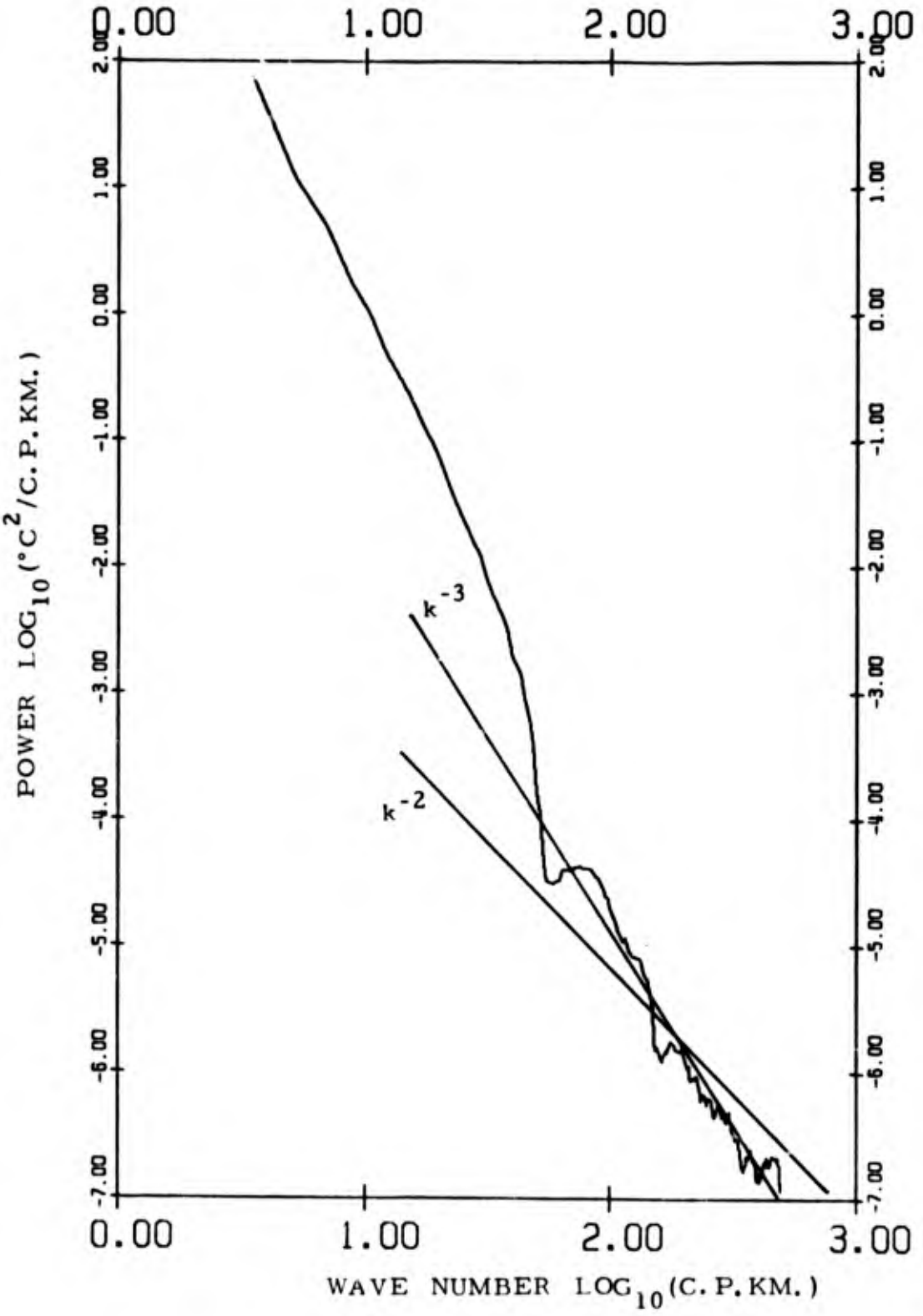

FIG. 12-9. Wave number spectra of temperature perturbations corrected for binomial filtering.
Depth interval 0 - 600 meters.
Station 16.

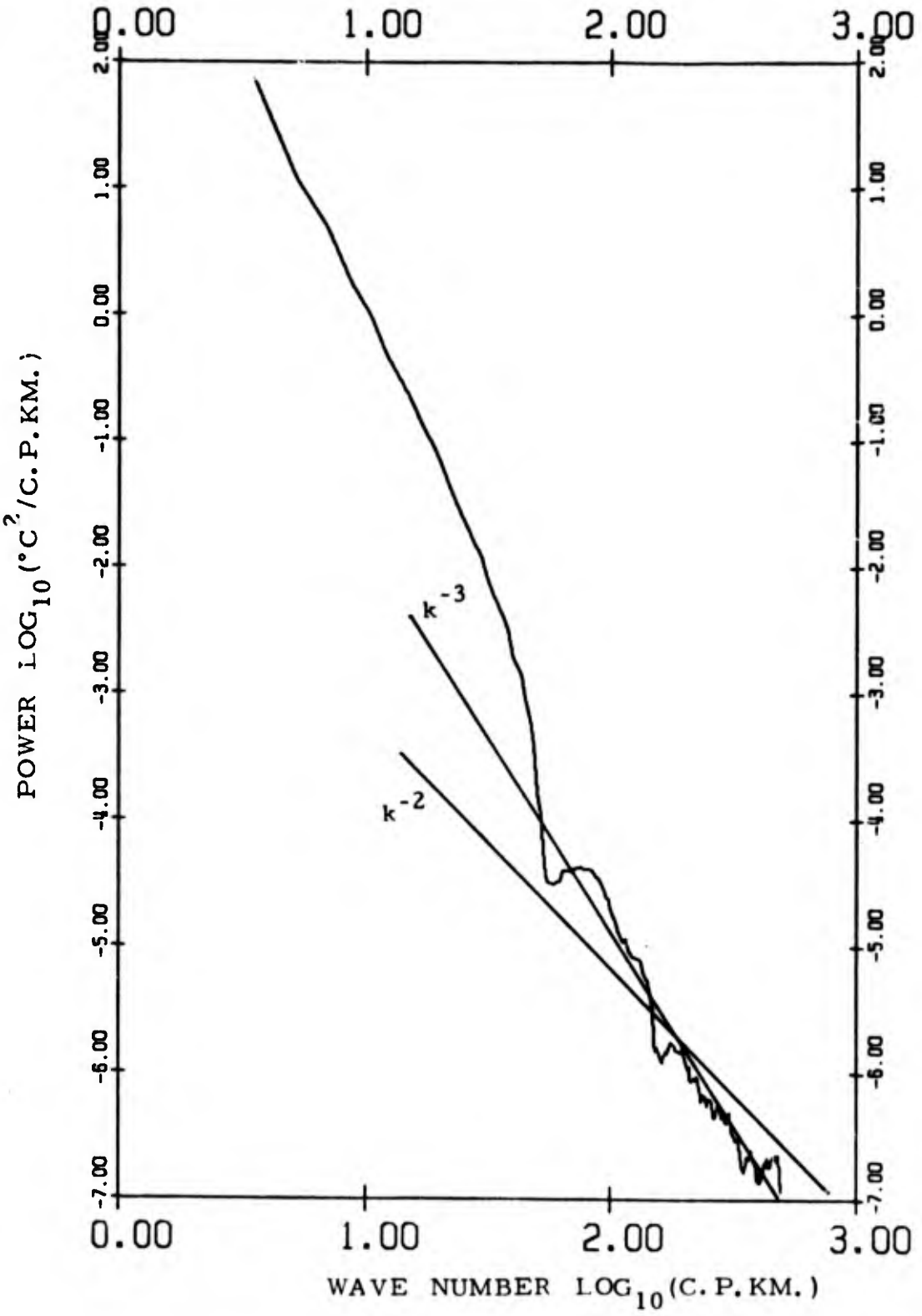

FIG. 12-9. Wave number spectra of temperature perturbations corrected for binomial filtering.
Depth interval 0 - 600 meters.
Station 16.

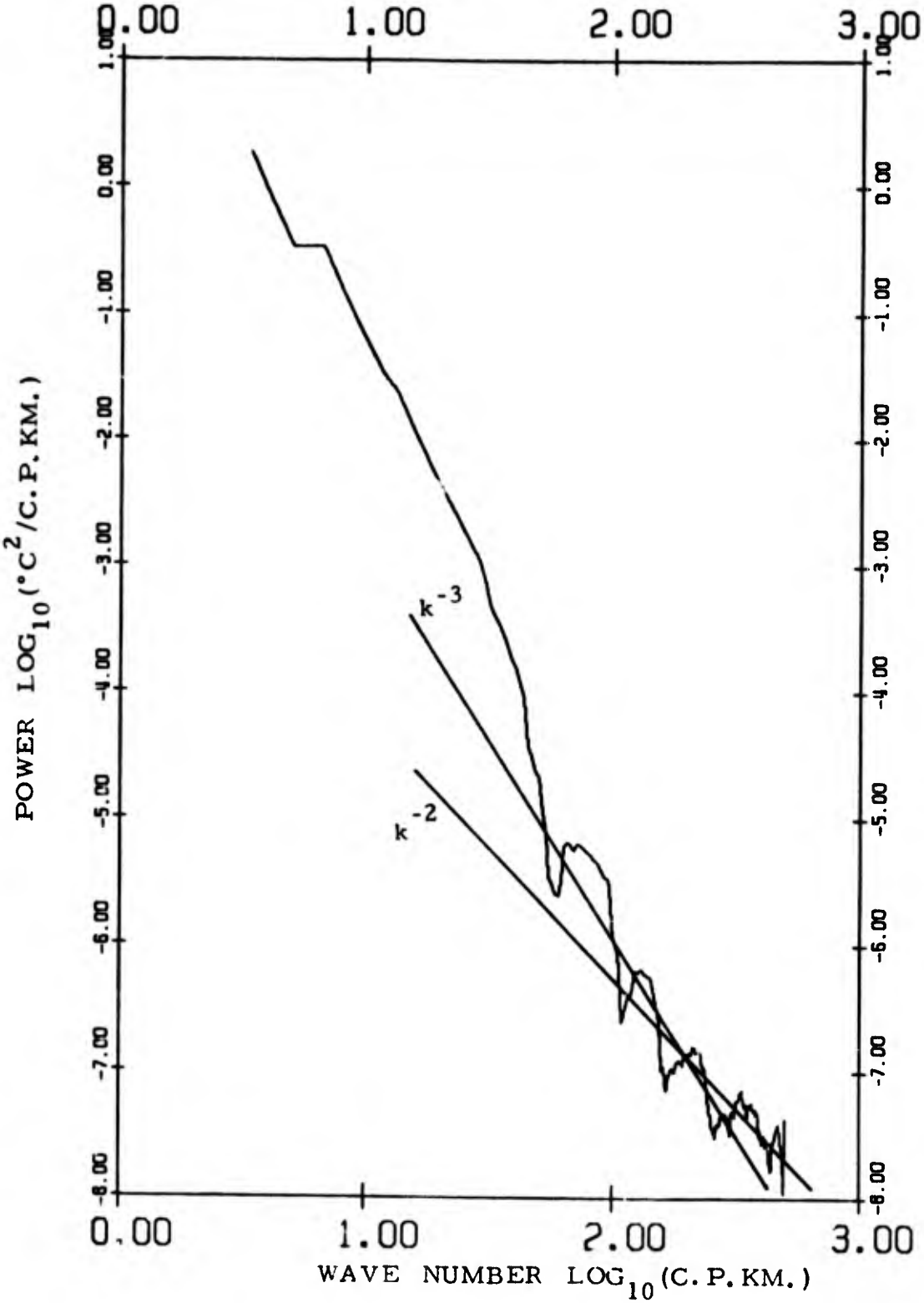

FIG. 12-10. Wave number spectra of temperature perturbations corrected for binomial filtering.
Depth interval 600-1200 meters.
Station 16.

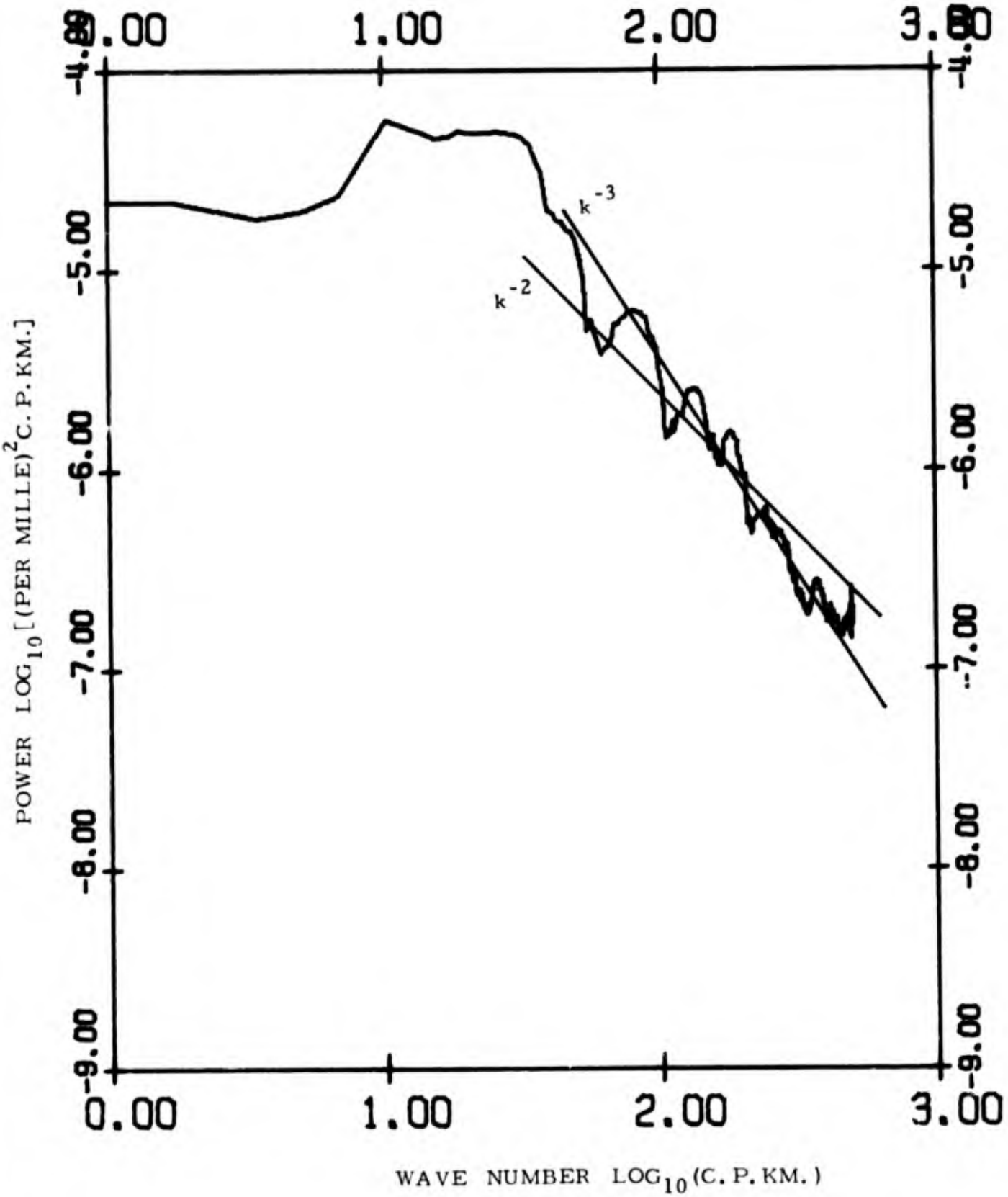

FIG. 13-1. Wave number spectra of salinity perturbations.
Depth interval 0-600 meters.
Station 9.

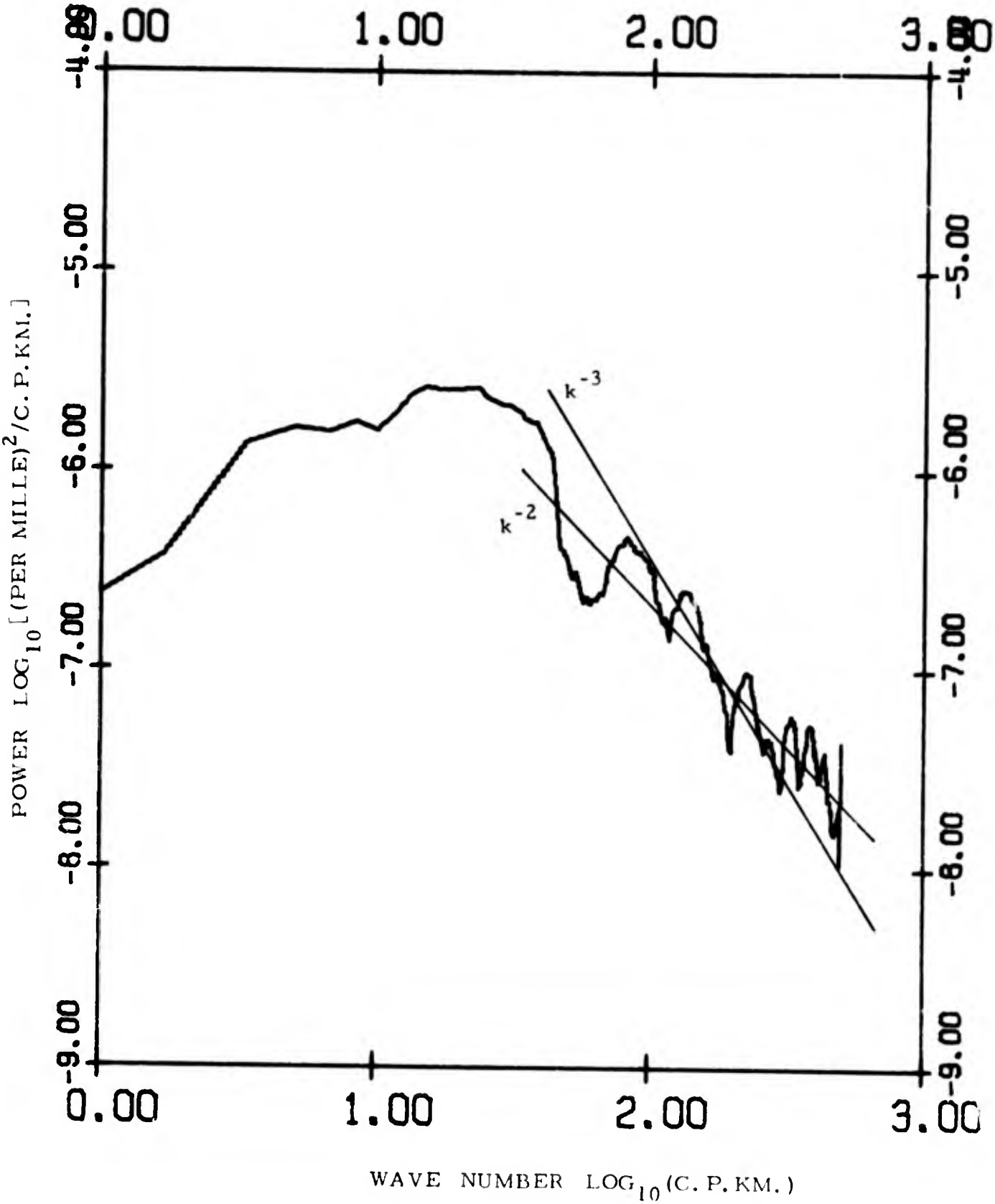

FIG. 13-2. Wave number spectra of salinity perturbations.
Depth interval 600-1200 meters.
Station 9.

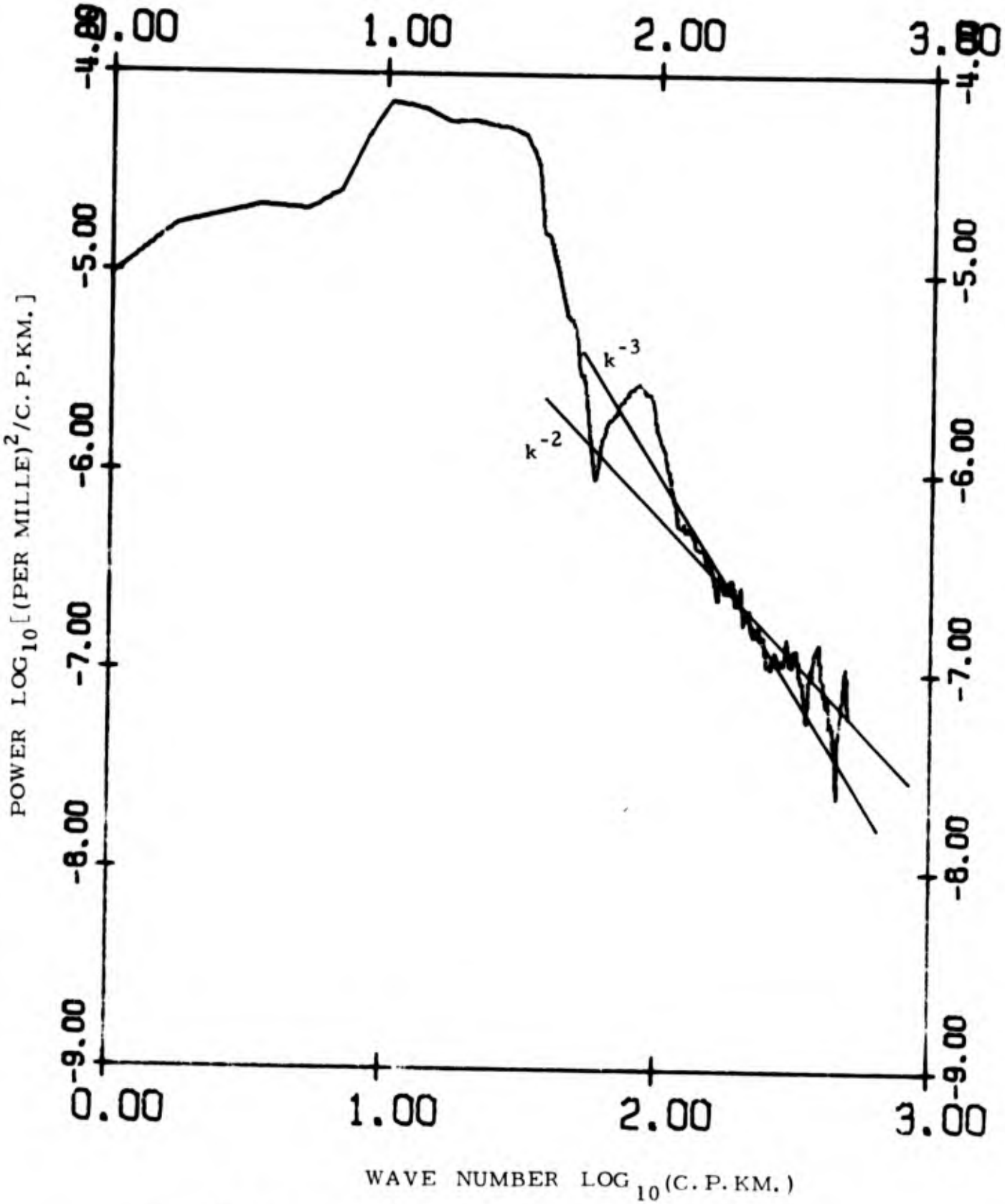

FIG. 13-3. Wave number spectra of salinity perturbations.
Depth interval 0-600 meters.
Station 10.

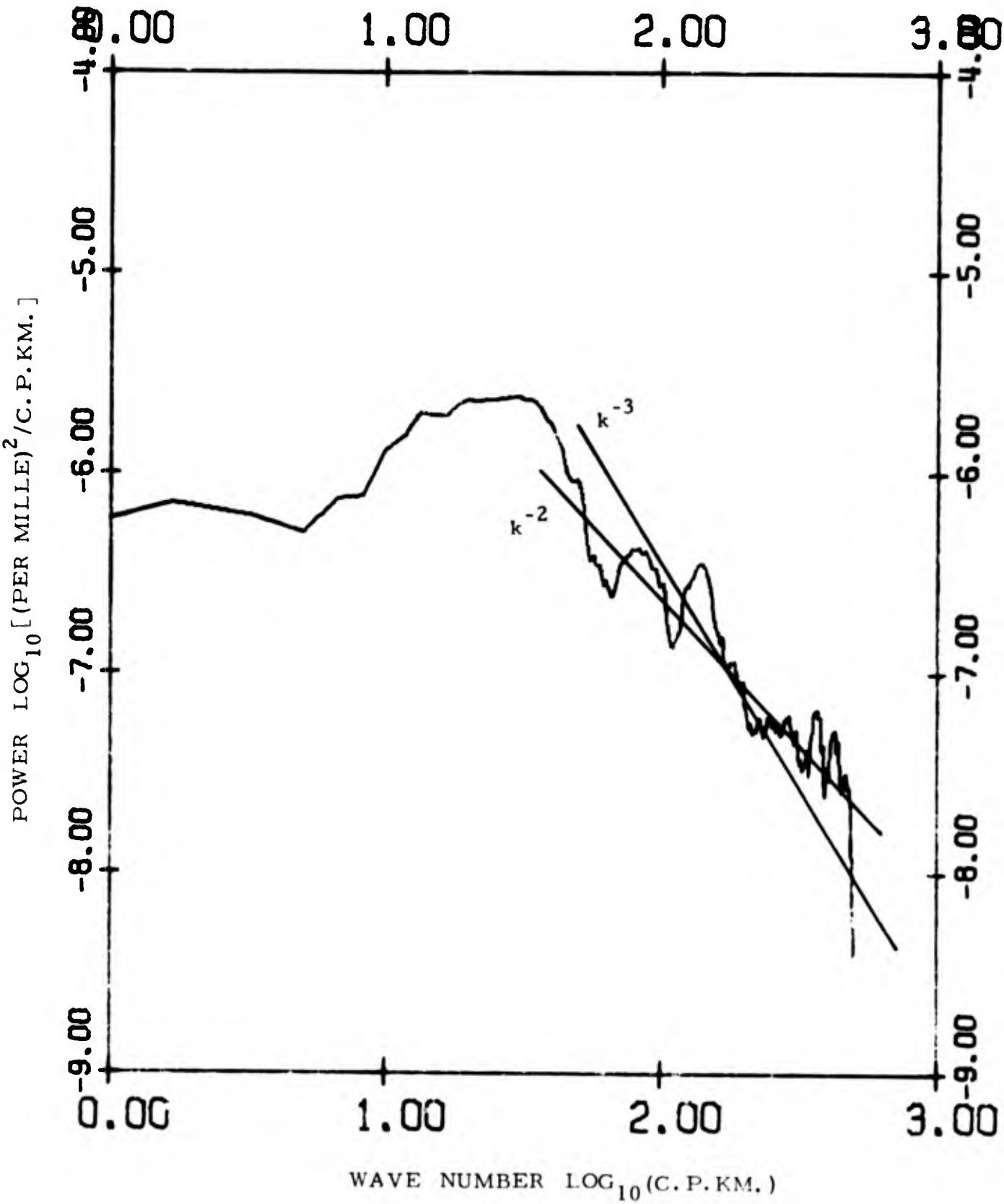

FIG. 13-4. Wave number spectra of salinity perturbations.
Depth interval 600-1200 meters.
Station 10.

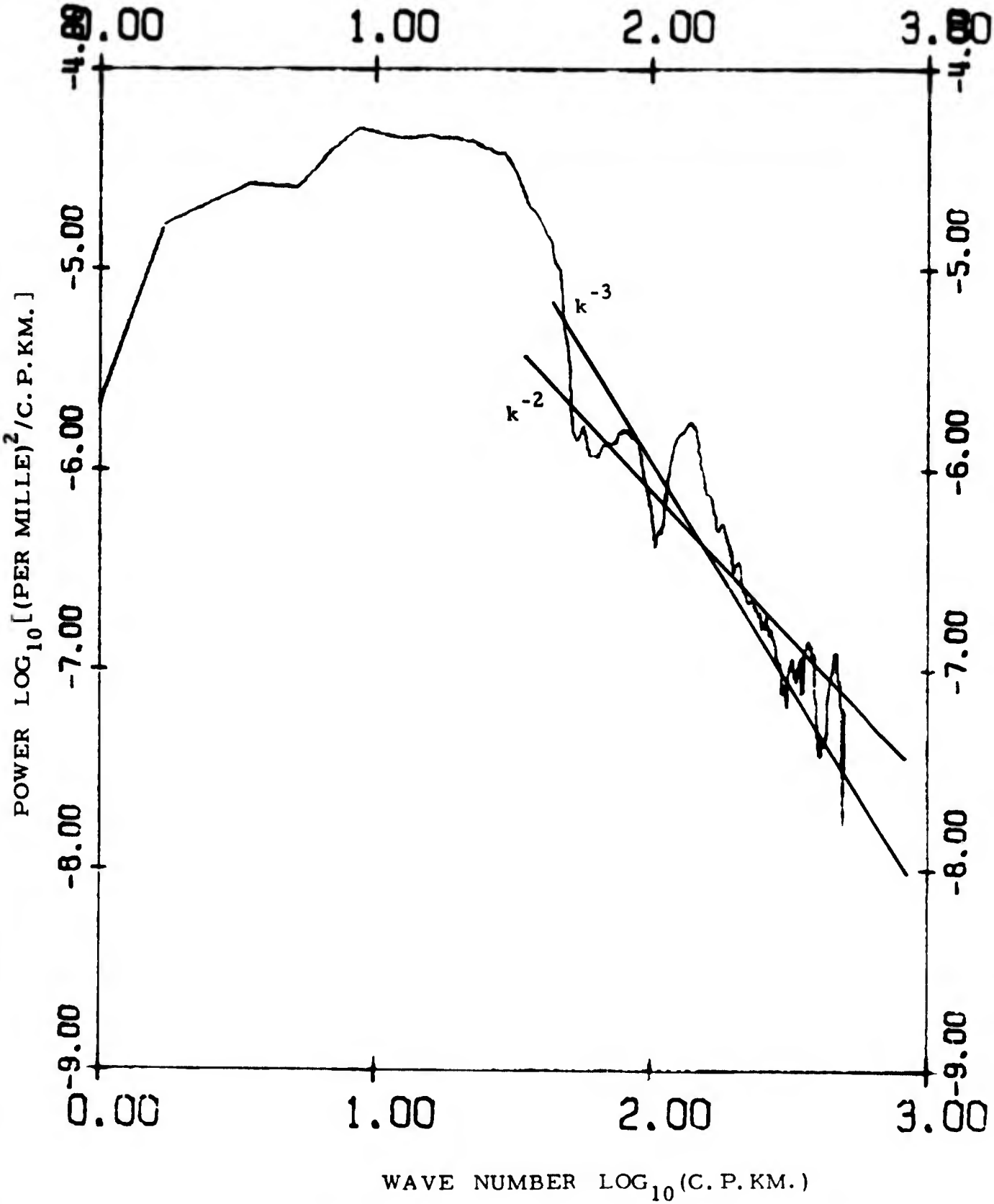

FIG. 13-5. Wave number spectra of salinity perturbations.
Depth interval 0-600 meters.
Station 11.

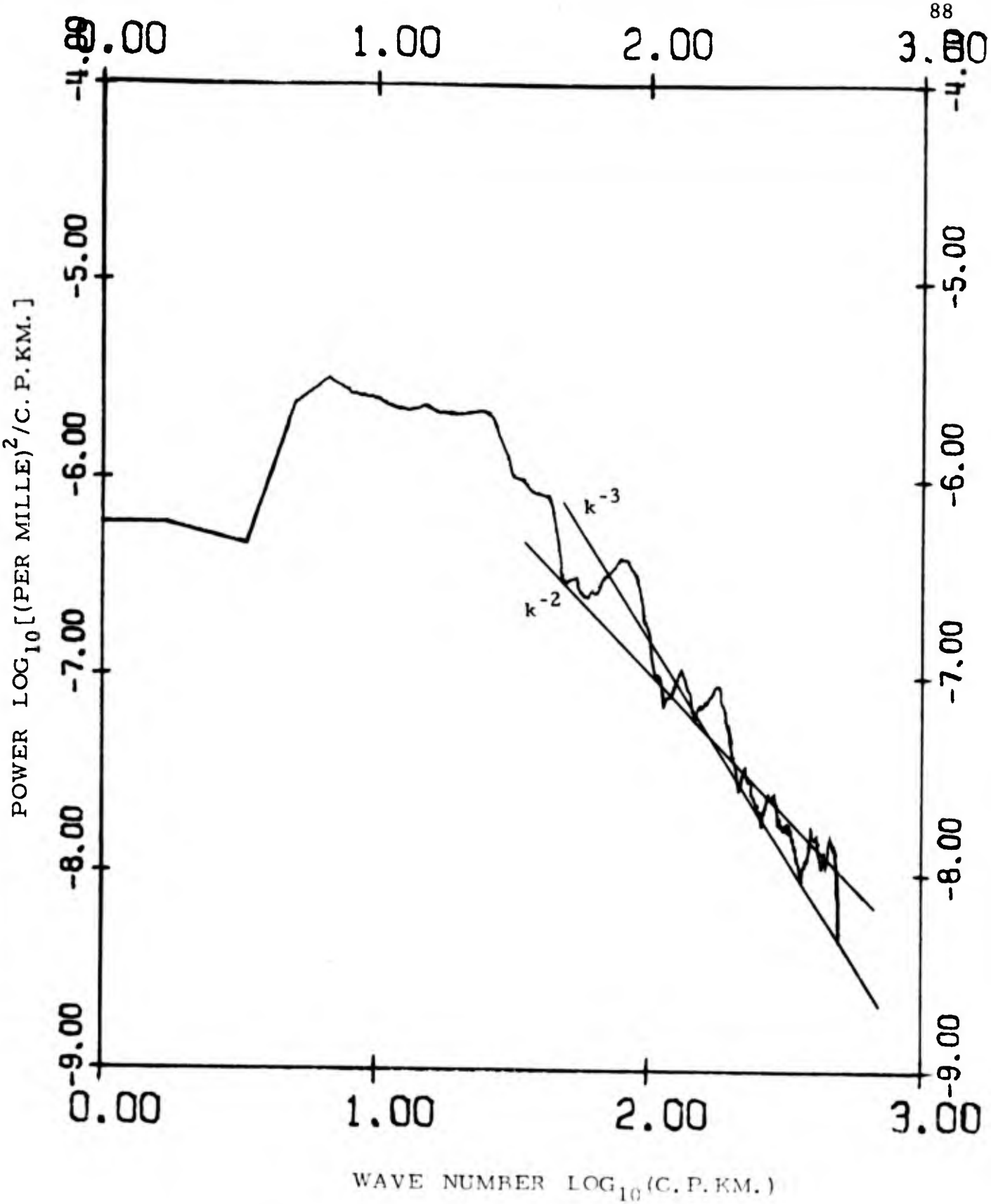

FIG. 3-6. Wave number spectra of salinity perturbations.
Depth interval 600-1200 meters.
Station 11.

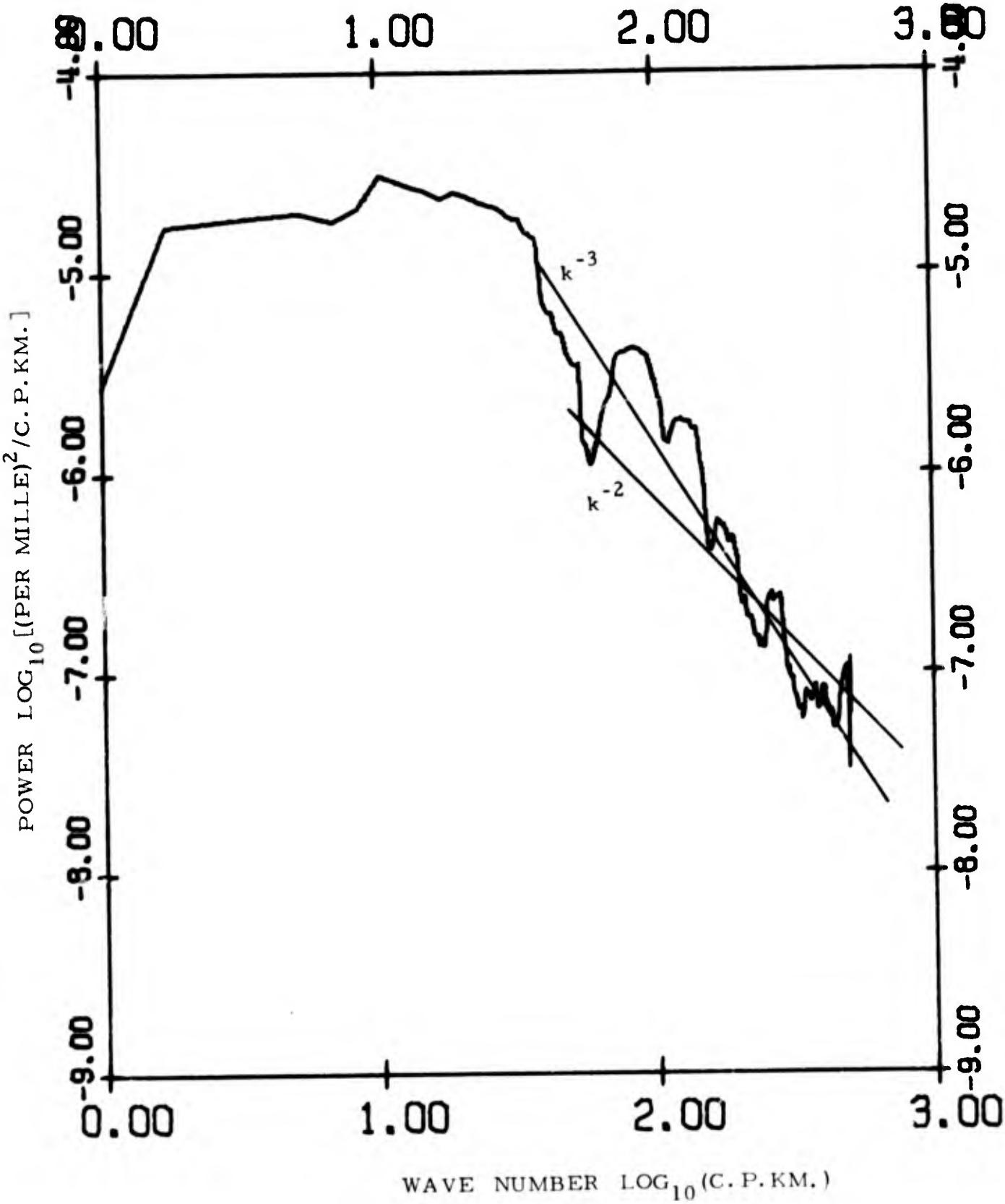

FIG. 13-7. Wave number spectra of salinity perturbations.
Depth interval 0-600 meters.
Station 15.

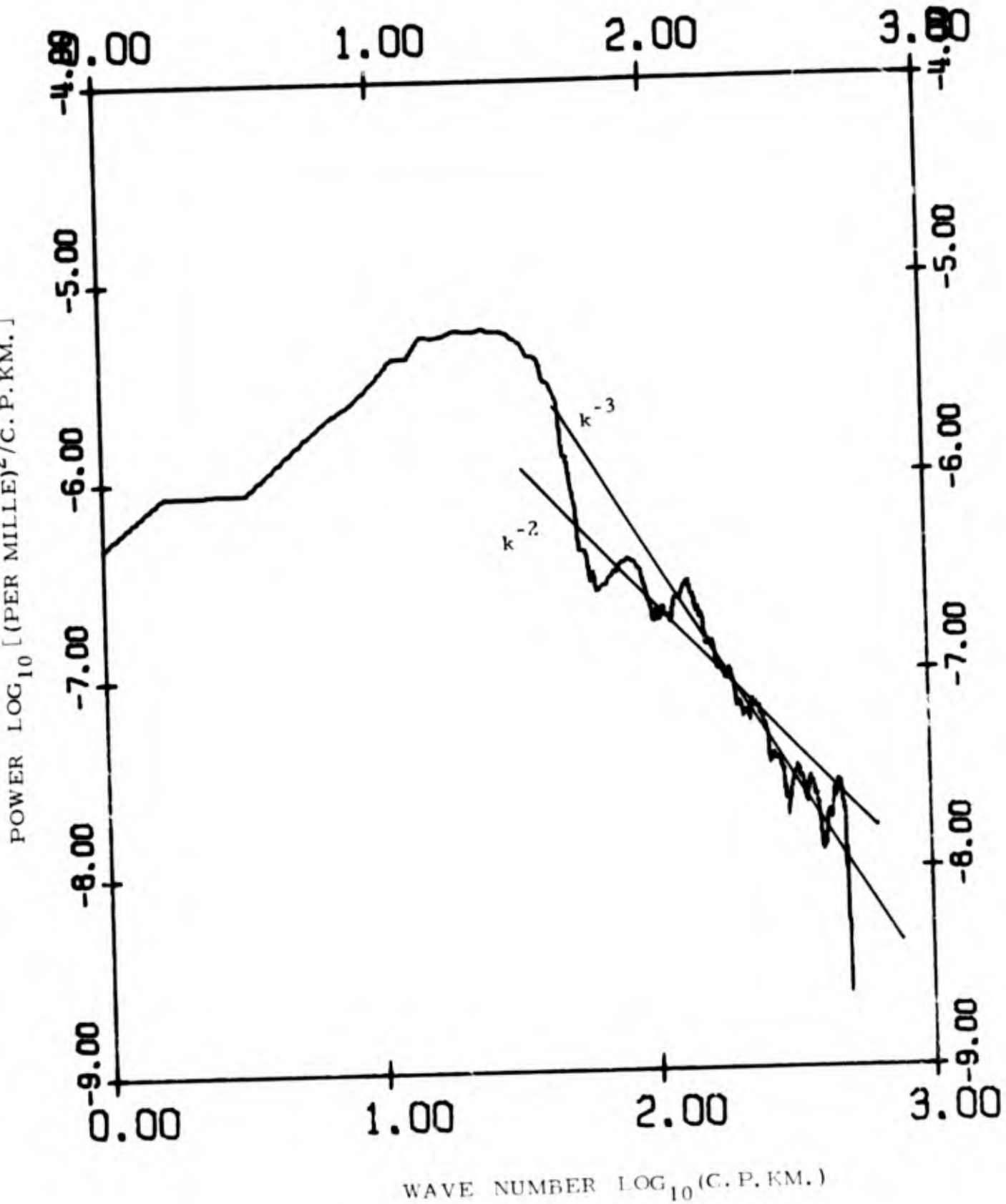

FIG. 13-8. Wave number spectra of salinity perturbations.
Depth interval 600-1200 meters.
Station 15.

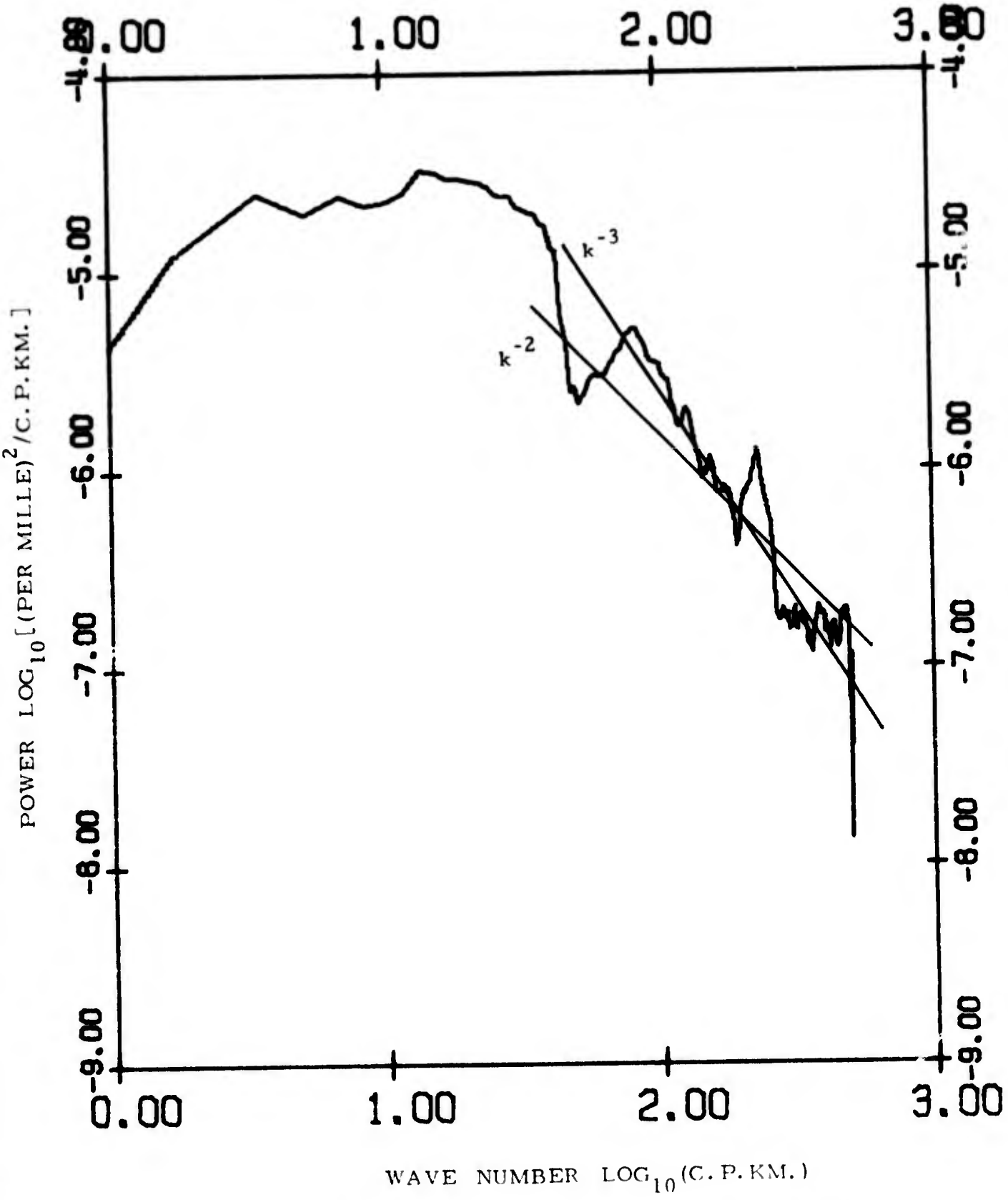

FIG. 13-9. Wave number spectra of salinity perturbations.
Depth interval 0-600 meters.
Station 16.

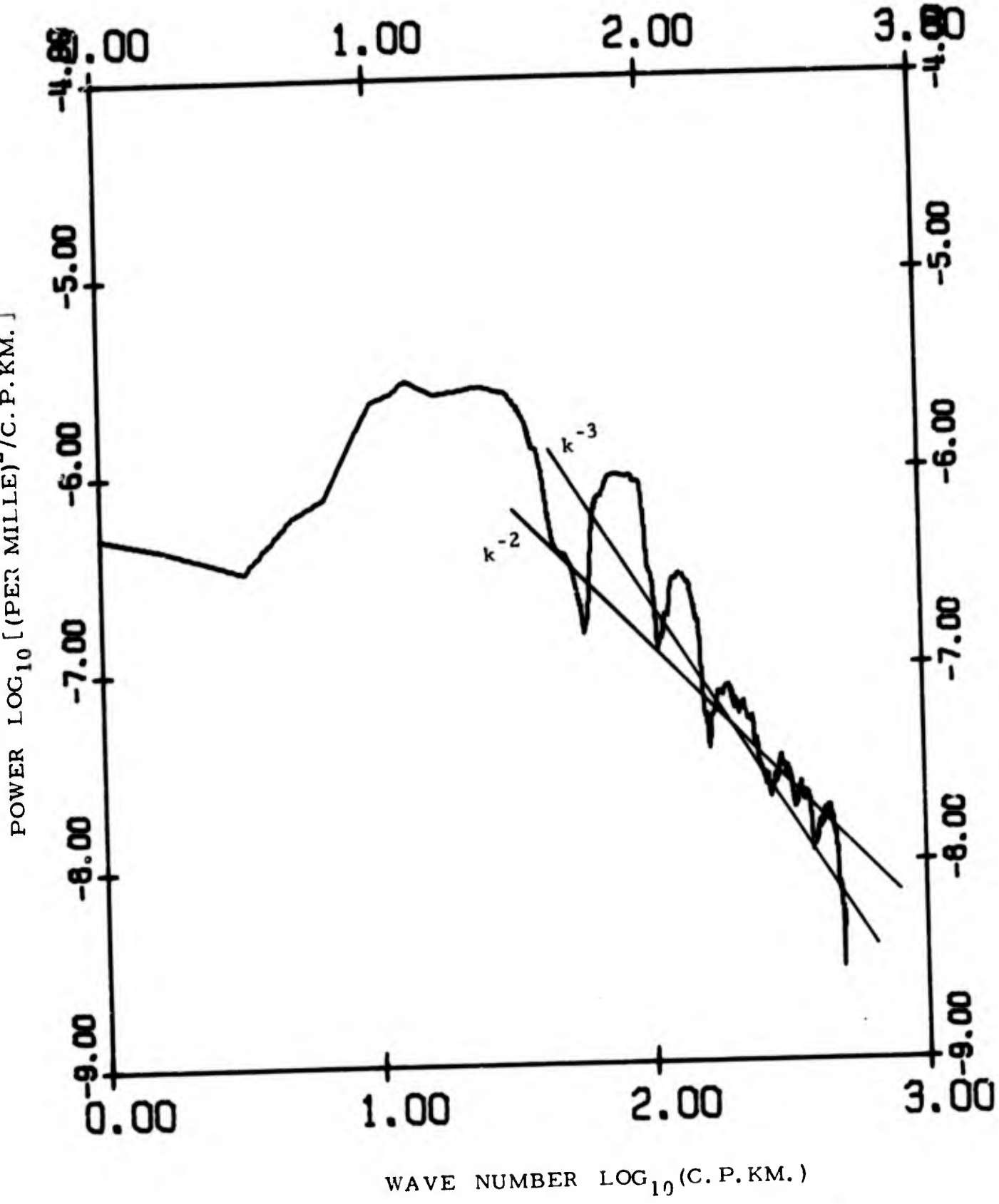

Fig. 13-10. Wave number spectra of salinity perturbations.
Depth interval 600-1200 meters.
Station 16.

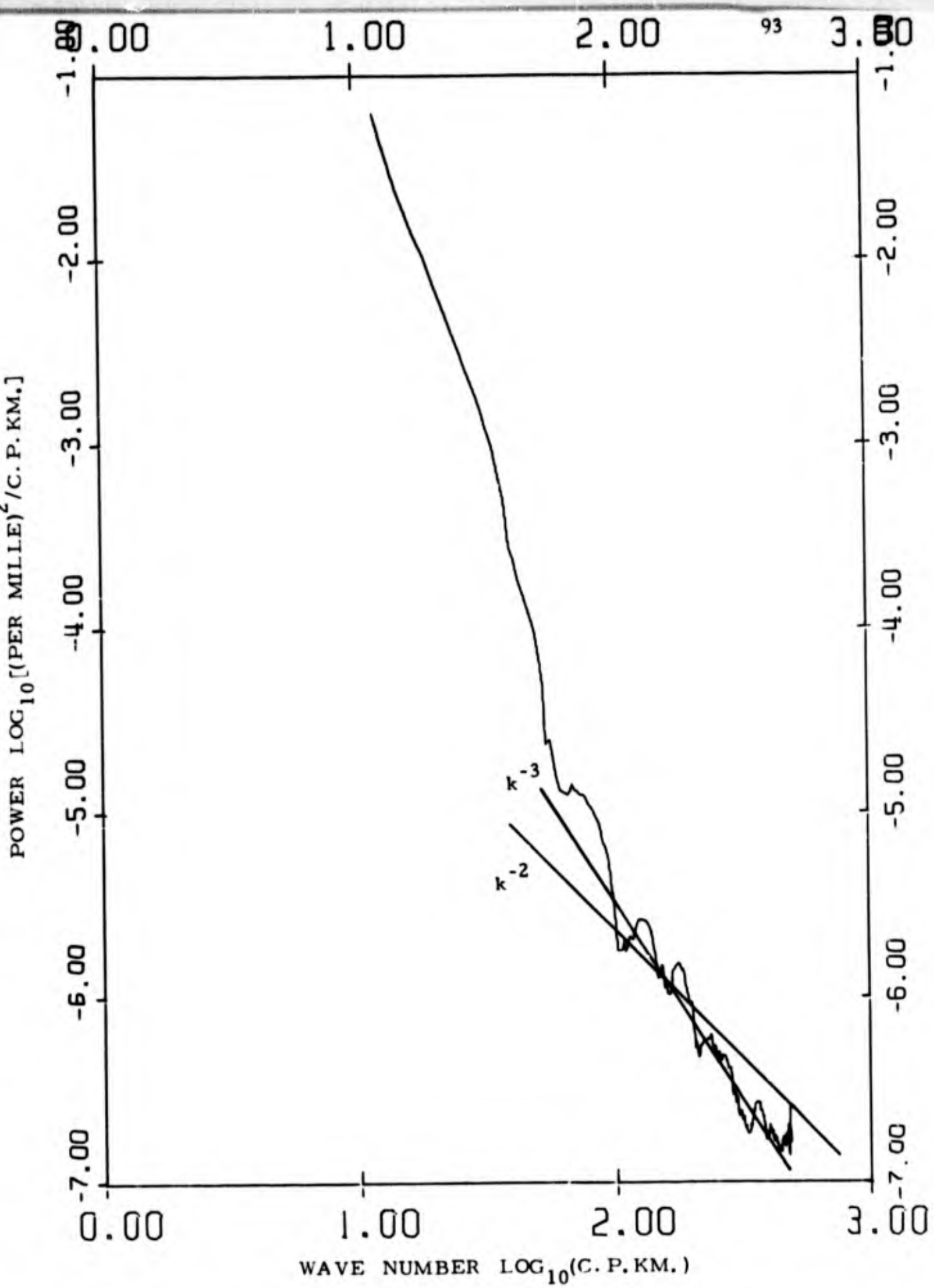

FIG. 14-1. Wave number spectra of salinity perturbations corrected for binomial filtering.
Depth interval 0 - 600 meters.
Station 9.

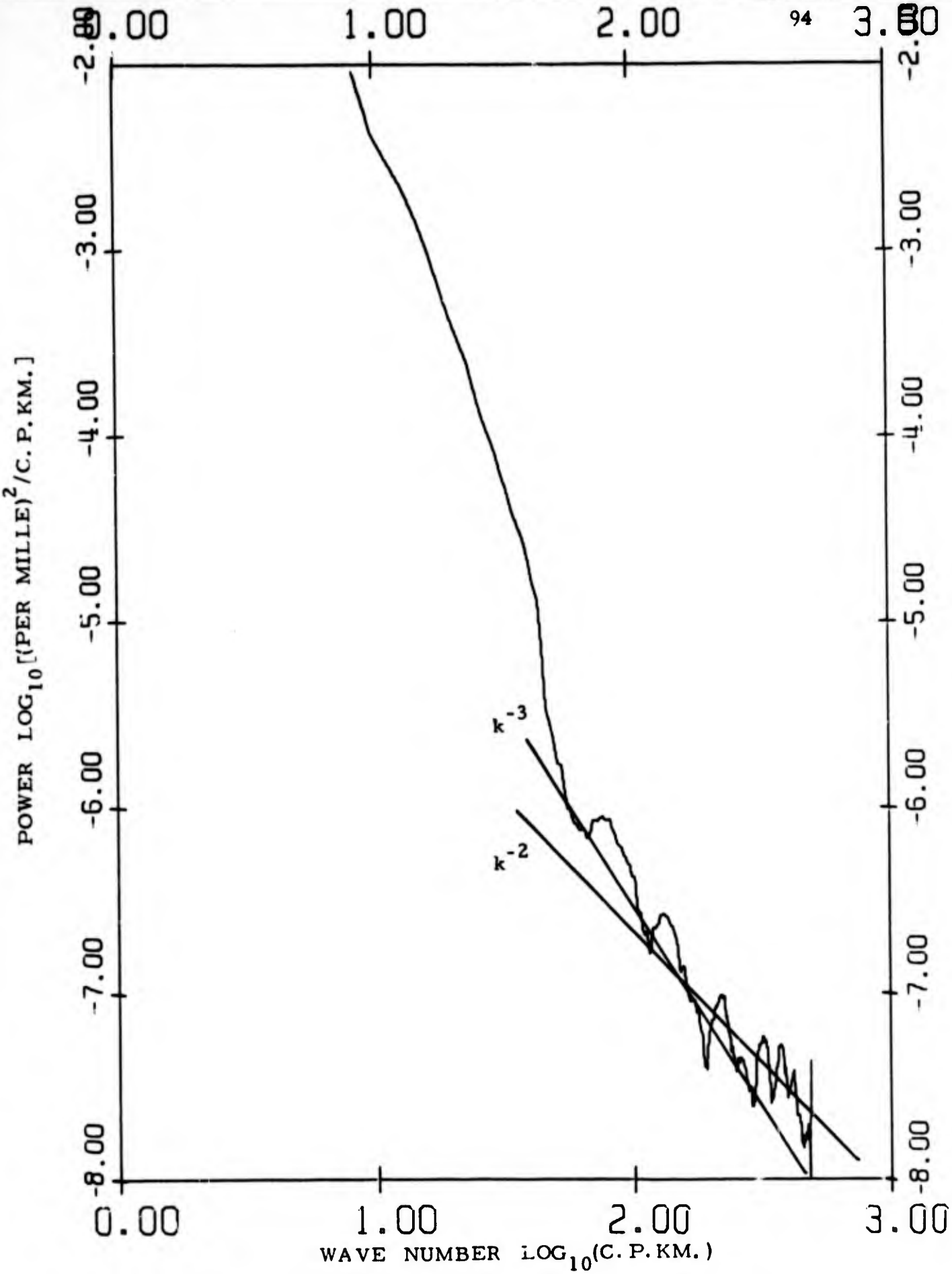

FIG. 14-2. Wave number spectra of salinity perturbations corrected for binomial filtering.
Depth interval 600-1200 meters.
Station 9.

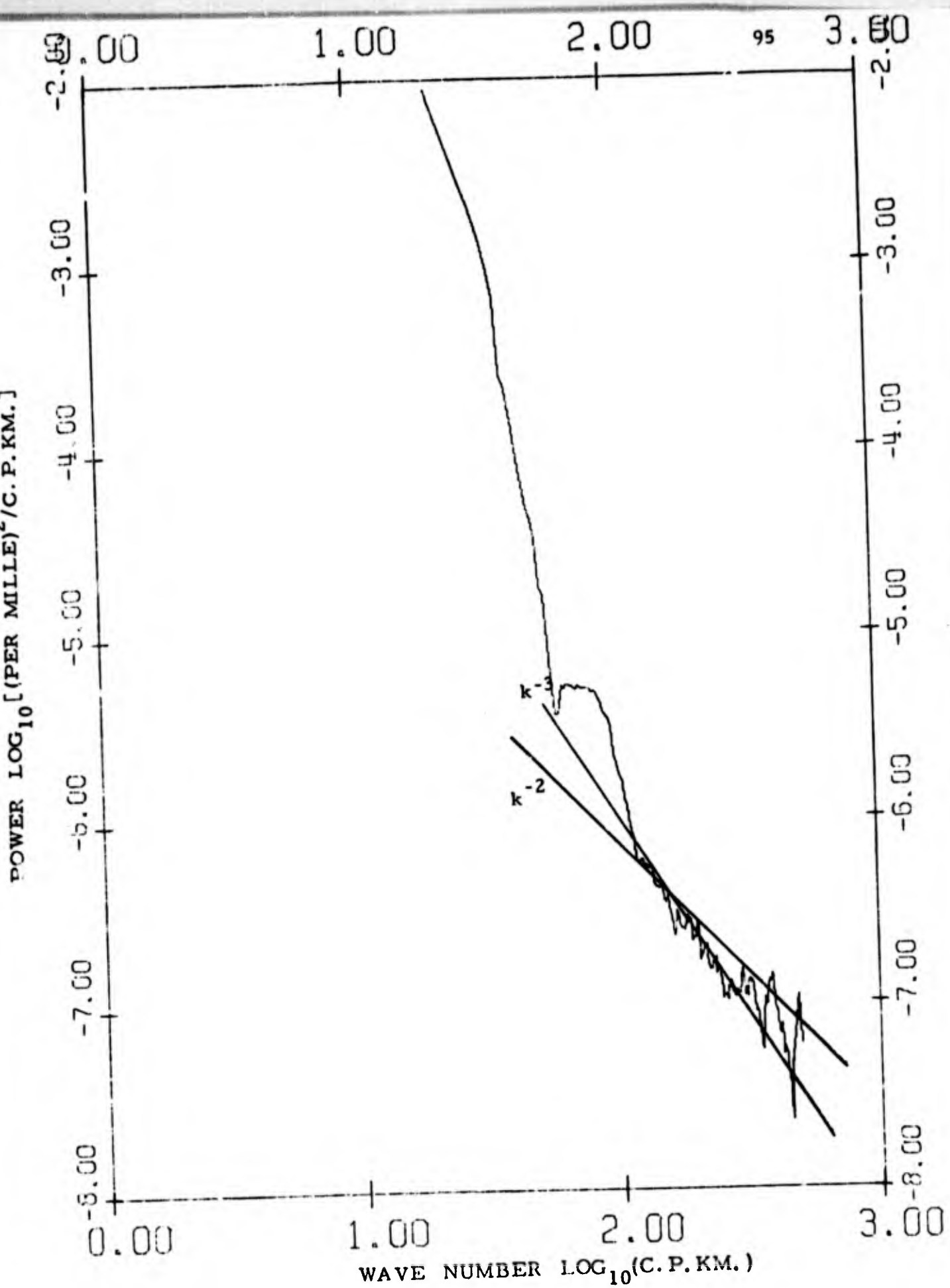

FIG. 14-3. Wave number spectra of salinity perturbations corrected for binomial filtering.
Depth interval 0 - 600 meters.
Station 10.

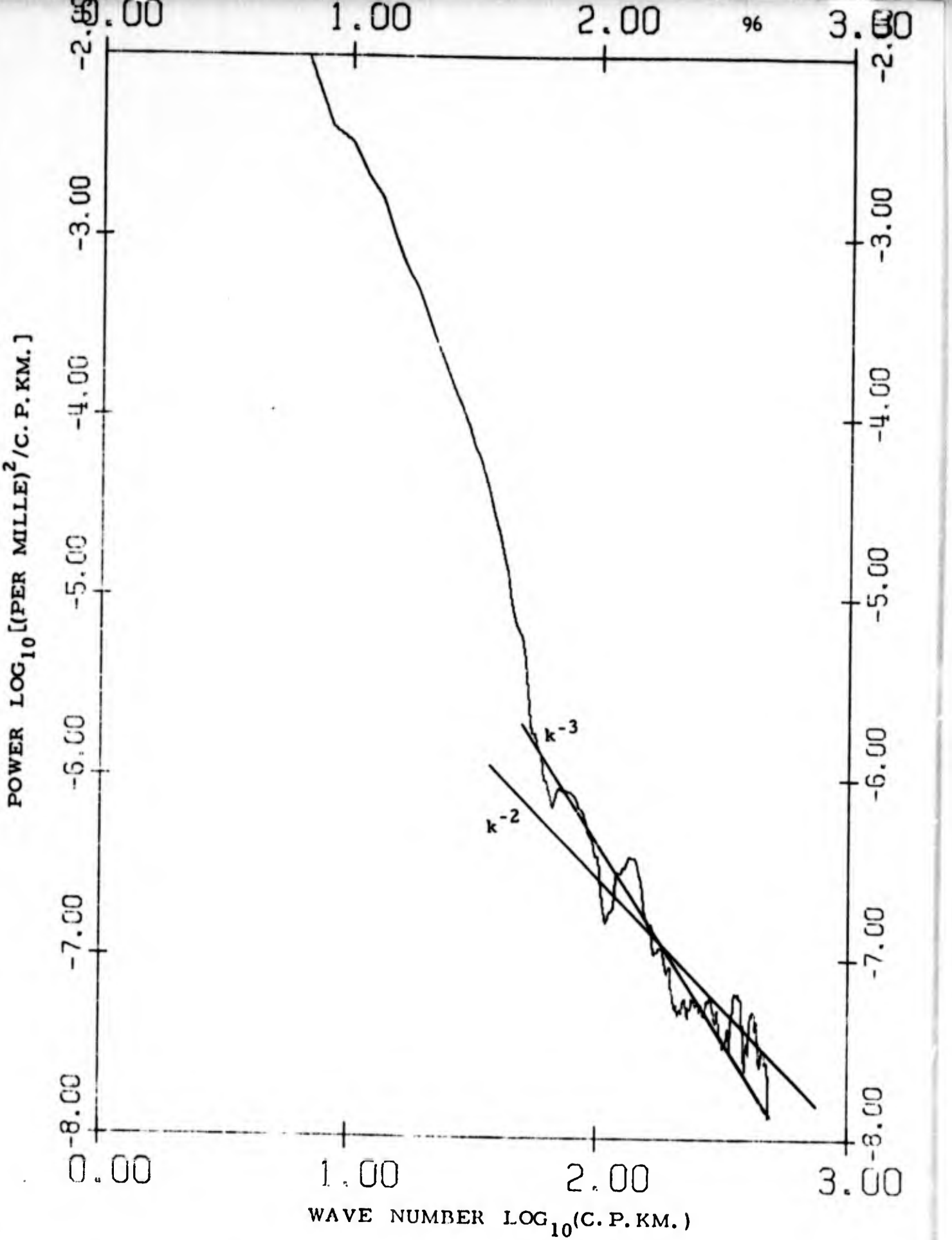

FIG. 14-4. Wave number spectra of salinity perturbations corrected for binomial filtering.
Depth interval 600-1200 meters.
Station 10.

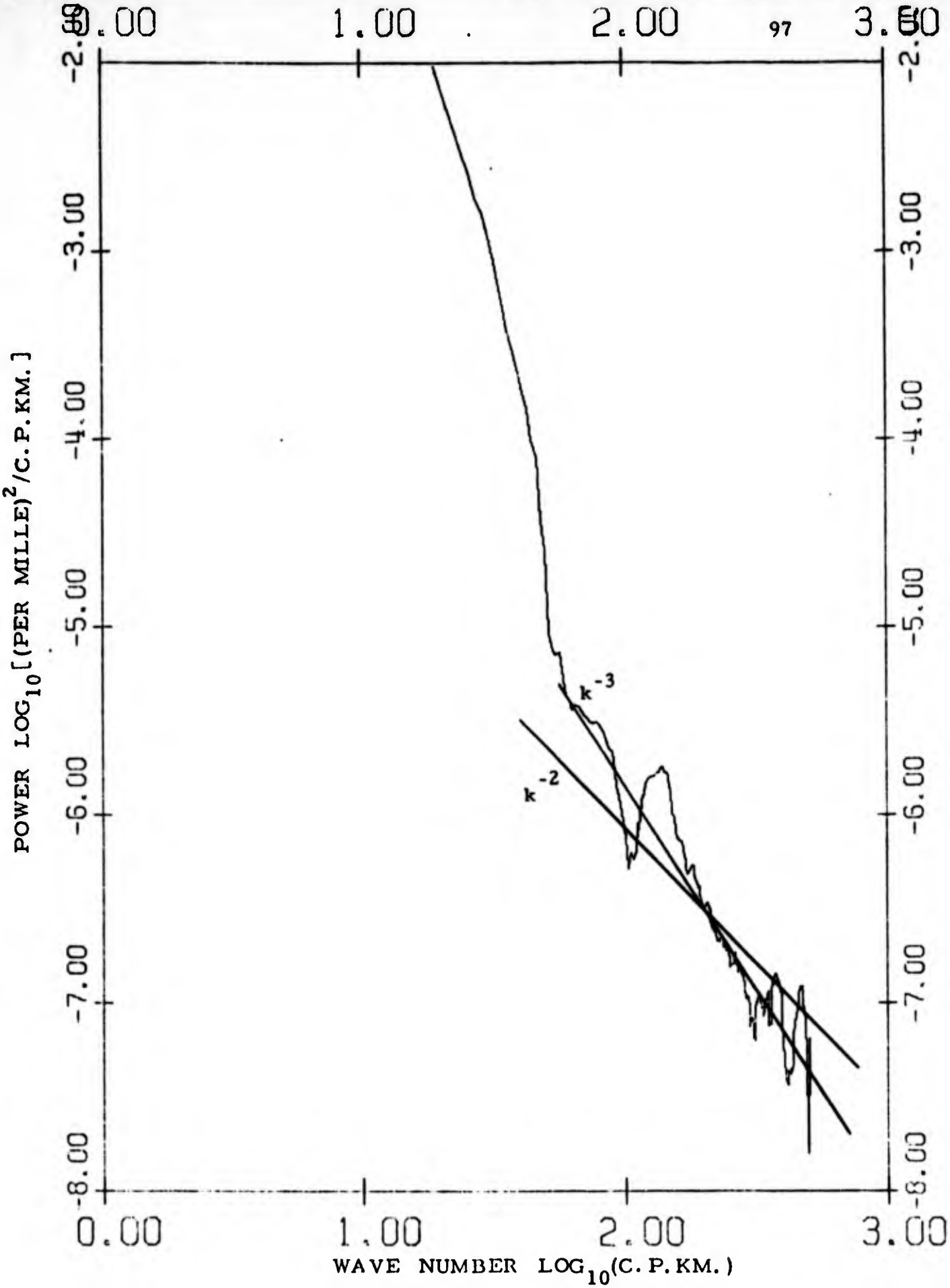

FIG. 14-5. Wave number spectra of salinity perturbations corrected for binomial filtering.
Depth interval 0 - 600 meters
Station 11.

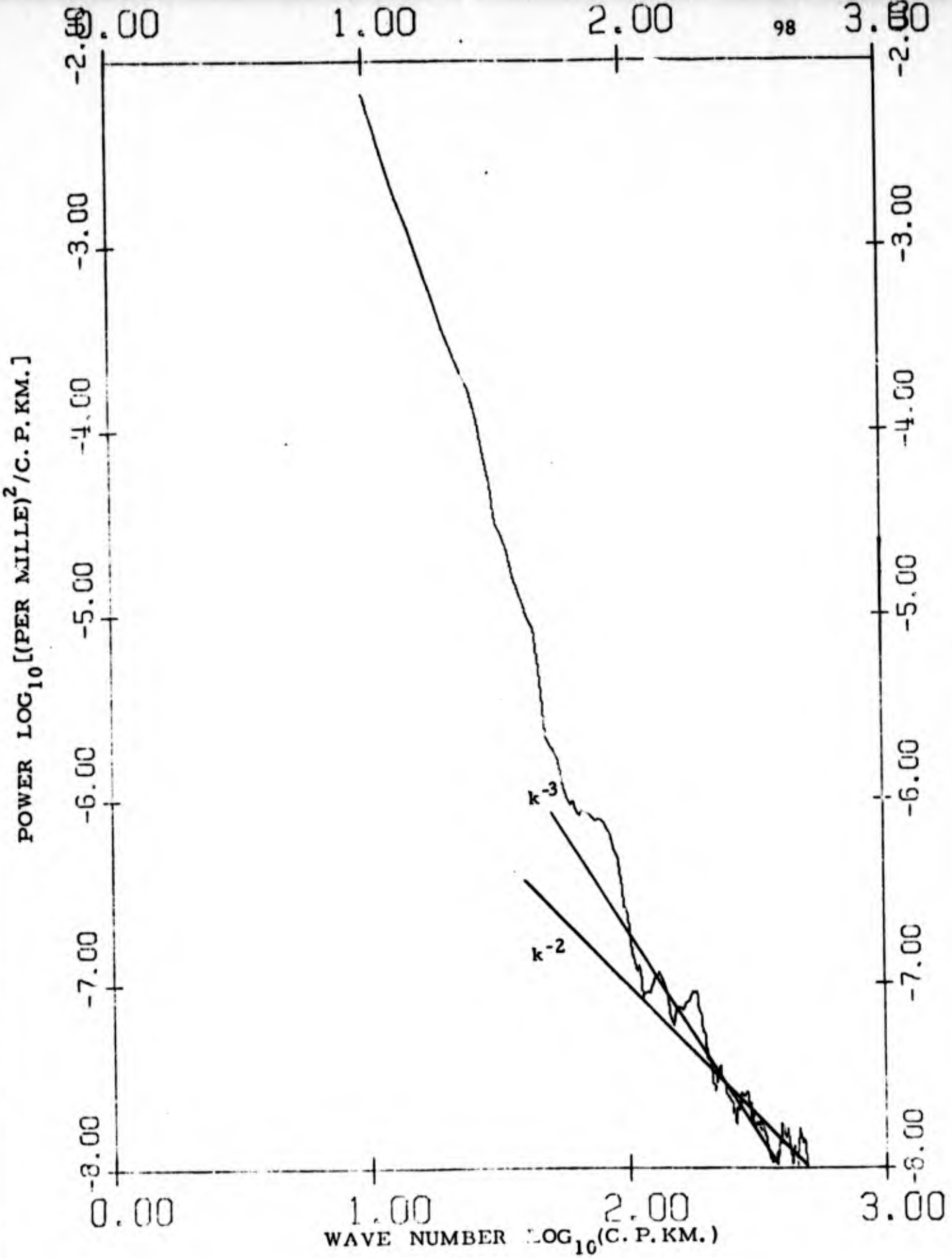

FIG. 14-6. Wave number spectra of salinity perturbations corrected for binomial filtering.
Depth interval 600-1200 meters.
Station 11.

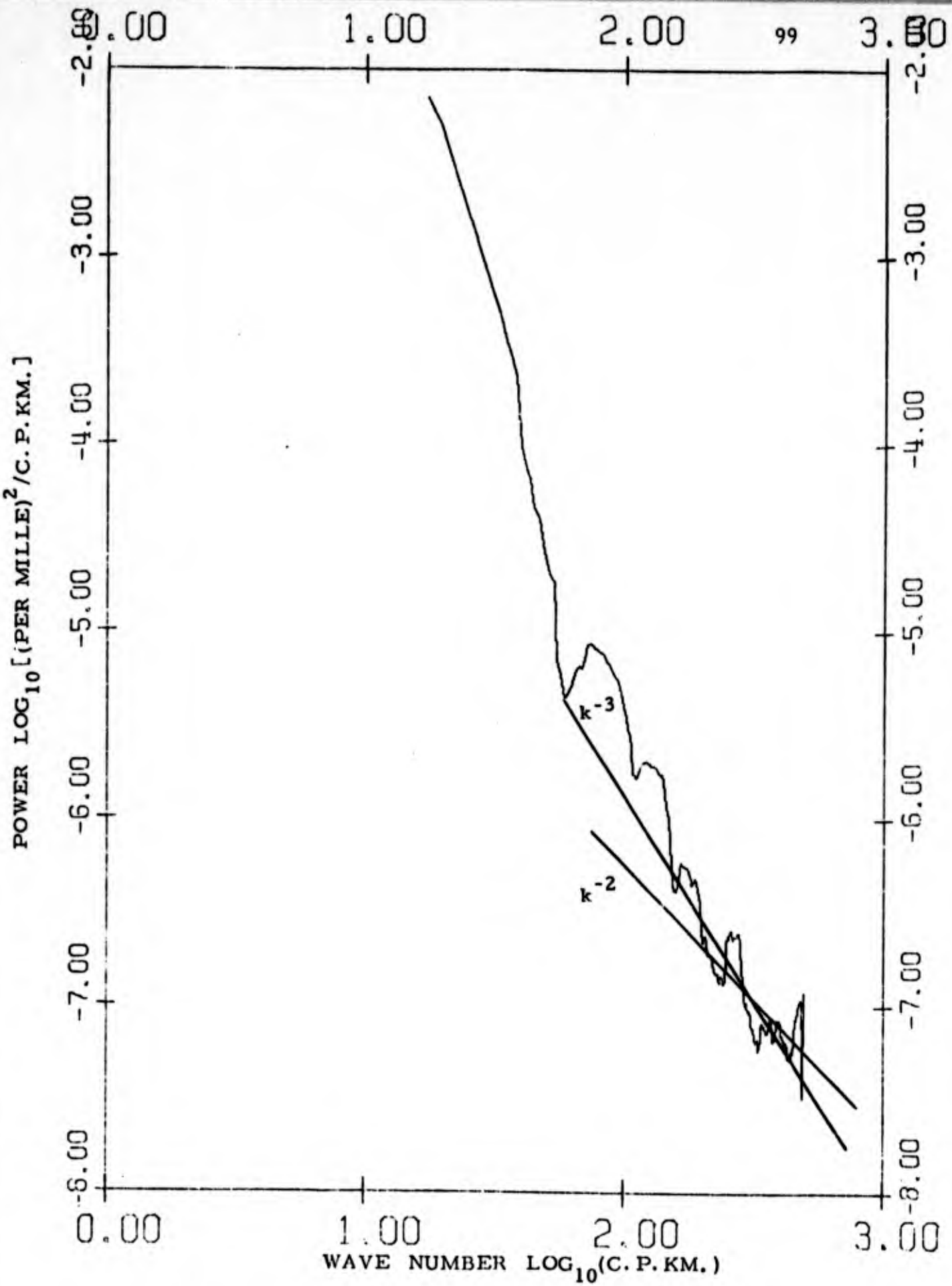

FIG. 14-7. Wave number spectra of salinity perturbations corrected for binomial filtering.
Depth interval 0 - 600 meters.
Station 15.

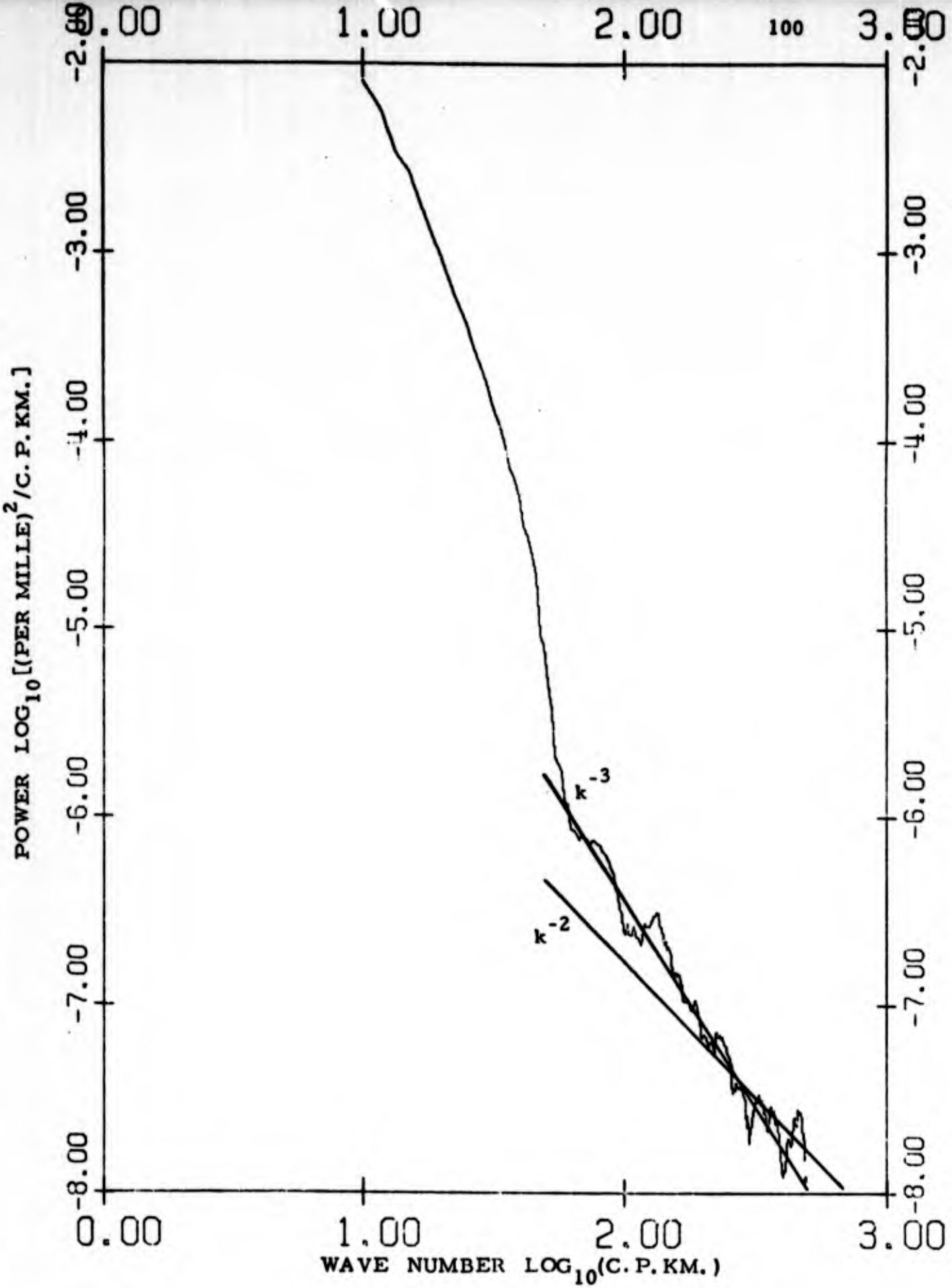

FIG. 14-8. Wave number spectra of salinity perturbations corrected for binomial filtering.
Depth interval 600-1200 meters.
Station 15.

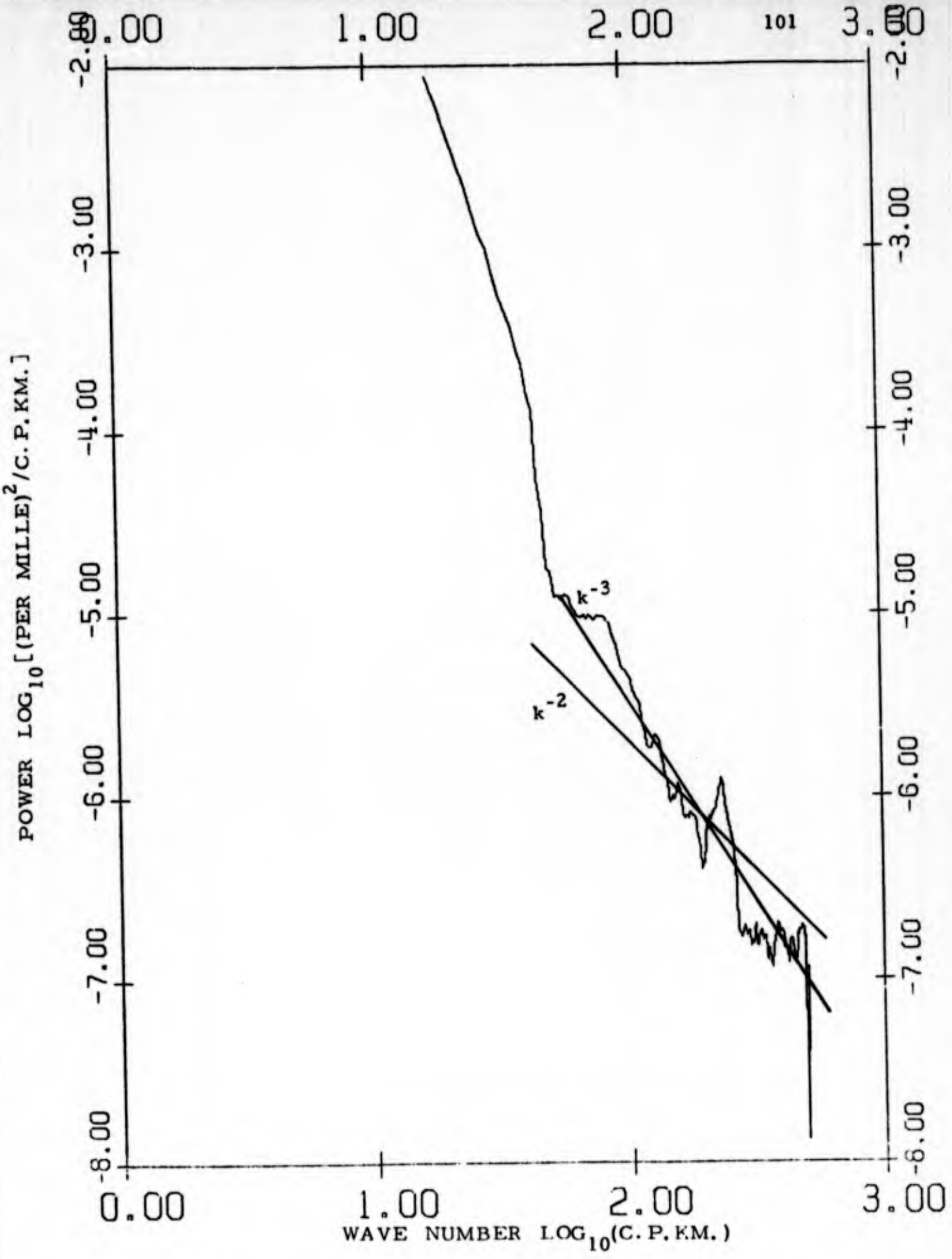

FIG. 14-9. Wave number spectra of salinity perturbations corrected for binomial filtering.
Depth interval 0 - 600 meters.
Station 16.

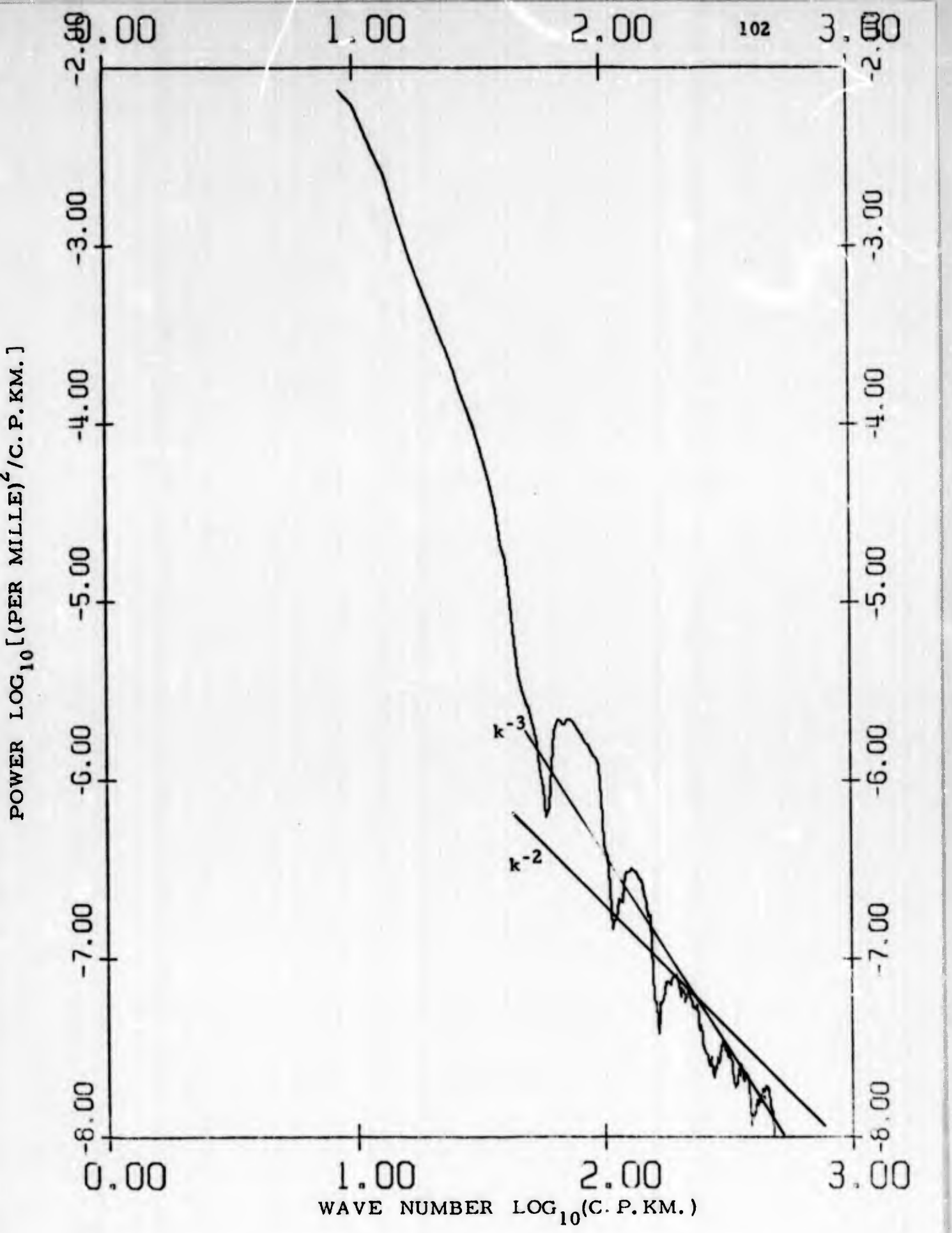

FIG. 14-10. Wave number spectra of salinity perturbations corrected for binomial filtering.
Depth interval 600-1200 meters.
Station 16.

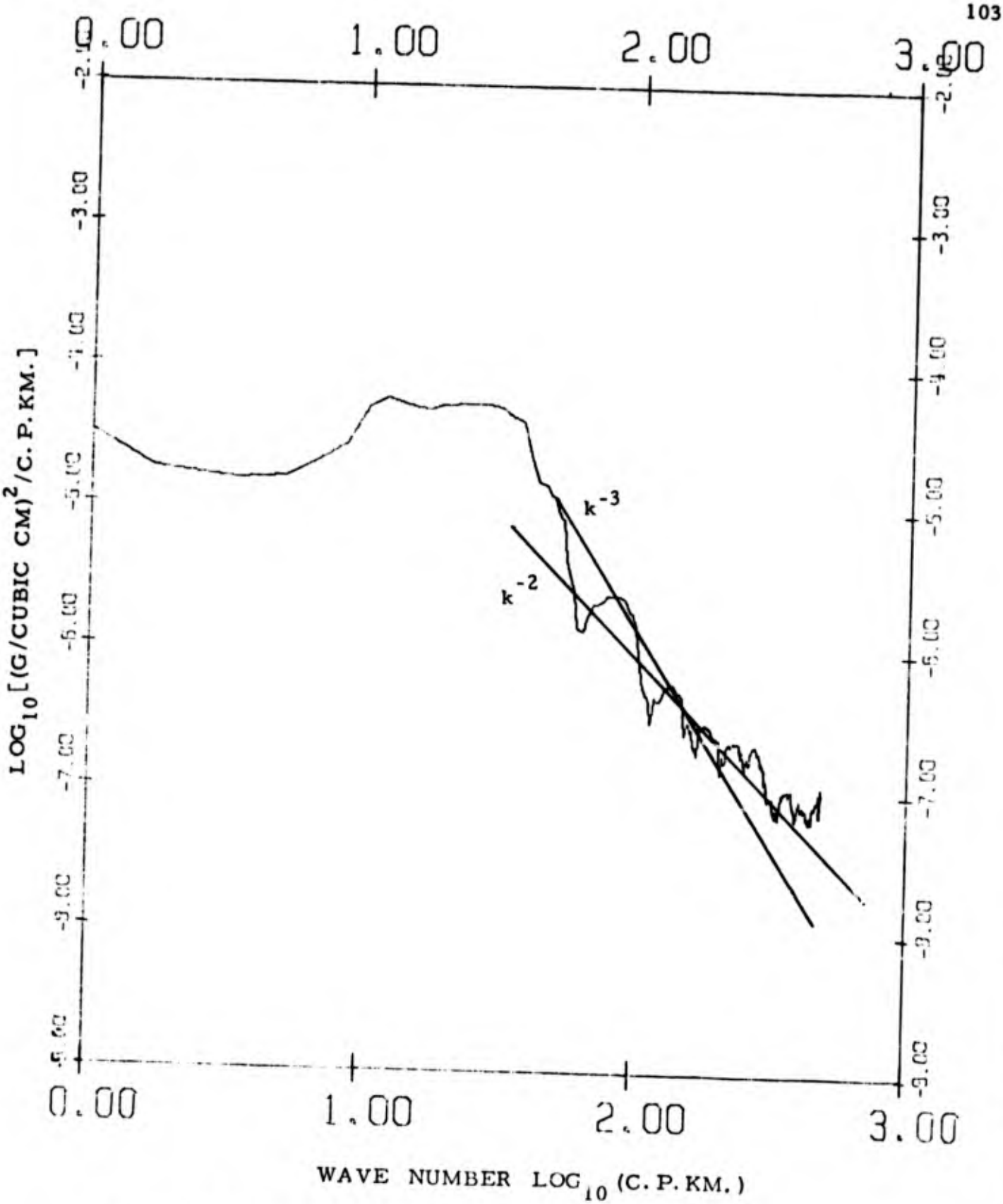

FIG. 15-1. Wave number spectra of sigma-t perturbations.
Depth interval 0-600 meters.
Station 9.

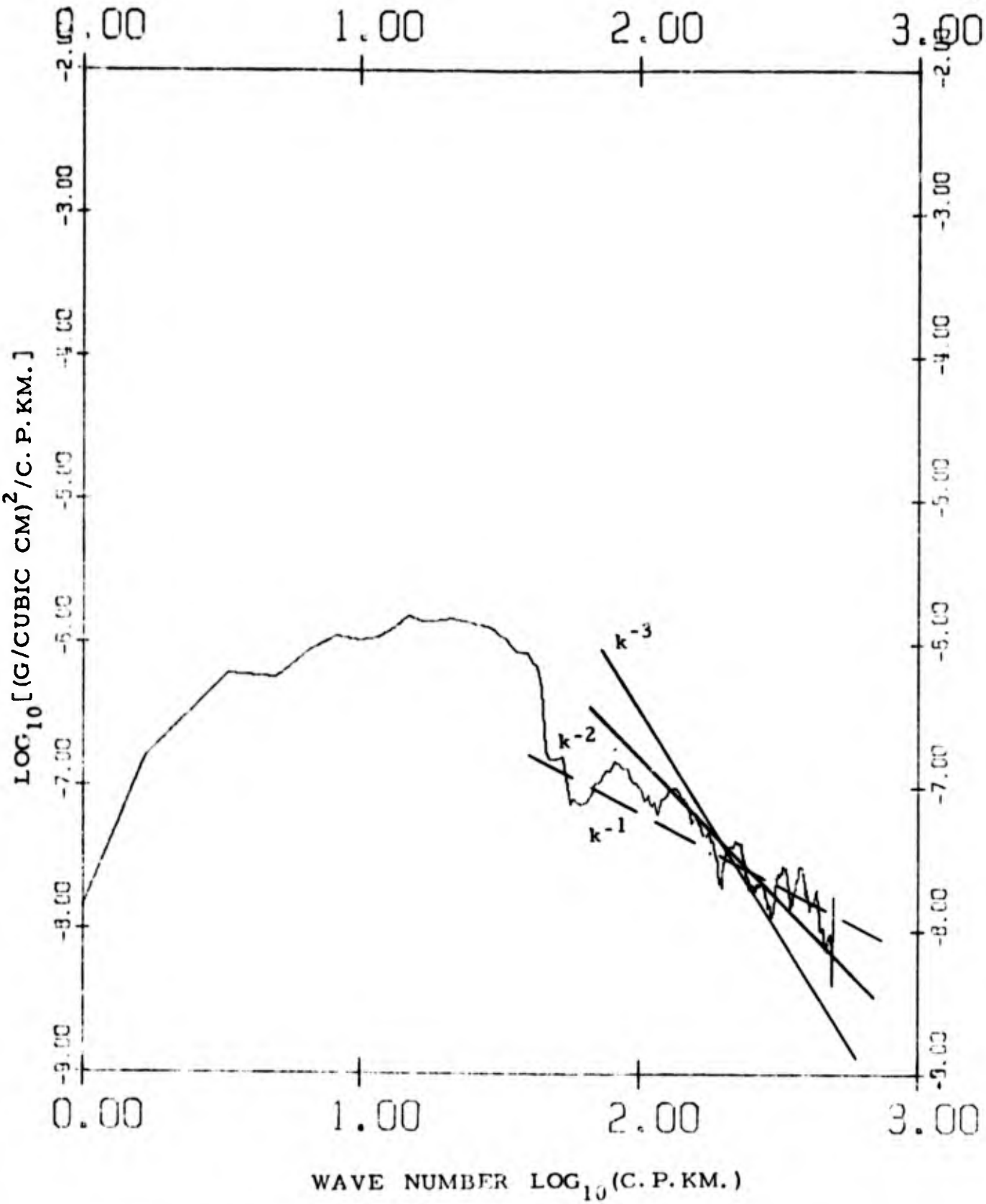

FIG. 15-2. Wave number spectra of sigma-t perturbations.
Depth interval 600-1200 meters.
Station 9.

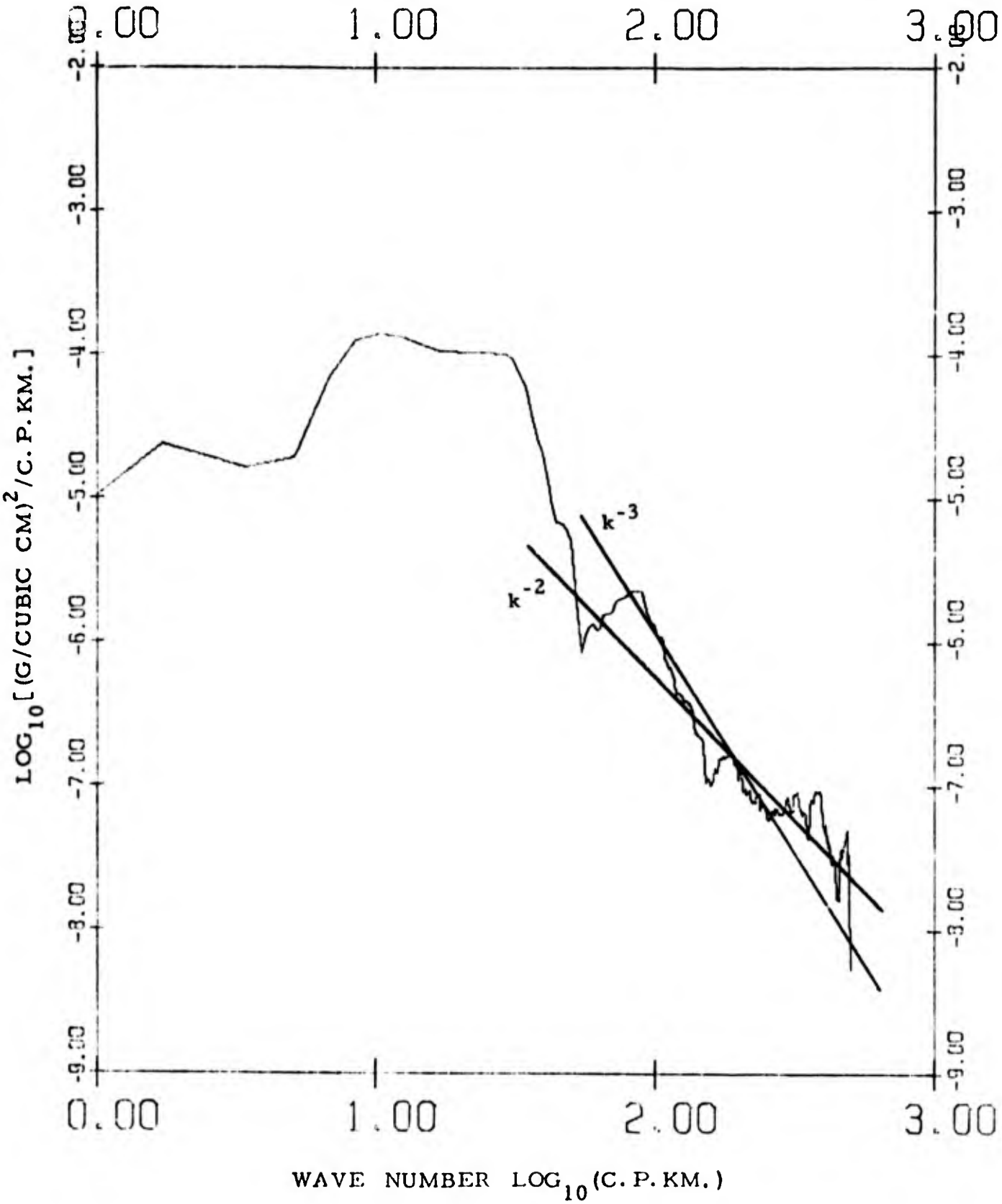

FIG. 15-3. Wave number spectra of sigma-t perturbations.
Depth interval 0 - 600 meters.
Station 10.

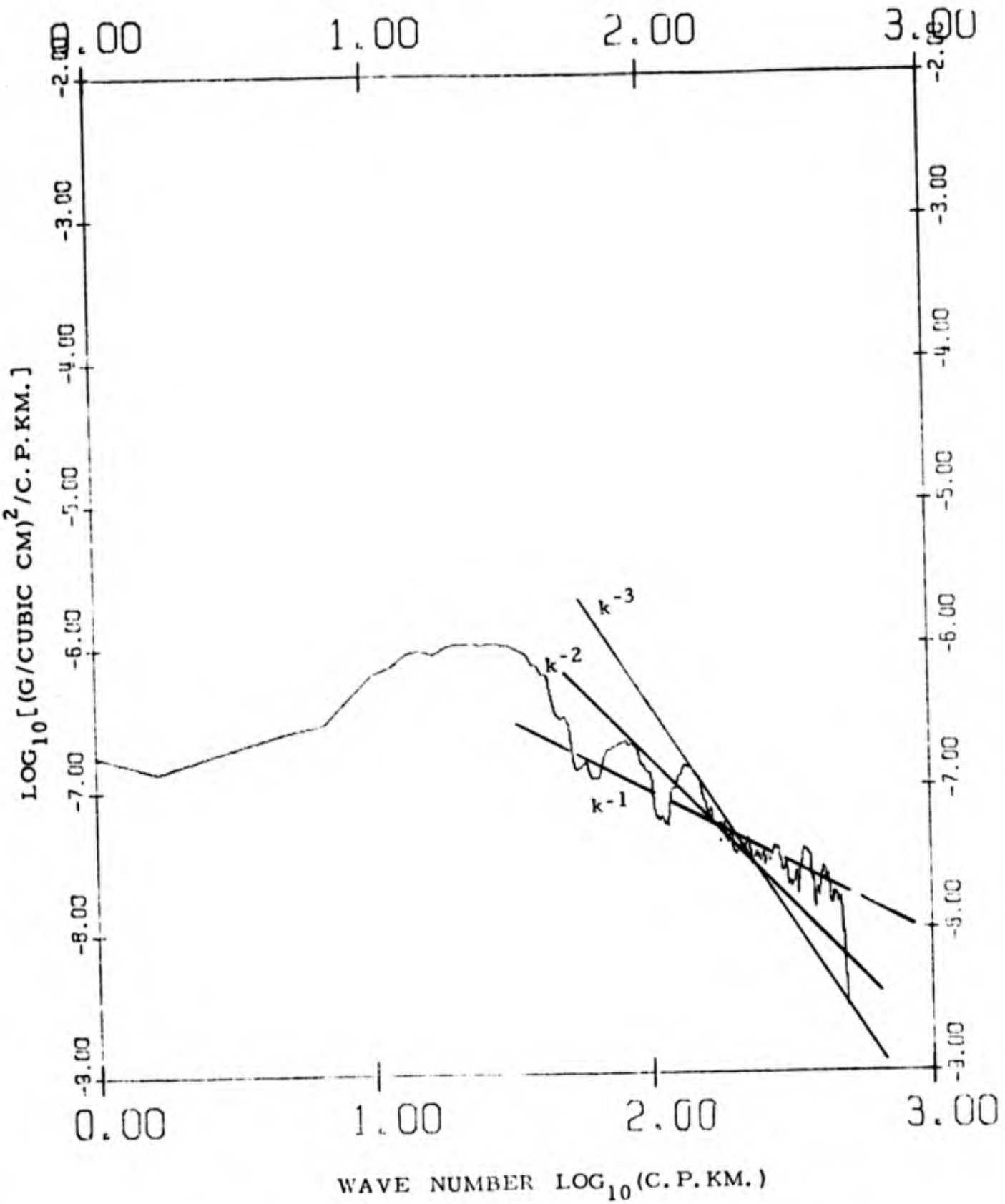

FIG. 15-4. Wave number spectra of sigma-t perturbations.
Depth interval 600-1200 meters.
Station 10.

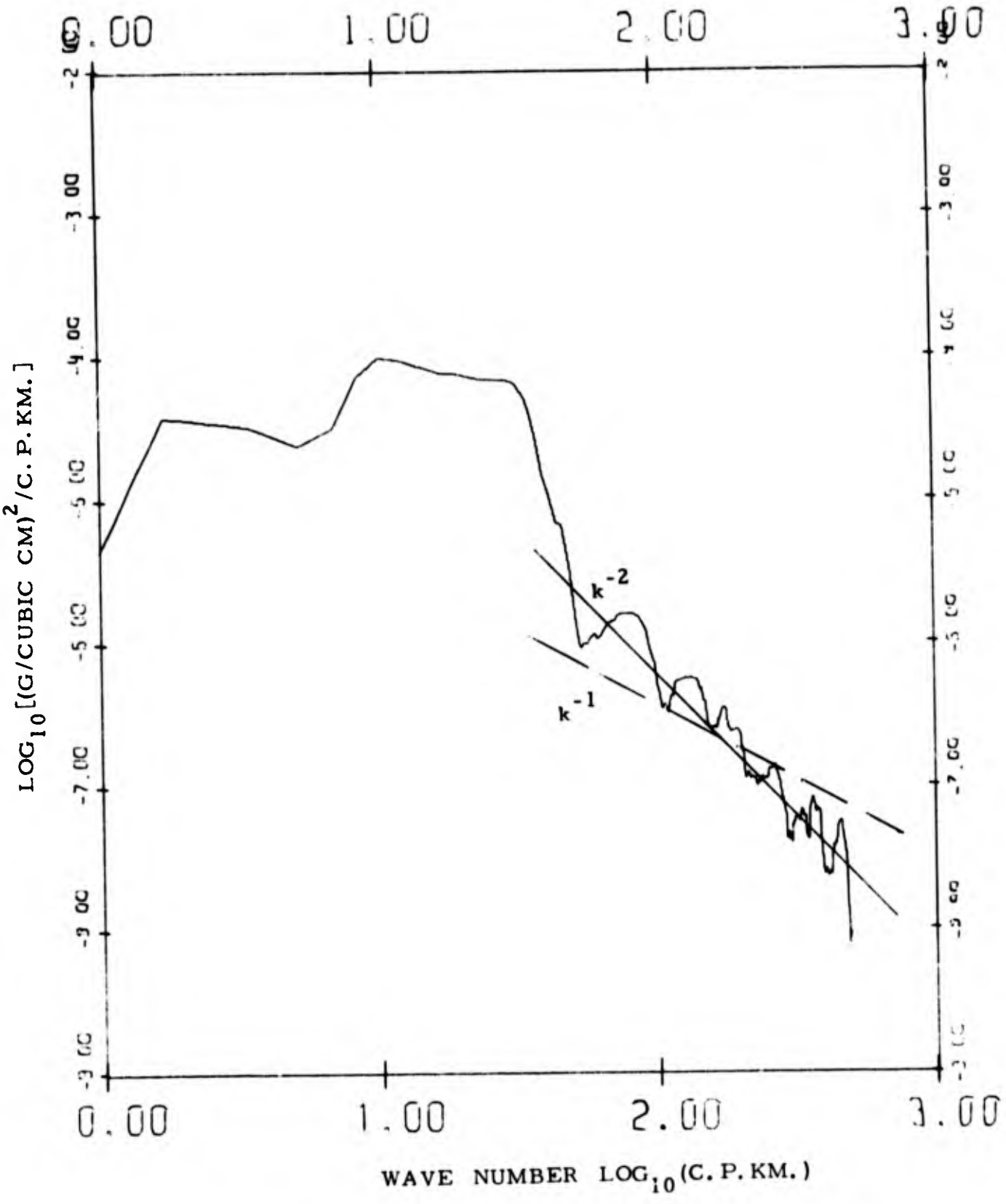

FIG. 15-5. Wave number spectra of sigma-t perturbations.
Depth interval 0 - 600 meters.
Station 11.

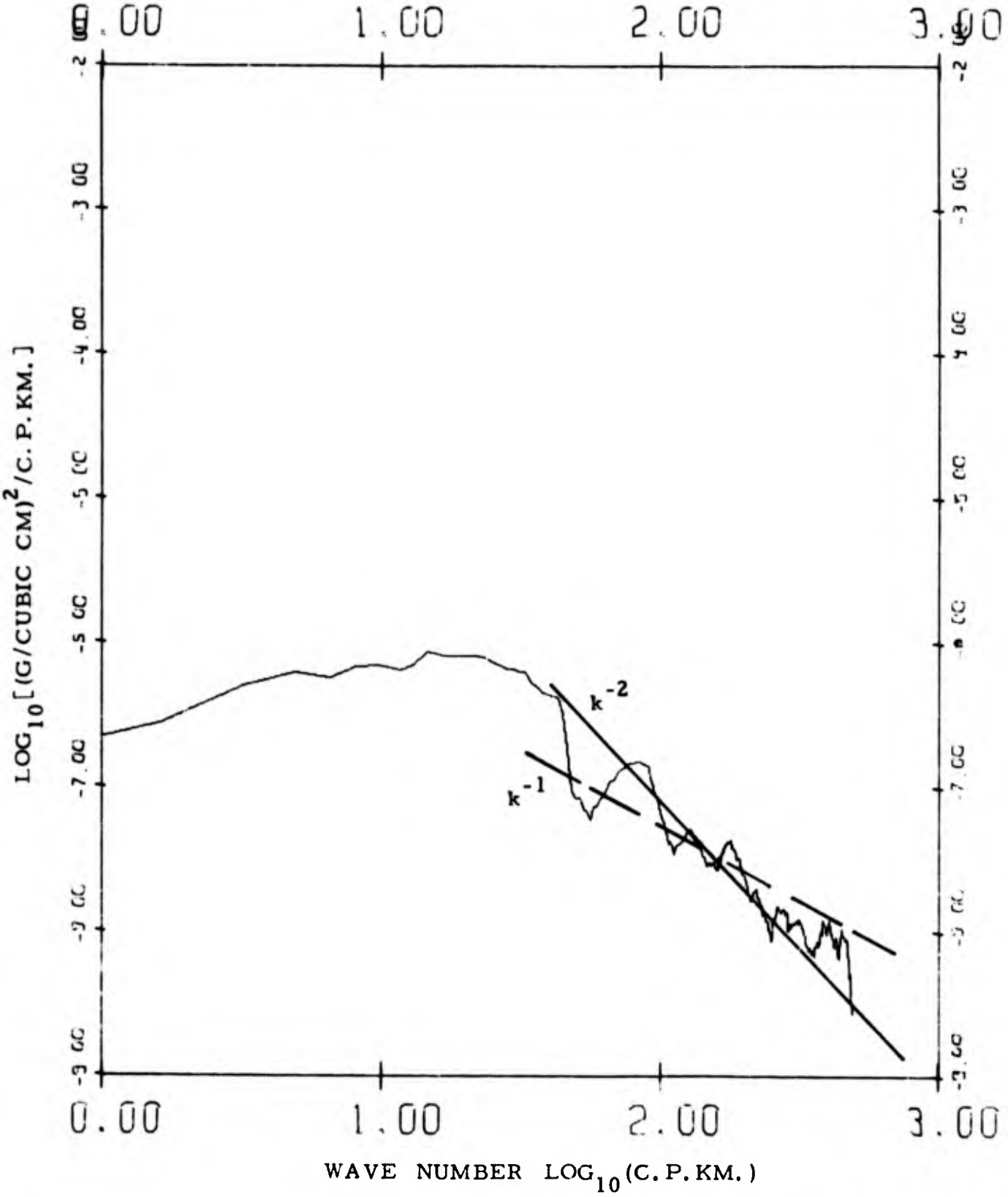

FIG. 15-6. Wave number spectra of sigma-t perturbations.
Depth interval 600-1200 meters.
Station 11.

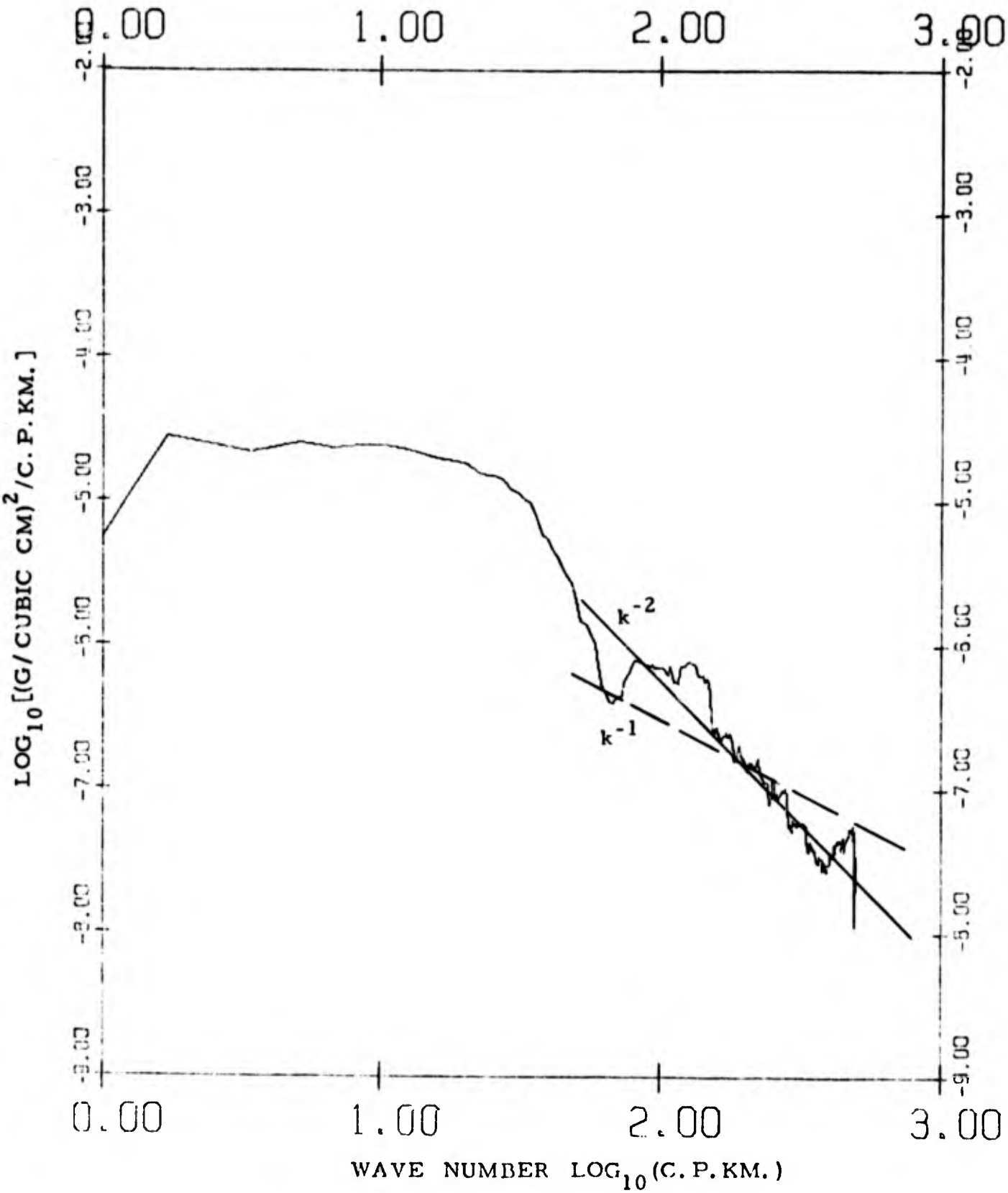

FIG. 15-7. Wave number spectra of sigma-t perturbations.
Depth interval 0 - 600 meters.
Station 15.

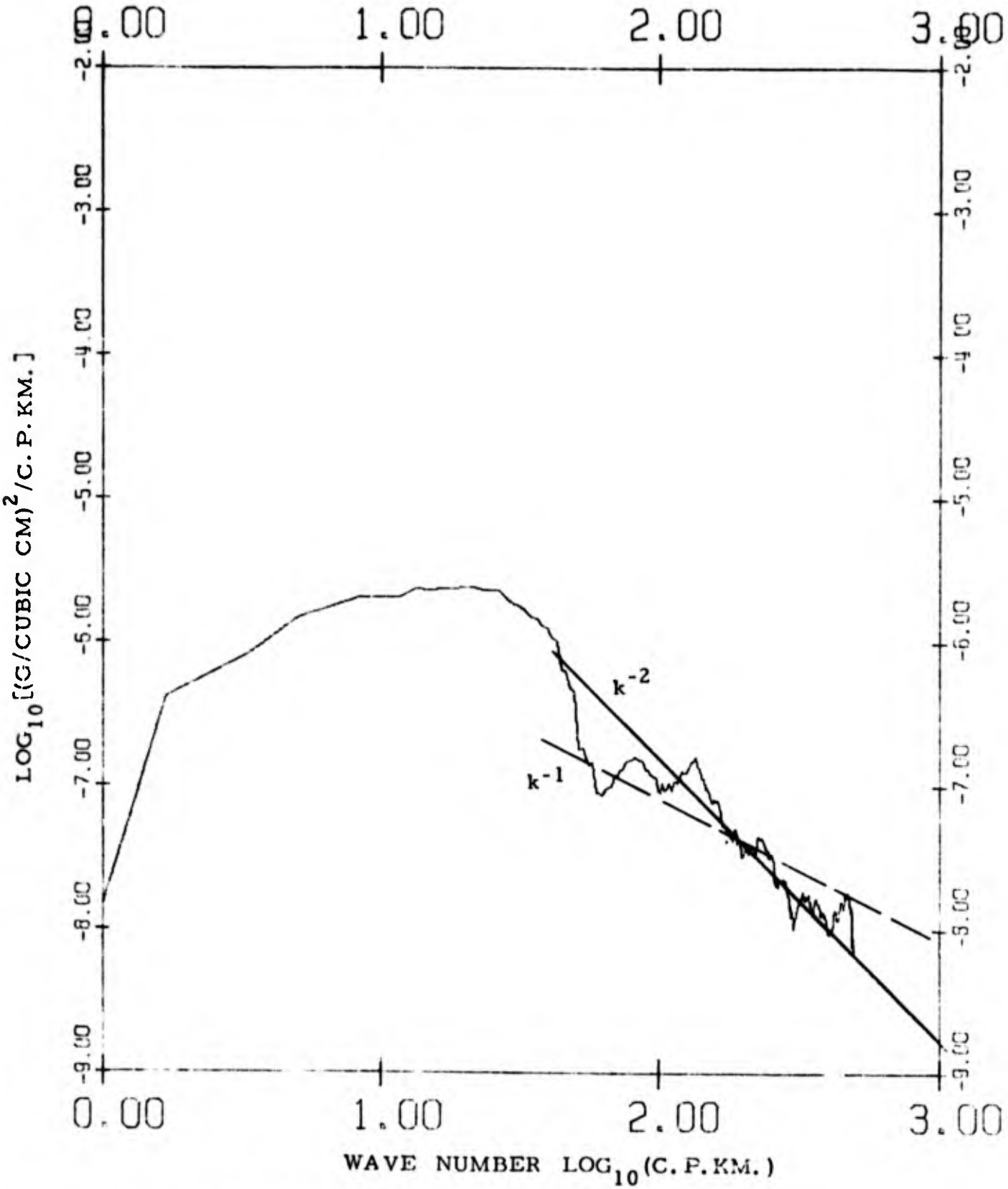

FIG. 15-8. Wave number spectra of sigma-t perturbations.
Depth interval 600-1200 meters.
Station 15.

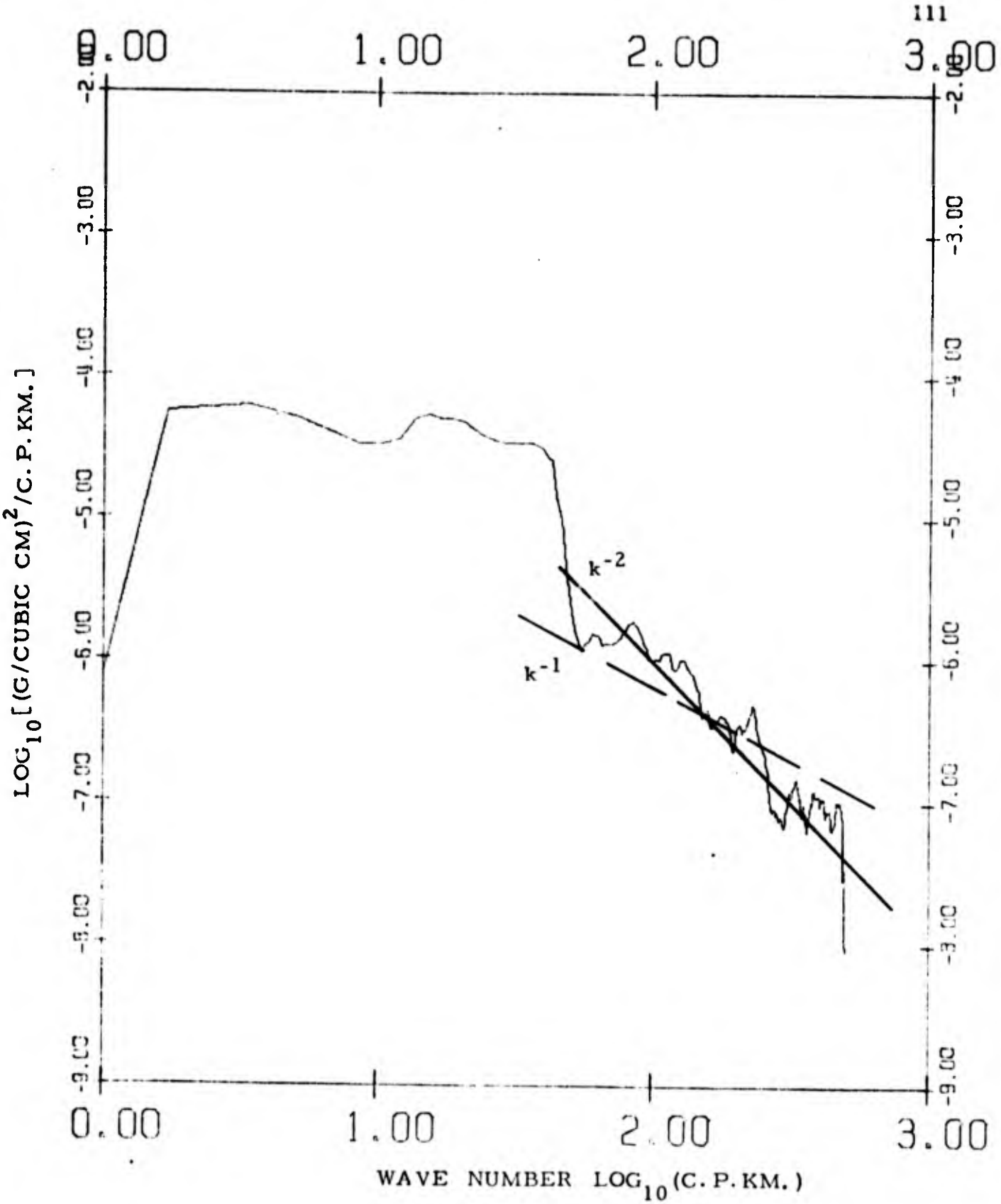

FIG. 15-9. Wave number spectra of sigma-t perturbations.
Depth interval 0 - 600 meters.
Station 16.

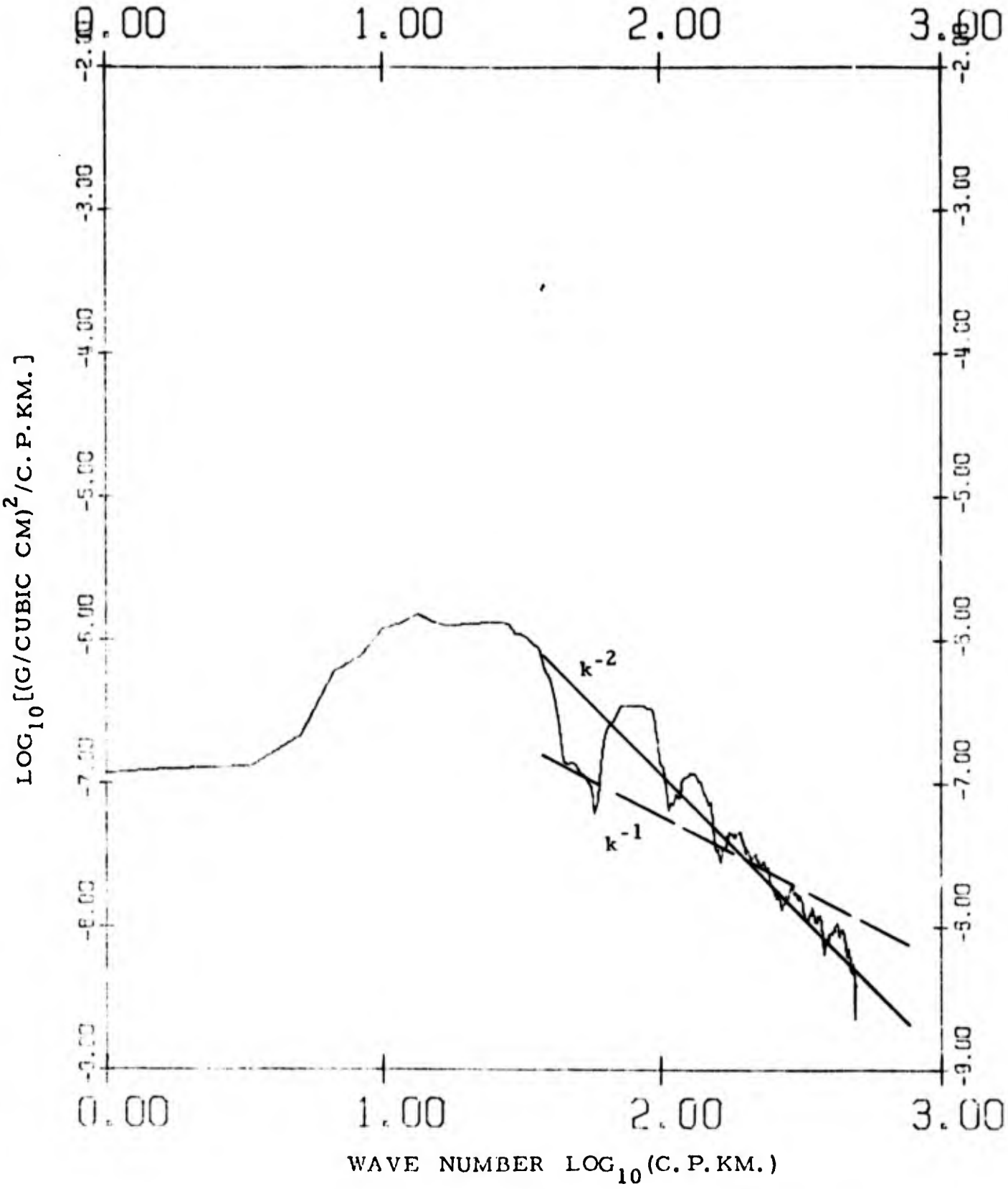

FIG. 15-10. Wave number spectra of sigma-t perturbations.
Depth interval 600-1200 meters.
Station 16.

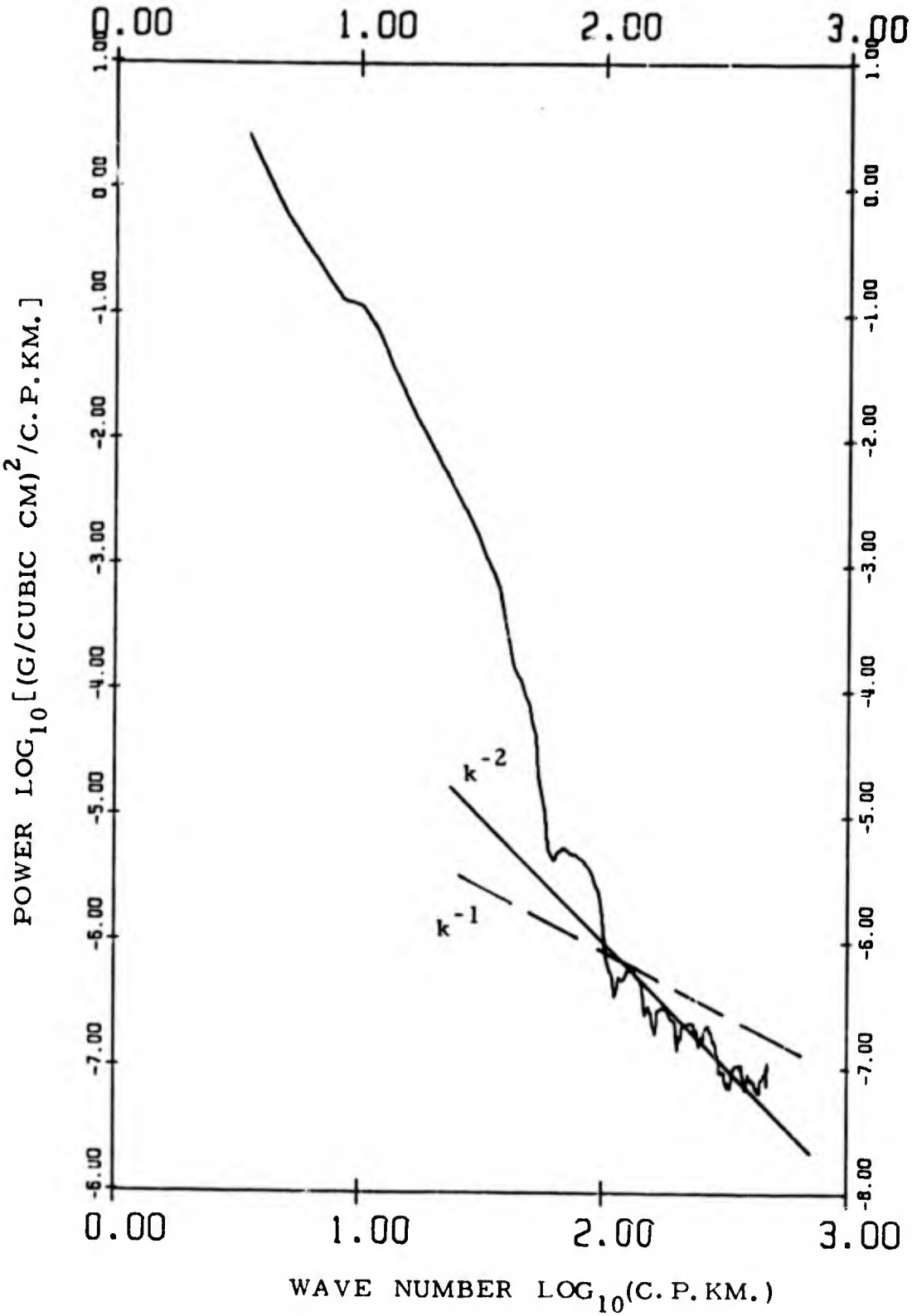

FIG. 16-1. Wave number spectra of sigma-t perturbations corrected for binomial filtering. Depth interval 0 - 600 meters. Station 9.

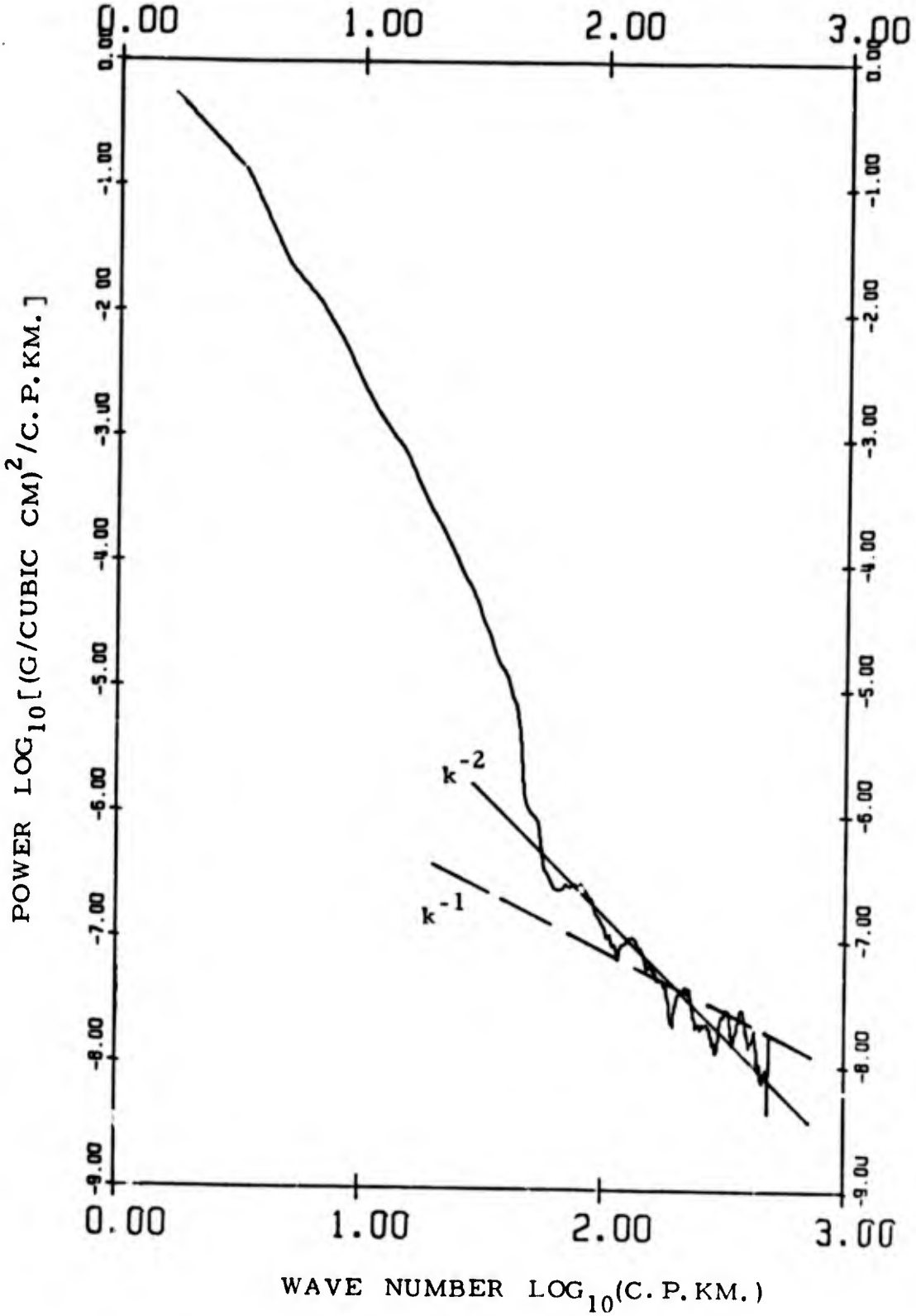

FIG. 16-2. Wave number spectra of sigma-t perturbations corrected for binomial filtering. Depth interval 600-1200 meters. Station 9.

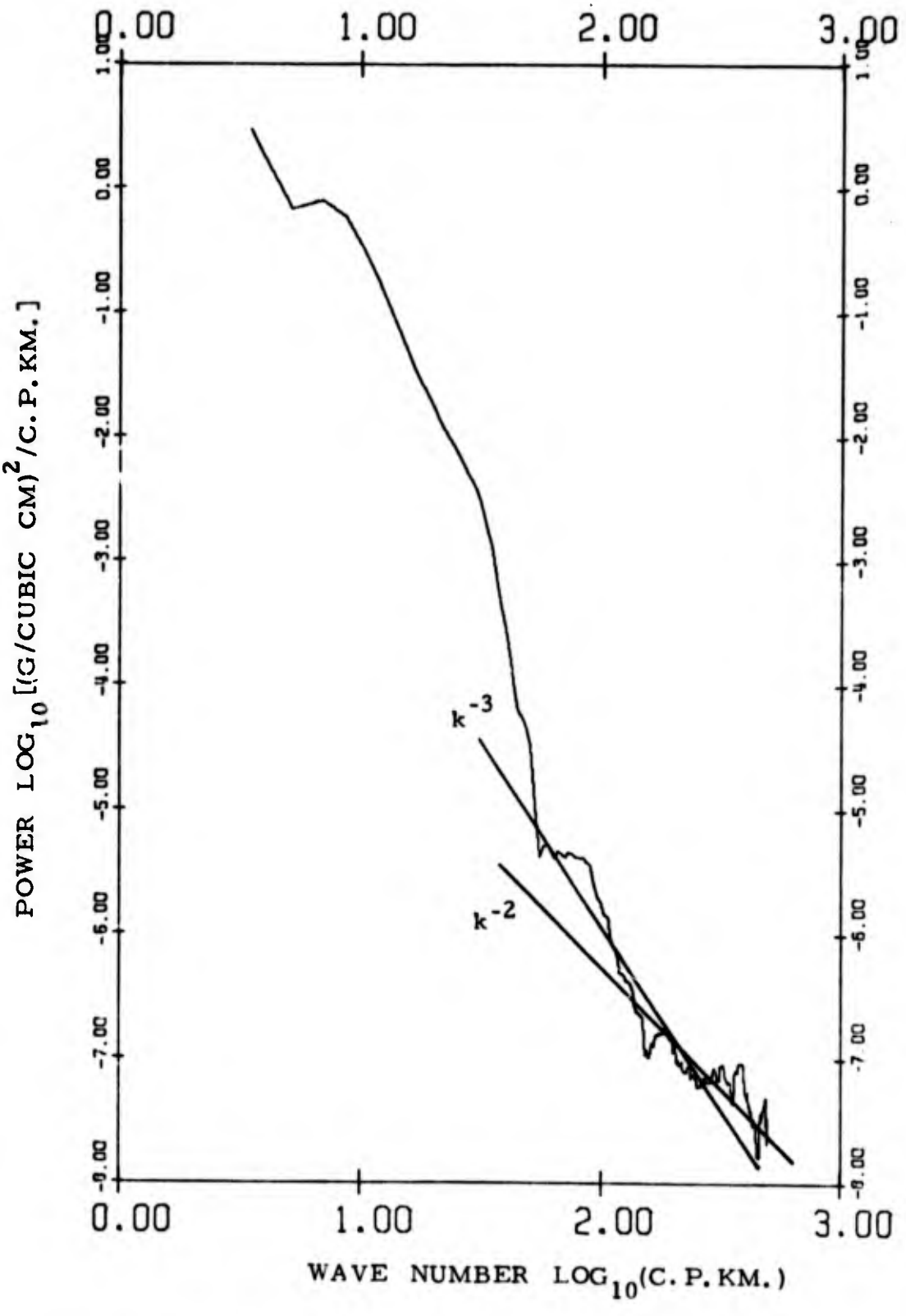

FIG. 16-3. Wave number spectra of sigma-t perturbations corrected for binomial filtering.
Depth interval 0 - 600 meters.
Station 10.

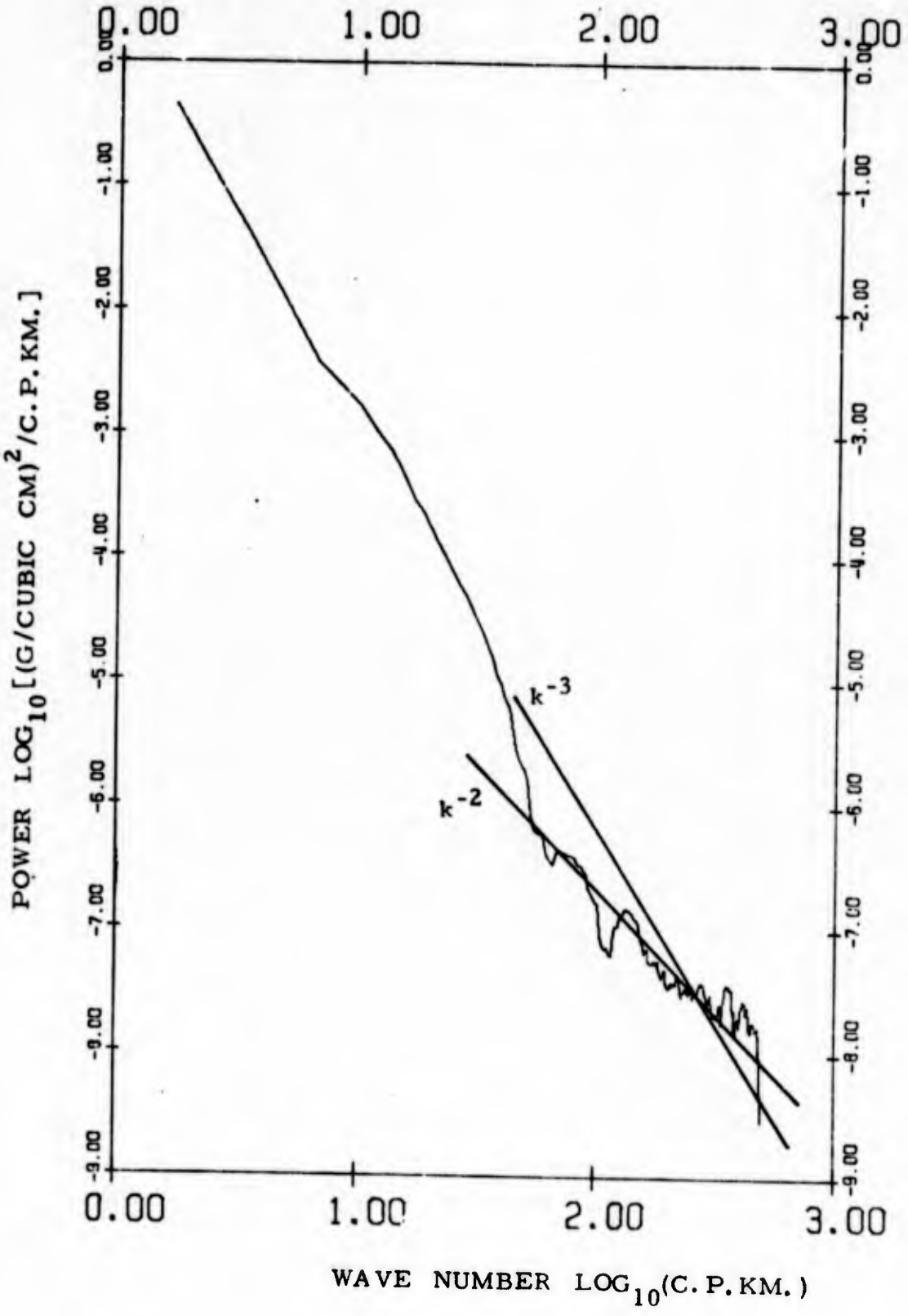

FIG. 16-4. Wave number spectra of sigma-t perturbations corrected for binomial filtering. Depth interval 600-1200 meters. Station 10.

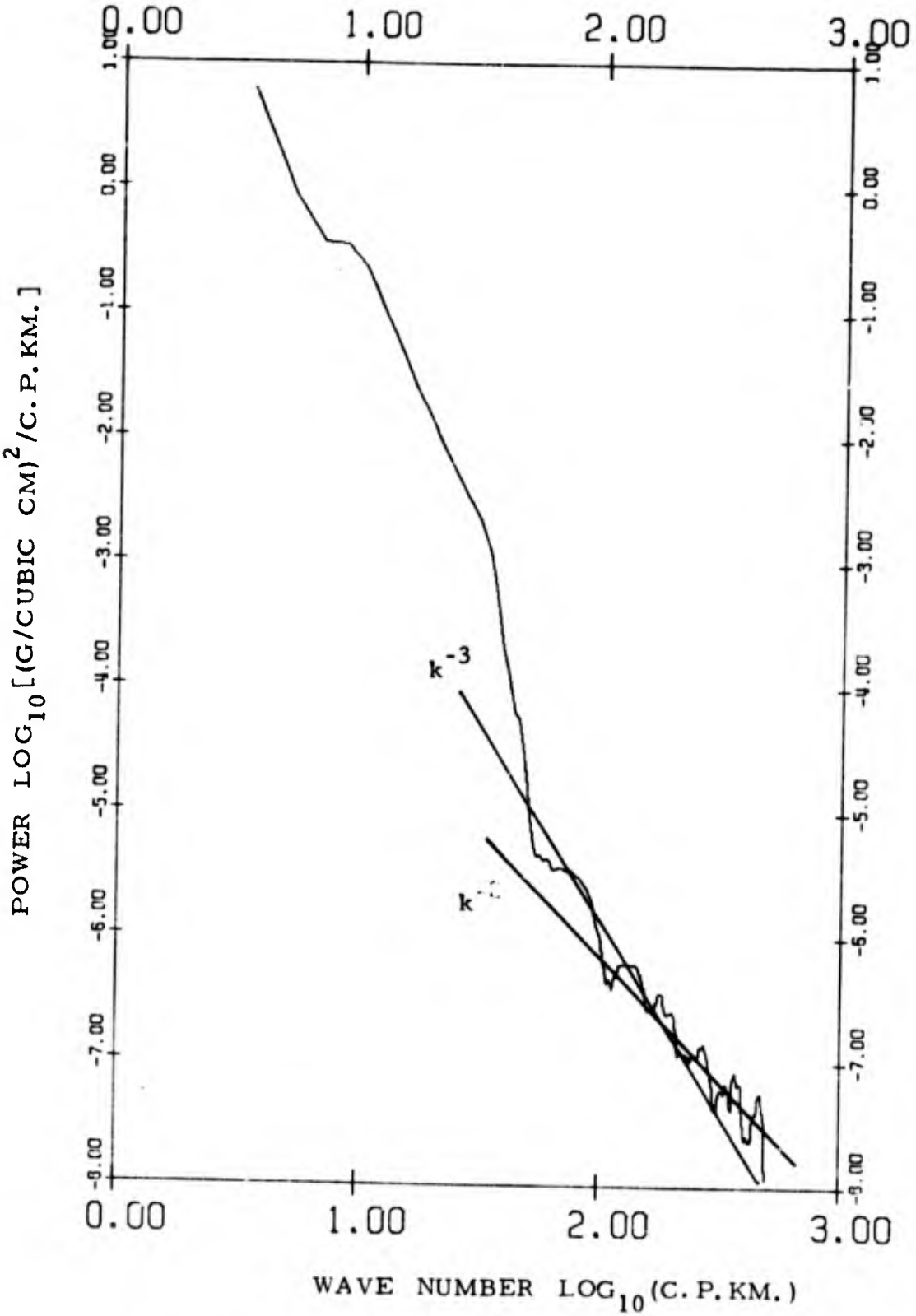

FIG. 16-5. Wave number spectra of sigma-t perturbations corrected for binomial filtering. Depth interval 0 - 600 meters. Station 11.

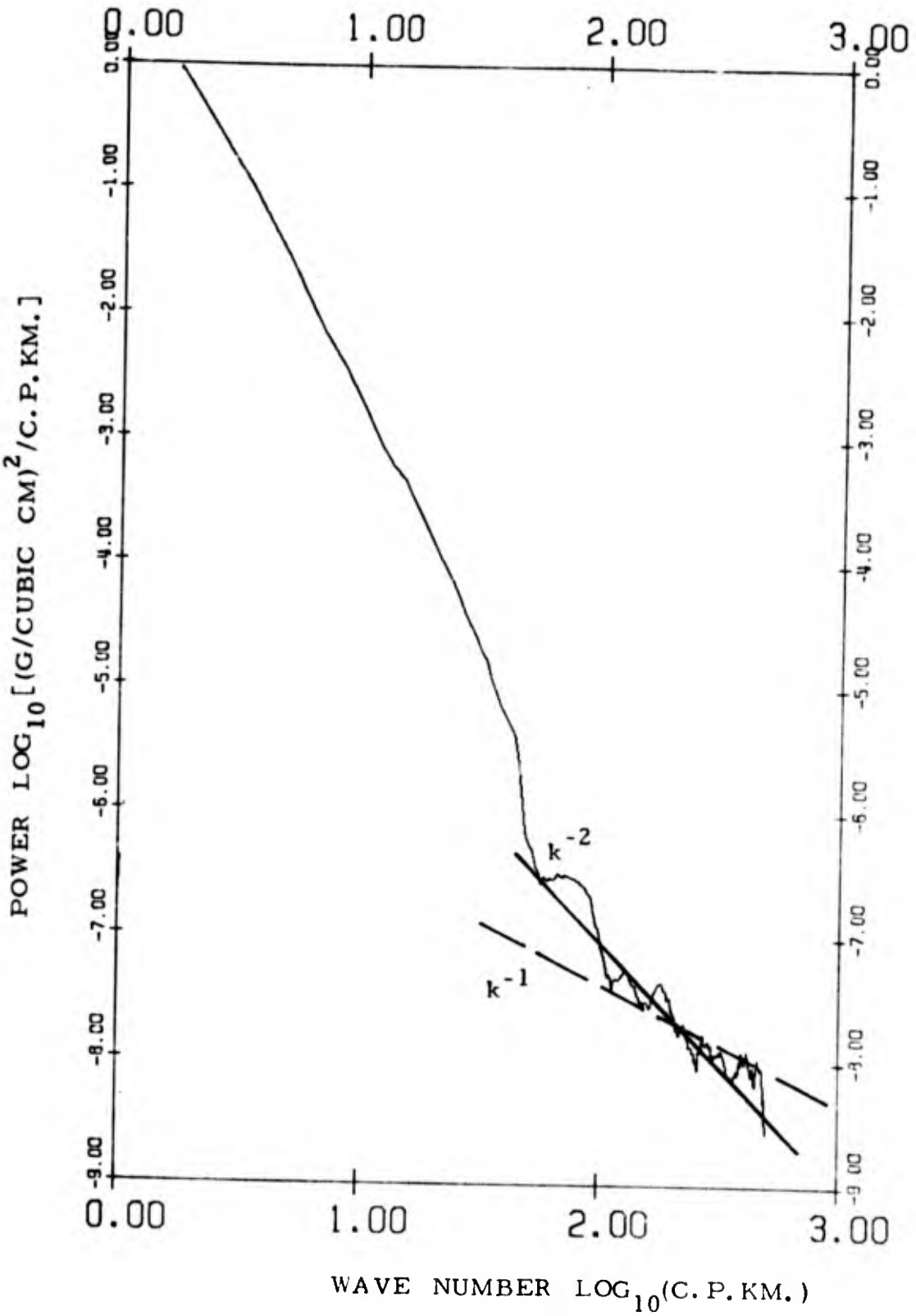

FIG. 16-6. Wave number spectra of sigma-t perturbations corrected for binomial filtering. Depth interval 600-1200 meters. Station 11.

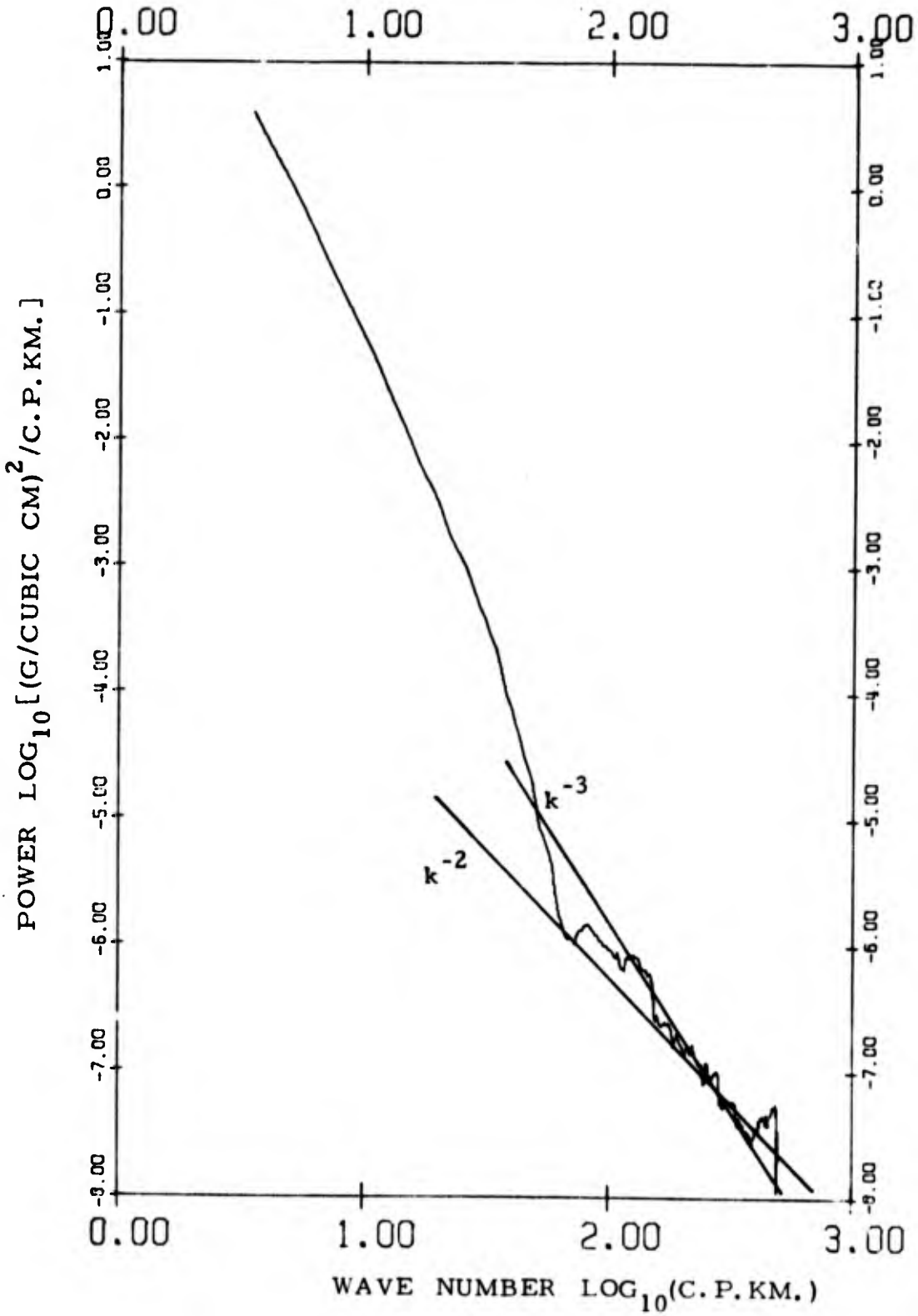

FIG. 16-7. Wave number spectra of sigma-t perturbations corrected for binomial filtering. Depth interval 0 - 600 meters. Station 15.

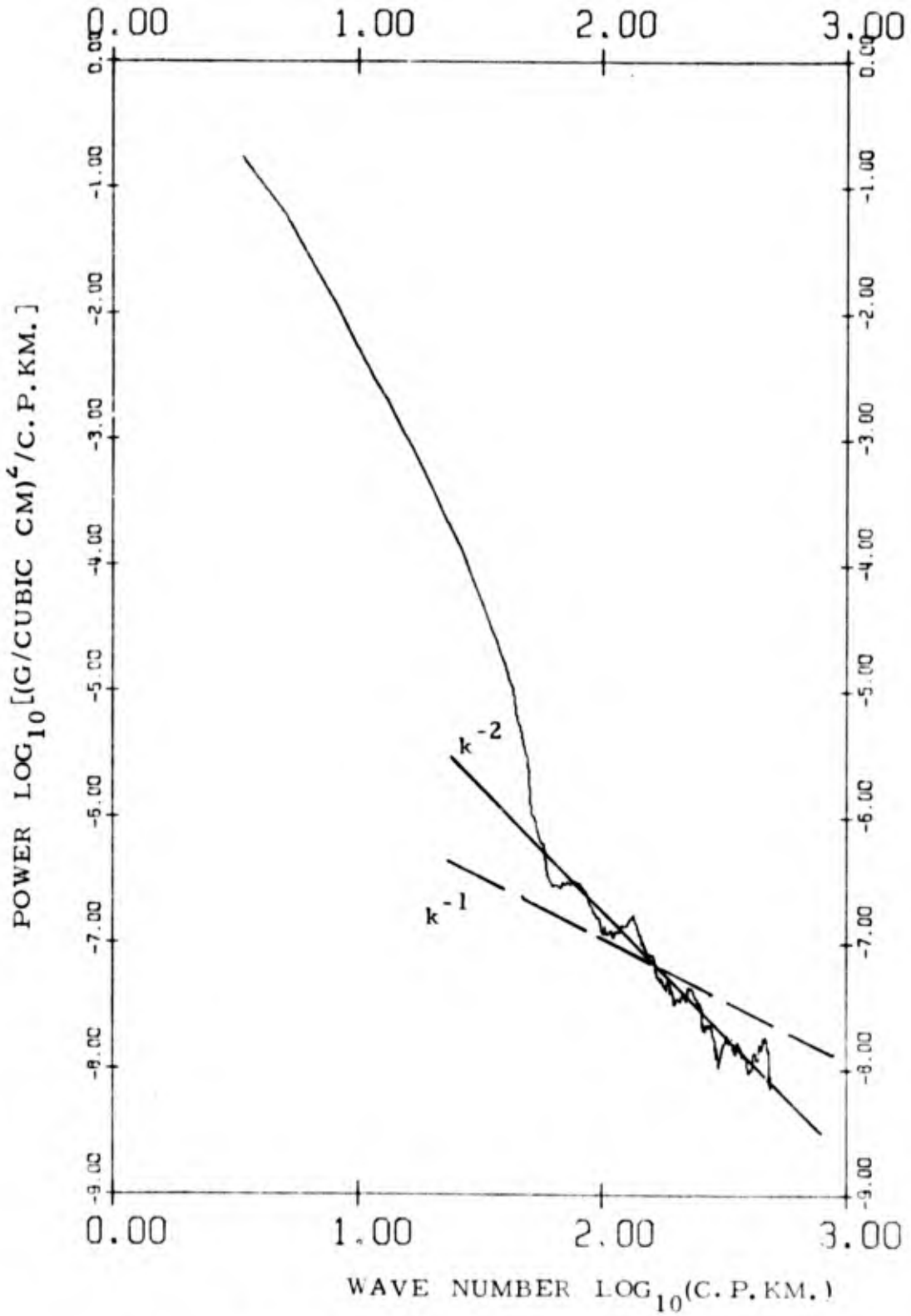

FIG. 16-8. Wave number spectra of sigma-t perturbations corrected for binomial filtering. Depth interval 600-1200 meters. Station 15.

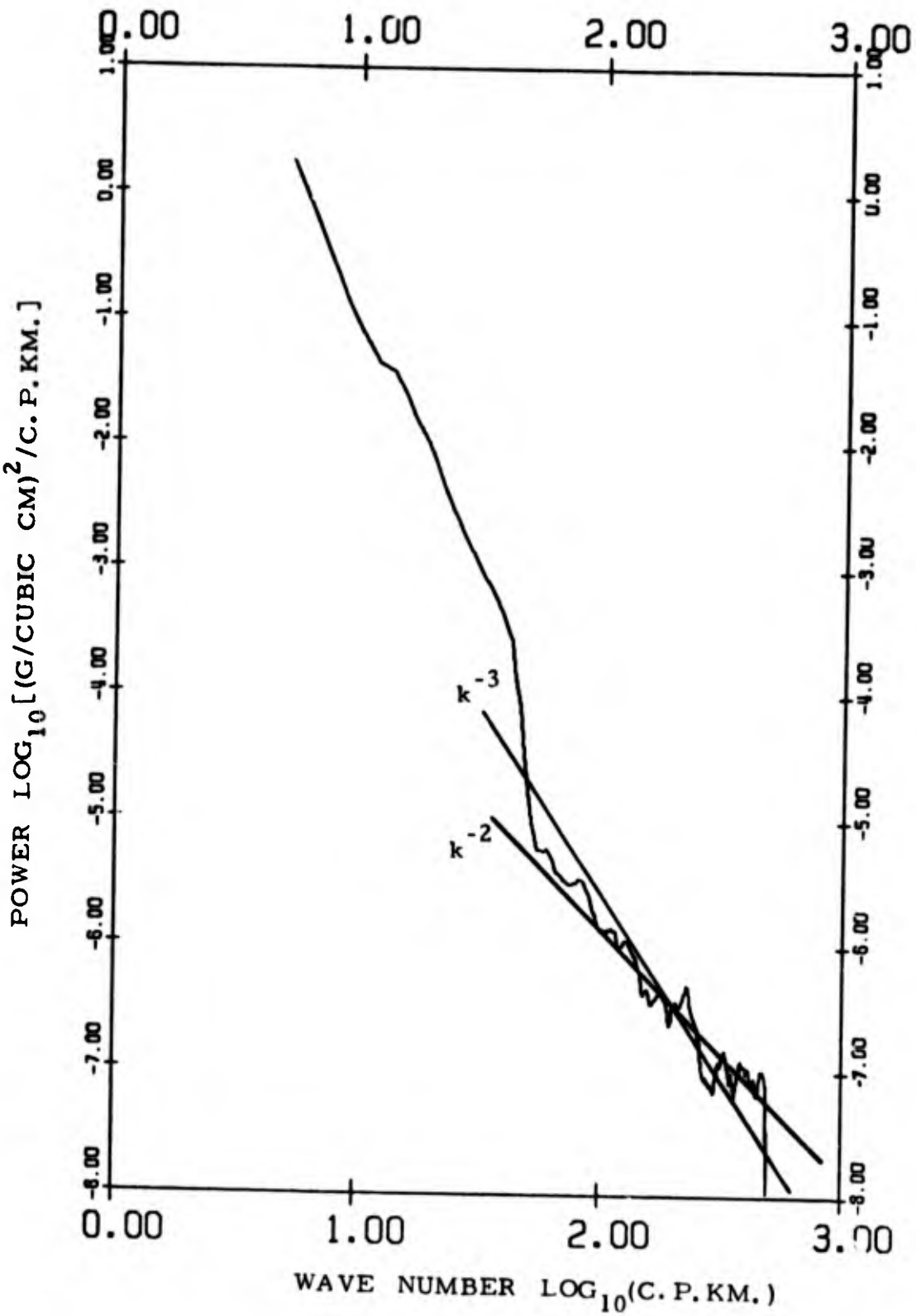

FIG. 16-9. Wave number spectra of sigma-t perturbations corrected for binomial filtering.
Depth interval 0 - 600 meters.
Station 16.

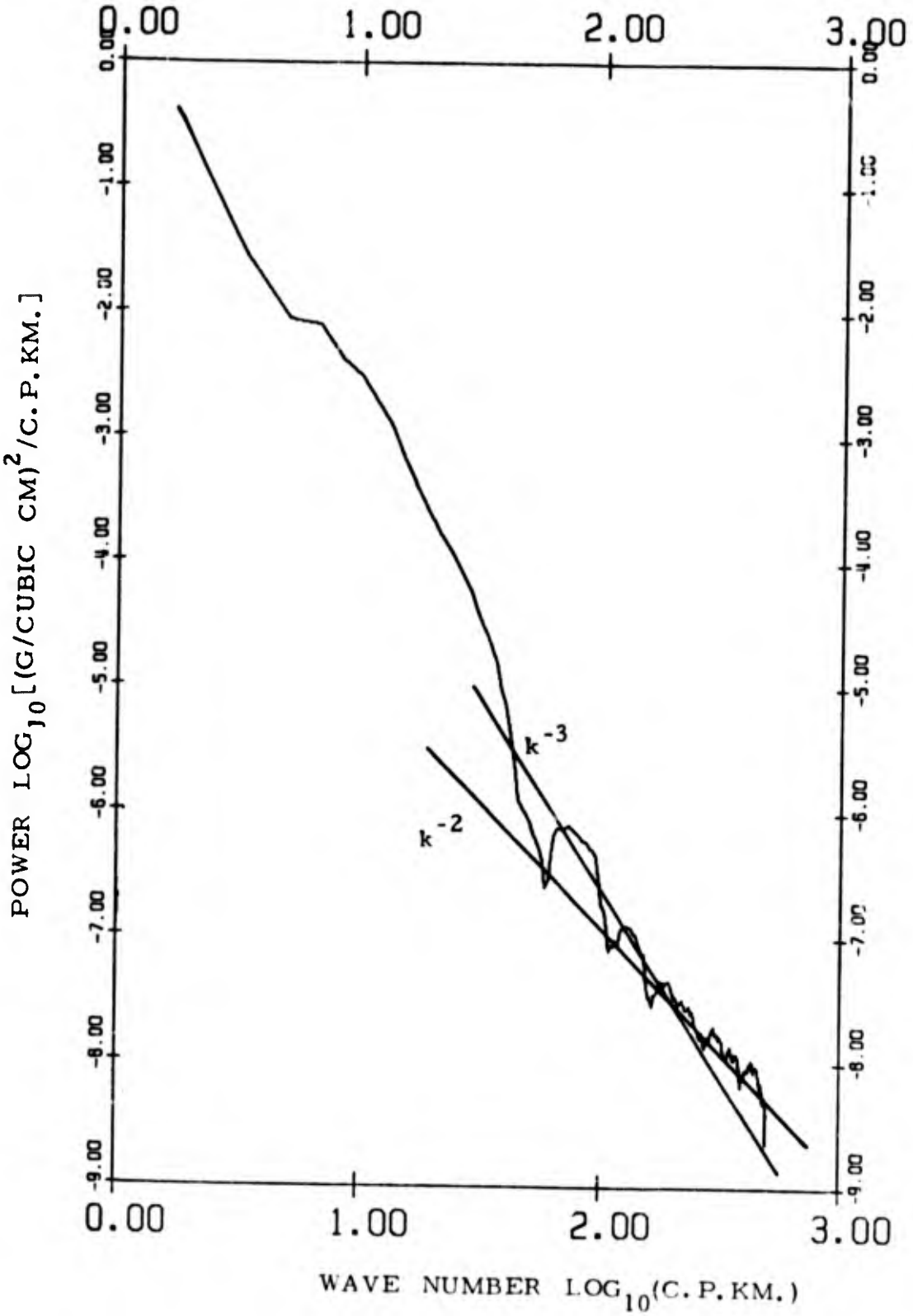

FIG. 16-10. Wave number spectra of sigma-t perturbations corrected for binomial filtering. Depth interval 600 - 1200 meters. Station 16.

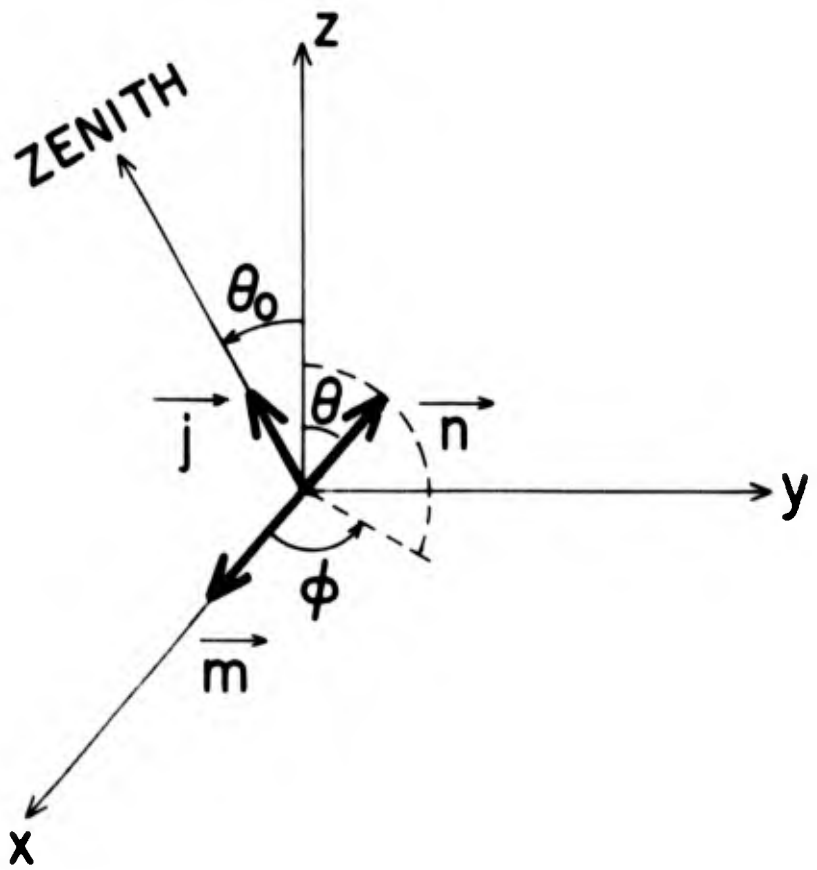

FIG. 17. Coordinate system for sound scattering problem.